UNIVERSIDADE DE SÃO PAULO
INSTITUTO DE FÍSICA

Quantum Field Theory and Space-Time Geometry

Jorge L. deLyra

Thesis submitted to the Physics Institute of the University of São Paulo as part of the requirements for obtaining the title of "Livre-Docente".

April 1997

Abstract

We study the generation of geometry in space-time as a consequence of the introduction in it of quantum matter fields. We use as definition of Quantum Field Theories their representation on the Euclidean lattice. The introduction of external sources in the $\lambda\phi^4$ model breaks the translational invariance of the model on the lattice. Due to this the physical scale that the model defines through its renormalized mass becomes dependent on position. The interpretation of this physical scale as the physical unit which defines distances generates on finite lattices a metric geometry with non-zero intrinsic curvature.

Dedication

On the occasion of the writing of this thesis, which I hope will be the last one I will ever write, I would like to leave recorded the intellectual legacy which I received from the persons who were my main mentors and teachers, among the many good teachers with whom I had the happiness of studying. Hence, I would like to dedicate this work to those persons who played a particularly important role in my scientific education and who, beyond that, guided me along the difficult paths of science.

I dedicate this effort to the memory of my father, Professor Carlos B. de Lyra, who left me not only the seeds of curiosity and intellectual honesty, but the belief in the redemption of the human being through science and wisdom; to Professor Henrique Fleming, who showed me for the first time, with extraordinary enthusiasm, the beauties of physics, and initiated me in my journey through science; to Professor Lee Smolin, who transmitted to me the fascination for the study of gravitation; to the memory of Professor Feza Gürsey, who showed me, even in the few contacts which we had, a profound vision of the relationship between physics and mathematics; and to Professor Bryce S. DeWitt, who guided me to scientific maturity.

Acknowledgements

I would like to thank in a special way the people who accompanied and helped me in a constant way during all the long and difficult period of our lives during which this work was slowly developed: my wife Maria Aparecida S. de Lyra and my children Alexandre e Cassandra. I would also like to thank all my work companions, friends, collaborators and students, for all the conversations, discussions, seminars and exchanges of ideas which were so important to us all in learning new things, in special Dr. Timothy E. Gallivan, Dr. See-Kit Foong, Prof. Carlos Eugênio I. Carneiro, Dr. André C. R. Martins and Prof. João Carlos A. Barata.

I would like to thank the Department of Mathematical Physics and in particular Prof. H. Fleming for their enduring support in my effort to obtain the facilities with which this work was done. The computer work involved in the elaboration of this thesis was all done on equipment of the University of São Paulo. The major part of the basic simulation work was done on the IBM-SP2 parallel computer of the Laboratory for Advanced Scientific Computing, to which I owe many thanks. The remaining simulation work, as well as all the work of analysis and elaboration of the results, was done on the machines of the Department of Mathematical Physics, with the extensive use of free software.

Contents

Chapter 1

Introduction and Overview

Contemporary theoretical physics is based on the two great and fundamental intellectual structures the discovery of which constituted the great revolution which occurred in the first half of this century: Relativity and Quantum Mechanics. More than descriptive theories of this or that aspect of the structure of nature, these intellectual structures are meta-theories containing the fundamental principles that rule all of physics. We say that these two intellectual structures are *theories of principle*, in contrast to the *theories of substance* which describe each aspect of the structure of nature.

Among the theories which describe the several fundamental forms of interaction between the particles which constitute the structure of matter the best known and also that with the most universal and familiar applications is, without question, Electrodynamics. Cradle of Relativity, it was also in this theory that the most successful application o the principles of Quantum Mechanics was realized. The classical principles of Electrodynamics are one of the most successful parts of physics and the application to them of the principles of Quantum Mechanics led to the creation of Quantum Electrodynamics, the most successful of the Quantum Field Theories.

The great successes of Quantum Electrodynamics motivated the formulation of generalizations of it, known as Gauge Theories, for the description of the short-range interactions which exist in nature. In contrast to Electrodynamics, which dominates the structure of matter at the level of atoms and molecules, these short-range interactions, called strong and weak interactions, dominate the dynamics of the structure of the atomic nucleus and of its components. These are the interactions discovered most recently, in this century, being also the least well understood.

The weak interactions are described and unified with Electrodynamics by a Gauge Theory with symmetry $U(1) \times SU(2)$, while the strong interactions are described by Quantum Chromodynamics, a Gauge Theory with symmetry $SU(3)$. While all these are quantum theories of vector fields describing various types of interactions, the constituents of matter itself are fermionic particles described by spinor fields and appear as *quarks* or *leptons* according to their being able or not to undergo strong interactions. This whole picture is called the *standard model* of the elementary particles.

On the other hand, the form of interaction longer known is undoubtedly gravitation,

the classical theory of which goes back to the origins of classical mechanics. In fact, the combined application of Classical Mechanics and the theory of Universal Gravitation to the problems of celestial mechanics was one of the first, great and lasting successes of classical physics. However, the situation of the theory of gravitation within the order of the ideas of physics has always been shrouded by a certain cloud of mystery.

At its inception the theory of gravitation was not even a field theory in the sense in which we use this concept today, but a theory of action at a distance. The question of the origin of this force was one which could not even be formulated clearly. With the discovery of Relativity the theory of gravitation was the main obstacle, resisting to the direct application of the relativistic principles. The compatibilization of the theory of gravitation with the principles of relativity was accomplished with the creation of the theory of General Relativity, now a well established theory and one of the most beautiful conquests of the human intellect. With this the theory of gravitation definitely becomes a field theory, although the gravitational waves predicted by it have not been, until now, observed directly. Besides, the theory presents an elegant explanation of the origin of the gravitational interactions in terms of the curvature of the geometry of space-time.

However, the status to be attributed to the theory remained rather obscure. Its geometric and profoundly non-linear character puts it in clear contrast with all other field theories of interaction of physics. If, on the one hand, General Relativity can be understood simply as a relativistic theory of gravitation, on the other hand it can also be understood as a kind of generalization of Relativity. While Relativity contains at its center the principle of the constancy of the speed of light and Quantum Mechanics contains the principle of uncertainty, General Relativity contains the principle of equivalence, which is intimately associated to the concept of locality which dominates the theory. Hence, General Relativity mixes up the concepts of theory of principle and theory of substance.

In no aspect the singularity of the theory shows itself more clearly than in the one related to the quantization effort. Since the beginning the theory resisted consistently to all the trials at making it compatible with the principles of Quantum Mechanics, which were many and varied. It must be said that there is no direct experimental evidence implying a need to quantize General Relativity. What exists is a logical imperative to make the theory of gravitation compatible with the fundamental concepts of Quantum Mechanics, if we want to believe that this last one is a true theory of principle with completely general validity.

In the effort, unsuccessful to this day, to bring the relativistic gravitation of General Relativity and Quantum Mechanics to a coexistence in a unique logical scheme, one has always started from the point of view that General Relativity is a classical field theory which should be quantized according to some scheme following the basic directives of the quantization of Electrodynamics and Gauge Theories. In this way, the dominant image of General Relativity in this effort is as a theory of substance, a classical theory of interaction, not as a theory of principle. However, after an enormous number of the most varied trials for the quantization of General Relativity, in which many different

techniques and many modifications of the classical theory were tried, no definitive results have been obtained.

Parallel to this, the semi-classical analysis of the theory, in which one studies the quantization of other fields in the presence of a classical gravitational field, that is the so-called Quantum Field Theory in Curved Space-Time, presents some interesting and suggestive results. These results, associated to the horizons which exist in the solutions of General Relativity, establish an interesting connection with thermodynamics. We must observe, however, that these results do not provide a complete view of the physics involved, containing in fact some paradoxes.

From whatever angle one examines the nature of the theory of gravitation, a cloud of doubt persists, specially with respect to its relationship with Quantum Mechanics. One may identify the very geometrical character of the classical theory as the root of the difficulties. Observe that the fundamental principle contained in the theory, the principle of equivalence, finds its expression exactly in this geometrical character. Indications are that the fundamental principle of locality in General Relativity conflicts in an unavoidable way with the non-local character introduced through Quantum Mechanics by the principle of uncertainty.

One of the difficulties one finds in the effort of quantization of General Relativity is our still limited knowledge of Quantum Field Theory in general. A fair portion of these difficulties is of a technical character, however, after so many trials for so long, it is no longer possible to believe that all difficulties which confront us in the quantization of gravity are of a technical character. Certainly there must be a fundamental difficulty of a conceptual character, even if we are not yet capable of identifying it clearly.

It is not surprising that our understanding of Quantum Field Theory is limited, for these are recent, complex and sophisticated theories, expressed by mathematics over which our control is still very limited. The extraordinary and even surprising success of the predictions of perturbation theory in Quantum Electrodynamics gives us, perhaps, a distorted idea of the depth of our understanding of Quantum Field Theory in general, even with respect to theories which are formally simpler that Quantum Electrodynamics, like the $\lambda\phi^4$ polynomial models.

In this work we wish to examine some aspects of this question, using as a laboratory the $\lambda\phi^4$ model. Through the analysis of some basic properties of the structure of this model we will be taken to the examination of a particularly interesting aspect, which relates the quantization of the model directly to the concept of a local geometry in space-time. Although the ideas will be presented in the restricted context of this laboratory model with scalar fields, they introduce the analysis of a new aspect of the quantization of field theories and suggest new and interesting lines of research for the exploration of the possibility of extension of these ideas to more realistic models, containing vector and spinor fields.

It is interesting to record here the philosophy which we adopt with respect to the definition of Quantum Field Theories. There is a way of thinking according to which a Quantum Field Theory is what one gets by applying to a given classical field theory

some "quantization process". This is not the standpoint which we adopt, because what is meant by the "quantization process" is not a unique and well-defined mathematical procedure. Unlike this, we adopt from the start a certain given definition of the quantum theory, while the corresponding classical theory should be obtained from the quantum theory by means of a classical limit, which consists of an approximation for long wavelengths.

In principle it is possible that several different definitions of the quantum theory have the same classical limit, or that no quantum theory has a given classical limit. The determination of the classical limit of a quantum theory is part of the analysis of the nature of this quantum theory and is not determined "a priori". If, on the one hand, we adopt a given definition for the quantum theory with the intention that it be complete and consistent, on the other hand we do not assume any "a priori" position about the uniqueness or physical relevance of this definition. The correctness of the choice of the detailed definition of a quantum theory can only be judged from the properties of the resulting theory.

In this work we will be using a laboratory model to which no fundamental physical relevance is intended, but which we believe to be a good laboratory to illustrate the working of the mathematics involved in the definition of a Quantum Field Theory. The definition we use for the quantum theory in this model by means of the Euclidean lattice is the definition which is universally used by the researchers in this area, for this particular model. However, it is certainly not the only possible definition.

Chapter 2

Quantum Fields on the Lattice

The first step for the definition of a quantum field theory within the formalism of the Euclidean lattice is the definition of a certain mathematical structure on finite lattices. This structure will contain exclusively a certain number, possibly large but finite, of dimensionless parameters and functions. The theory will be defined as the limit of a sequence of finite lattices, with increasingly larger sizes, satisfying certain conditions. We will call this limit the *continuum limit*.

Some physical quantities are defined at the beginning of this process and remain unaltered until its end. One quantity of this type is the the integer number d of dimensions of the Euclidean space-time in which we define the theory. Another quantity of this type is the order $\mathcal{N}$ of the symmetry group we use to define the model. Other quantities will be parameters that, although constant in each lattice, will vary in the continuum limit. Among these is the number N of lattice sites in each space-time direction, which characterizes the size of the lattice. Other parameters of this type will be the mass parameter α and the dimensionless coupling constant λ. Finally, we will have dimensionless random variables, which fluctuate in each finite lattice according to a given probability distribution, that is, the dimensionless dynamical field variables, defined in an internal space of dimension $\mathcal{N}$, which we will denote as $\vec{\varphi}$, or by its components φ_i, $i = 1, \ldots \mathcal{N}$.

2.1 Definition of the Classical Theory

Initially we will illustrate the process considering the definition on the lattice of the *classical* field theory, using as an example the $\lambda\phi^4$ model. Later we will examine in some detail the definition of the quantum theory. We consider, therefore, a hyper-cubic lattice of size N in d dimensions, that is, a set of N^d points, which we will call *sites*, arranged as a d-dimensional cube with N points along each side. We associate to these points the concept of next neighbor, symbolized by the introduction of connections or *links* between them. We include links connecting the sites at the boundary of the cube with the sites at the opposite boundary, so as to implement periodic boundary

conditions. Note that, at this stage, there is no notion of distance in the lattice.

We define now the Euclidean action of the system as

$$S_N = \frac{1}{2}\sum_{l}^{dN^d} \Delta_l\vec{\varphi}\cdot\Delta_l\vec{\varphi} + \frac{\alpha}{2}\sum_{s}^{N^d}\vec{\varphi}\cdot\vec{\varphi} + \frac{\lambda}{4}\sum_{s}^{N^d}(\vec{\varphi}\cdot\vec{\varphi})^2 - \sum_{s}^{N^d}\vec{j}\cdot\vec{\varphi}, \tag{2.1}$$

where $\sum_l^{dN^d}$ represents a sum over all the dN^d links of the lattice, $\Delta_l\vec{\varphi}$ is the difference between the fields at each of the two ends of a link, $\sum_s^{N^d}$ represents a sum over all the N^d sites of the lattice, the dot denotes scalar product in the internal space of the fields and $\vec{j}$ is an external source. Note that we may separate this action in two parts, as $S_N = S_0 + S_V$, where S_0 is the action of the free theory, which is quadratic on the fields and hence exactly soluble,

$$S_0 = \frac{1}{2}\sum_{l}^{dN^d} \Delta_l\vec{\varphi}\cdot\Delta_l\vec{\varphi} + \frac{\alpha}{2}\sum_{s}^{N^d}\vec{\varphi}\cdot\vec{\varphi} - \sum_{s}^{N^d}\vec{j}\cdot\vec{\varphi},$$

while S_V is the part involving the quartic term of the potential, which couples the field components in a non-linear way,

$$S_V = \frac{\lambda}{4}\sum_{s}^{N^d}(\vec{\varphi}\cdot\vec{\varphi})^2.$$

The classical solution of the model on a finite lattice is the configuration of the field $\vec{\varphi}$ which minimizes the function S_N, which has a lower bound if $\lambda > 0$ or if $\lambda = 0$ with $\alpha \geq 0$. In order to take the continuum limit, it is necessary that we establish a *scale* in the system, introducing a dimensional parameter, in such a way that it will be possible to define the concept of distance between points on the lattice. Classically, we do this by introducing an *external* scale in the system.

We assume that, in some system of units external to the system, our cubic lattice has sides of length L. We define then the lattice spacing as $a = L/N$, the squared mass as $m^2 = \alpha a^{-2}$, the dimensional coupling constant as $\Lambda = \lambda a^{d-4}$, the dimensional field as $\vec{\phi} = \vec{\varphi}a^{(2-d)/2}$ and the dimensional external source as $\vec{J} = \vec{j}a^{-(d+2)/2}$. Besides, we may decompose the sum over links, conveniently, as $\sum_l^{dN^d} = \sum_s^{N^d}\sum_\mu^d$, where $\sum_\mu^d$ is a sum over the d positive directions from a given site. With all this, we may write the action as

$$S_N = \sum_{s}^{N^d} a^d \left[\frac{1}{2}\sum_{\mu}^{d}\frac{\Delta_\mu\vec{\phi}}{a}\cdot\frac{\Delta_\mu\vec{\phi}}{a} + \frac{m^2}{2}\vec{\phi}\cdot\vec{\phi} + \frac{\Lambda}{4}(\vec{\phi}\cdot\vec{\phi})^2 - \vec{J}\cdot\vec{\phi}\right],$$

where Δ_μ is a difference between neighbors in the direction μ. Taking now the limit $N \to \infty$ with fixed L and $a \to 0$, we have that the sum $\sum_s^{N^d} a^d$ approximates the integral $\int d^d x$, the ratio Δ_μ/a approximates the partial derivative ∂_μ, and we have therefore that $S_N \to S$ where

$$S = \int d^d x \left[\frac{1}{2} \sum_{\mu}^{d} \partial_\mu \vec{\phi} \cdot \partial_\mu \vec{\phi} + \frac{m^2}{2} \vec{\phi} \cdot \vec{\phi} + \frac{\Lambda}{4} (\vec{\phi} \cdot \vec{\phi})^2 - \vec{J} \cdot \vec{\phi} \right]. \tag{2.2}$$

Hence we recover the classical field theory in its usual form. Note that the dimensional parameters are relative to the external scale which was introduced to define L. Note also that, in order that m and $\vec{J}$ be finite in the limit, it is necessary, respectively, that $\alpha \to 0$ and $\vec{j} \to \vec{0}$. Naturally, for point sources we will have that $\vec{J}$ diverges at a certain point as a delta function. Besides, in order that Λ be finite and non-zero in the limit, it is necessary that $\lambda \to 0$ (for $d < 4$), $\lambda \approx 1$ (for $d = 4$) or $\lambda \to \infty$ (for $d > 4$). Finally, in order that ϕ_i be finite and non-zero in the limit, we must have $\varphi_i \to \infty$ (for $d < 2$), $\varphi_i \approx 1$ (for $d = 2$) or $\varphi_i \to 0$ (for $d > 2$).

Note that the introduction of an external scale could be, in principle, avoided, since the theory contains the internal dimensional parameter m which can, in principle, be used as a unit to measure the others, as for example the size L of the box. In fact, if we wish to see our model as a laboratory for the universe and not as a model for only a localized part of it, then the introduction of an external scale does not make sense and we are forced to use this internal scale. However, in the classical theory it is not clear what is the procedure associated to m which could be used to define distances. On the other hand, in the quantum theory there is such a procedure, as we shall see. This is precisely the point of view which we want to explore in this work, in the context of the quantum theory.

2.2 Definition of the Quantum Theory

We may use the lattice to define the quantum theory in a way which is similar to the process described above. The fundamental difference between this procedure and the traditional approach is that, instead of first taking the continuum limit and then consider the quantization of the classical continuum theory which results, we invert the order of these operations. We first define a version of the quantum theory on each finite lattice and afterwards we consider the limit of the sequence of these finite quantum theories as we increase the lattice indefinitely, keeping satisfied certain conditions on some of the observables of the model. This limit produces the Euclidean quantum field theory and, as a final step, the Lorentzian quantum field theory is defined by means of the analytic extension of the observables, by taking imaginary Euclidean times.

In each finite lattice we define the quantum theory as a statistical model with a finite number of degrees of freedom. The physically relevant quantities of the theory are the average values, on a certain ensemble, of certain functions $\mathcal{O}[\varphi]$ of the fields. The ensemble in question is defined by the Euclidean action. The observables are defined as

$$\langle \mathcal{O} \rangle = \frac{\int [d\varphi] \mathcal{O}[\varphi] e^{-S_N[\varphi]}}{\int [d\varphi] e^{-S_N[\varphi]}}, \tag{2.3}$$

where $[d\varphi] = \prod_s^{N^d} \prod_i^{\mathcal{N}} d\varphi_i(s)$ and the multiple integrals are over all the components of the field at all the sites, having therefore dimension $N^d\mathcal{N}$. The observables formed by simple products of the fields, which we call correlation functions and which, by analytic extension, produce the Green's functions of the system, are particularly important. We will be paying particular attention to the one- and two-point functions, which relate respectively to the expectation value of the field and the renormalized mass, which in turn measures the inverse of the correlation length of the system,

$$\begin{aligned} g_{(1),i}(s) &= \langle \varphi_i(s) \rangle, \\ g_{(2),i}(s,s') &= \langle \varphi_i(s)\varphi_i(s') \rangle. \end{aligned}$$

In order to take the continuum limit we consider some conditions involving these observables. For example, for the case $\vec{j} = \vec{0}$, we may take a limit in which we impose that the renormalized mass m_R and the expectation value of the field $\vec{v}_R = \langle \vec{\varphi} \rangle$ are given constants. The maximum number of conditions that we can impose is the number of free parameters we have in the model, which allow us to adjust the values of these observables in each finite lattice. In our case we have two parameters, α and λ, hence we may impose at most two conditions, like the ones above. However, it is possible that the structure of the model correlates the values of the observables in such a way that it may, in fact, not be possible to give to them any values that we may wish.

As an example of the continuum limit we may take the free theory, where $\lambda = 0$ and which has the single free parameter α. In this case it is necessary that we have $\alpha > 0$ for the theory to be well-defined. Assuming also, for simplicity, the absence of external sources, that is that $\vec{j} = \vec{0}$, we may take in this case a limit in which $\vec{v}_R = \vec{0}$ and $m_R \neq 0$. In this model it results from direct calculation that $m_R^2 = \alpha a^{-2}$, so that in this limit we will necessarily have $\alpha \to 0$. We may also take a limit in which $m_R = 0$ and $\vec{v}_R \neq \vec{0}$, but it is not possible to have both $\vec{v}_R$ and m_R non-zero.

The renormalized mass m_R is defined as the position of the pole of the two-point function. In general it will not be related to α in such a simple way as in the free theory. In most models the renormalized mass will be a non-trivial function of both α and λ. It is convenient to define a renormalized version of α as $\alpha_R = m_R^2 a^2$. We see then that, in any physically interesting limit, we must have $\alpha_R \to 0$, otherwise the renormalized mass will be infinite and there will be no propagation of particles in the Lorentzian version of the theory.

In the Euclidean version the parameter α_R is related to the dimensionless correlation length of the model, which is measured in terms of the number of sites and links crossed in order that the correlation between two values of the field fall by a certain factor and which can be obtained from the two-point correlation function. In this way it becomes clear that it can be used to define distances: in order to know the distance between two points on the lattice it suffices to count the number of correlation lengths that one can fit between them.

In a similar way the expectation value $\vec{v}_R$ of the field can be obtained from the one-point functions and the renormalized coupling constant λ_R from the two- and four-point functions. The solution of the theory consists of the determination, on each finite

lattice, of the functions $\vec{v}_R(\alpha,\lambda)$, $\alpha_R(\alpha,\lambda)$ and $\lambda_R(\alpha,\lambda)$ which relate the renormalized quantities to the parameters of the theory and the subsequent taking of the continuum limit with conditions on some of the observables.

2.3 Stochastic Monte-Carlo Simulations

Stochastic simulations are the main exploration and calculation technique in this research area. They enable us to obtain good numerical estimates for the observables defined in (2.3). Their foundations are well known and will not be repeated here. It suffices to say that they are a technique which allows us to evaluate, with a measurable precision, the ratios between high-dimensional multiple integrals which appear in the definition (2.3) for the observables. This is done by the generation of a sequence of field configurations in such a way that the statistical distribution of these configurations converges to the distribution defined by the exponential of the Euclidean action. In this way, the simulation techniques are identical to those used in the study of Statistical Mechanics, except for the fact that the simulations are realized more often in four than in three dimensions.

There are many different ways to generate an appropriate sequence of configurations. We denominate as *stochastic evolution* the process of successive generation of configurations. In order that the generated statistical distribution of fields converge to the correct limit, it is sufficient that the algorithms used to generate each configuration form the previous one satisfy a condition which is known by the name of *detailed balancing*. The algorithms used in our programs are of several types. The stochastic variations of the fields in the $\lambda\phi^4$ model are decomposed into radial and angular parts. For the stochastic evolution of the angular part we use the Wolff algorithm [1]. For this, it was necessary to adapt it to models with variable-length vectors in the presence of external sources. The Wolff algorithm is extremely efficient and improves considerably the quality of the numerical results.

For the evolution of the radial part we used the Metropolis algorithm [2]. In this sector of the code the part of the action involving the potential, being strictly local, is treated in a particular way, by means of a change of variables and an interpolation of the inverse of the integral of the exponential of the potential. This approach for the radial part is very efficient for dealing with the usual theory, without sources, but revealed having some limitations in the presence of very strong external sources, forcing us to limit the simulations to values of the external source below a certain maximum limit. A re-structuring of the code to eliminate these limitations is currently in our plans, but they did not actually compromise the utility of the current code for this work.

It is interesting to record here the relation between the boundary conditions and the critical behavior of the model. We use in the simulations performed in this work periodic boundary conditions. In this case the internal $SO(\mathcal{N})$ symmetry of the models is always broken on finite lattices and there are no phase transitions except in the continuum limit. However, it is possible to define representations of the models which

present phase transitions even on finite lattices. For this it is necessary to use on the finite lattices, instead of periodic boundary conditions, *fixed* boundary conditions. In this kind of representation, instead of connecting each boundary of the lattice to the opposite boundary through links, we simply fix the value of some of the quantities of the theory, in general the field itself, along the boundary.

This kind of boundary condition may be useful in the future for the development of the work we present here, due to the fact that it would allow us to examine in greater detail the geometry of small regions of space. However, these boundary conditions are still poorly developed and the current versions cause distortions in the critical exponents of the models. There are ideas to improve this kind of boundary condition, which are currently subject of research in our group [3]. The basic idea is that we should not fix the quantum fields at the boundary but instead the values of some observables. It will be necessary to first develop these ideas if fixed boundary conditions are to be of real use in this work.

Chapter 3

Some Relevant Facts

We describe in this chapter some of the most important properties of the theory according to its definition in the Euclidean lattice. From these fundamental properties we will induce the basic motivation for this work.

3.1 Critical Behavior

As we saw before, in the continuum limit of the free theory we necessarily have that $\alpha_R = \alpha \to 0$, while in the interacting theory we have $\alpha_R(\alpha, \lambda) \to 0$. On the other hand, the Euclidean system that we define in each finite lattice is a statistical system which, in the continuum limit, has a second-order phase transition the order parameter of which is the expectation value of the field, $v_R = |\vec{v}_R|$. The transition region, in this case a critical curve in the (α, λ) plane, is the region where $\alpha_R \to 0$, and therefore any physically interesting continuum limit should converge to this critical curve.

This is a general property of the definition of Quantum Field Theories on the Euclidean lattice. If we cannot find a representation on the finite lattices which leads to a statistical system with a second-order phase transition, we cannot define the theory, for in first-order phase transitions, in which $\alpha_R \not\to 0$ in the critical region, it is not possible to take well-defined continuum limits, with finite renormalized masses.

The critical diagram of the $\lambda\phi^4$ model can be found in figure 3.1. This is a diagram in the space of the parameters of the model, in our case the (α, λ) plane. The continuum limits can be represented by paths in this diagram, which we call *flows*. All limits of physical interest converge to the critical curve. The ensemble of the theory is Gaussian in the half-axis $\alpha \geq 0$, $\lambda = 0$ and the free theory limits flow along this axis converging to the Gaussian point $\alpha = 0$, $\lambda = 0$, where the critical curve begins. The theory does not exist in the half-axis $\alpha < 0$, $\lambda = 0$ and in the half-plane $\lambda < 0$.

The critical curve divides the diagram in two regions, which constitute the two phases of the model. The symmetric phase is characterized by having $\vec{v}_R \to \vec{0}$ in the $N \to \infty$ limit, while in the broken-symmetric phase we have, for one of the components of the field, $v_{R,i} \neq 0$ even in the $N \to \infty$ limit. By convention we choose the component

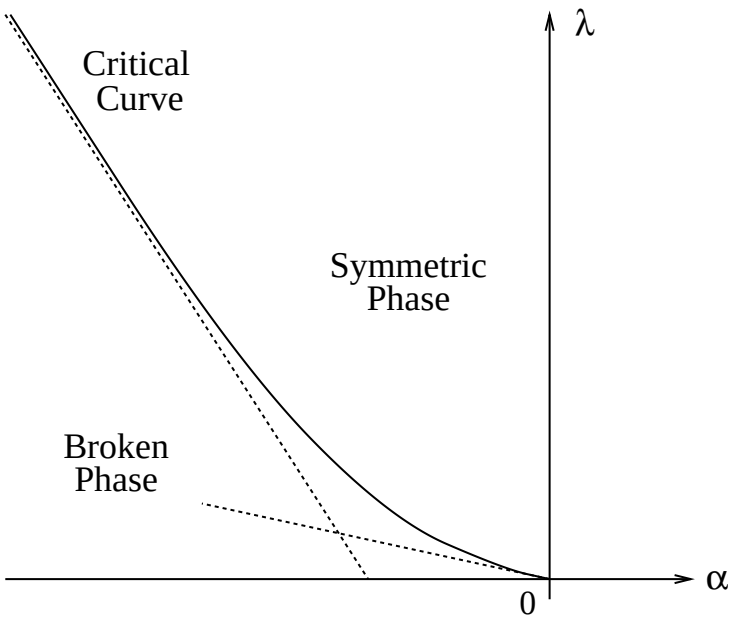

Figure 3.1: The critical curve of the $\lambda\phi^4$ model.

in the direction of which the symmetry is broken, which we name the *longitudinal* component, as the $\mathcal{N}$-th component of the field. For the other components, which we name *transversal* components, we always have $v_{R,i} = 0$, even on finite lattices. With periodic boundary conditions we will always have $v_{R,\mathcal{N}} \neq 0$ for the longitudinal component on finite lattices.

In the neighborhood of the Gaussian point the critical curve differs very little from a straight line. For the model with $SO(2)$ symmetry which we used in the simulations described later, it is at approximately 60^o from the $\alpha < 0$ half-axis in $d = 4$ and at approximately 45^o in $d = 3$. In $d = 4$ the larger lattice which we used, with $N = 8$, already has a behavior reasonably close to the critical behavior of the continuum limit. In $d = 3$ the $N = 8$ lattice is relatively more distant from the limit, so that we will examine the critical situation performing the simulation at 50^o. This is due to the fact that the proximity to the continuum limit, in terms of the critical behavior, is approximately proportional to the total number N^d of sites of the lattice.

3.2 Discontinuity of the Configurations

One property of the continuum limit of the $\lambda\phi^4$ model which interests us in particular is the fact that the typical configurations of the fields of the model, which contribute in a dominant way to the expectation values, are discontinuous functions at all points. One can show, analytically in the case of the free theory and numerically for the interacting models, that the quantity $\langle(\Delta_l\varphi_i)^2\rangle$ on any link of the lattice has a finite and non-zero

limit [4].

Since the difference Δ_l is taken between neighbors this means that, on average, values of the fields $\vec{\varphi}$ at infinitesimally close points differ by a finite quantity in the limit and hence that the fields are typically discontinuous at all points. For $d > 2$ this implies that the discontinuities of the dimensional field $\vec{\phi}$ become infinite in the continuum limit. The same conclusions can be derived analytically in the case of open electrodynamics without sources [4] and observed numerically in other cases like, for example, the Non-Linear Sigma Models.

This basic fact of the structure of the theory immediately puts in profound doubt the usual notion we have about what it means to quantize the gravitational field. The usual way to think about the process of quantization of General Relativity involves the conception of the field configurations in the form of a fluctuating geometry for space-time. It is extremely artificial to think of the quantized gravitational field as a fluctuating geometry if the configurations are so profoundly discontinuous, completely preventing the introduction of the concept of configurations of the theory as geometrical objects.

This property of the dominant configurations of the quantum fields has important consequences for the analysis of the perturbative expansion of the model on the Euclidean lattice. It constitutes the basic mechanism responsible for the divergences which appear in the perturbative expansion in the continuum limit. Besides, it immediately introduces doubts about the role that the topology of the field configurations may play in the dynamics of the model.

3.3 Triviality of the Model

A remarkable property of the $\lambda\phi^4$ models in four or more dimensions is what is usually called the *triviality* of these models. This triviality is a property of the structure of the models and means that, in the continuum limit, the correlation functions of the models are identical to the corresponding correlation functions of the free theory.

The most important aspect of this fact is that the four-point functions are factorizable in products of two-point functions. This, in the interpretation of the Lorentzian theory, means that the particles of the model behave as free particles and do not interact with one another. This appears in the observables as the fact that the dimensional coupling constant Λ_R vanishes. In $d > 4$ this simply means that λ_R is finite, while in $d = 4$ it means that $\lambda_R \to 0$ in the limit. In $d = 3$ it is known that the theory is not trivial, having a finite and non-zero limit for Λ_R, which, once more, means that $\lambda_R \to 0$ in the limit.

All this implies that we should have $\lambda_R = 0$ over the critical curve in $d = 3$ and $d = 4$. Simulations which we realized under certain specific conditions seem to indicate that, in fact, $\lambda_R = 0$ in all the parameter space of these models, even on finite lattices. However, our statistics is still very poor and we cannot state this with certainty. For this it will be necessary to improve the numerical techniques and perform much more

extensive numerical work.

However, in chapter 4 we will show some facts which seem to indicate the same conclusion. In the analysis of the local observables for the renormalized mass, presented in that chapter, we will see that certain relations of the free theory seem to be satisfied by the interacting model even on finite lattices. We do not know yet whether it is possible to use this approach to perform a deeper analysis of the question of triviality, something which we intend to try to do in the future.

3.4 Action of External Sources

The introduction of external sources in the model will play a fundamental role in this work. In the usual treatment this introduction is done primarily within the framework of the effective action formalism and is limited to infinitesimal sources. In that formalism the external sources are used basically to allow the generation of the correlation functions by means of functional differentiation and, at the end of the process, the sources are put to zero. In this work, in contrast to this, we will be introducing strong external sources and examining in more detail their action on the system.

The physical interpretation of the external sources is that they represent the introduction of classical objects in the theory, which generically can be sources of particles, such as accelerators, or absorbers of particles, such as detectors. For this reason, they are represented in the theory as given fixed functions and not as fluctuating random variables. The idea is that in a more complete representation the sources are related to some other physical system, which we are not representing directly in our model. For the purpose of studying their effect in our model we exchange the fluctuating variables of the quantum objects of this other system by their expectation values, which we treat as given fixed functions.

The most immediate effect of the introduction of an external source in our model is a change in the expectation value of the field $\vec{v}_R$, which becomes different from zero in either phase. Besides, if the external source is not constant over the lattice, $\vec{v}_R$ becomes dependent on position. We will be examining in particular the case of a point source oriented in the direction of $\varphi_{\mathcal{N}}$. In the case of the free theory we can present a general solution for $\vec{v}_R$, given a generic source:

$$\vec{v}_R(s) = \sum_{s'}^{N^d} \vec{j}(s') K(s,s'),$$

where K is the propagator in coordinate space,

$$K(s,s') = \frac{1}{N^d} \sum_{k}^{N^d} \frac{\cos\left[\frac{2\pi}{N} k_\mu (n_\mu - n'_\mu)\right]}{\rho^2(k) + \alpha}$$

and where n_μ are the integer coordinates of a site s of the lattice, in units of numbers of sites. The dimensional coordinates x_μ which describe the positions of the sites are

given by $x_\mu = a\, n_\mu$, where $n_\mu = 1, \ldots, N$ for $\mu = 1, \ldots, d$. The sum $\sum_k^{N^d}$ runs over the N^d Fourier modes of the lattice and k_μ are integer variable that index these modes. In general we adopt for them the interval of values $k_\mu = k_m, \ldots, 0, \ldots, k_M$, where $k_m = 1 - N/2$ and $k_M = N/2$ for lattices with even N, while $k_m = -(N-1)/2$ and $k_M = (N-1)/2$ for lattices with odd N. The quantities

$$\rho^2(k) = 4\left[\sin^2\left(\frac{\pi k_1}{N}\right) + \ldots + \sin^2\left(\frac{\pi k_d}{N}\right)\right]$$

are the eigenvalues of the Laplacian on the lattice. In the continuum limit the square of the momentum relates to these eigenvalues by $p_\mu p^\mu = p^2 = \lim_{a\to 0}[\rho^2(k)/a^2]$. The sums may be written explicitly as

$$\begin{aligned}\sum_s^{N^d} &= \sum_{n_1=1}^{N} \cdots \sum_{n_d=1}^{N}, \\ \sum_k^{N^d} &= \sum_{k_1=k_m}^{k_M} \cdots \sum_{k_d=k_m}^{k_M}.\end{aligned}$$

Subtracting from the field its expectation value we have the shifted field variable $\vec{\varphi}' = \vec{\varphi} - \vec{v}_R$, which has zero expectation value and all correlation functions identical to the ones for the free theory without external sources. This is, clearly, a consequence of the linearity of the free theory. For a point source at the origin we have, in particular, that $\vec{j}(s') = \vec{j}_0 \delta_{0,s'}$ and then

$$\vec{v}_R(s) = \vec{j}_0 K(s,0) = \frac{\vec{j}_0}{N^d} \sum_k^{N^d} \frac{\cos\left(\frac{2\pi}{N} k_\mu n_\mu\right)}{\rho^2(k) + \alpha}.$$

Note that, at the position of this singular source, $\vec{v}_R(s=0)$ has a finite and non-zero continuum limit for $d > 2$, because the quantity $K(0,0) = f_0(N,d,\alpha)$, where

$$f_0(N,d,\alpha) = \frac{1}{N^d} \sum_k^{N^d} \frac{1}{\rho^2(k) + \alpha}, \tag{3.1}$$

has a finite and non-zero limit for $d > 2$ [4]. At this point the expectation value of the dimensional field $\vec{V}_R = \langle \vec{\phi} \rangle$ diverges for $d > 2$. On the other hand, since we will have a finite $\vec{V}_R$ at all other points, it follows that at all points except the location of the source we shall have $\vec{v}_R \to 0$ in the limit, for $d > 2$.

3.5 Finite Invariances

There are symmetries of several types in the model. All these symmetries are familiar and have complete and explicit realizations in the continuum limit, if we also make the

dimensions of the box containing the model tend to infinity. Both the representation of the model inside a finite box and its realization on a discrete lattice affect some of these symmetries. However, the representation on the lattice keeps remnants of the complete symmetries, which allow us to identify that the symmetries will be restored in the infinite-volume continuum limit.

First we have the internal invariance with which we defined the model, in our case an invariance by transformations of $SO(\mathcal{N})$ in the space of the fields. This invariance is the only one that stays intact on the classical model defined on a finite lattice. It is not affected by either the finiteness of the box or the discrete character of the lattice and, for $\mathcal{N} > 1$, it is a continuous symmetry. This symmetry is broken, however, by the dynamics of the quantum theory and may or may not be recovered in the continuum limit. It is this symmetry that defines the phase structure in the critical diagram of the model.

The spatial symmetries of rotation are broken, of course, by the introduction of a discrete lattice in a finite cubic box. However, the rotation symmetries remain encoded in the system in an indirect way. For example, we have the fact that the propagator of the theory in momentum space is a function only of $\rho^2(k)$ and not of the several components and values of k_μ independently. In fact, the propagator has, as a function of $\rho^2(k)$, exactly the same form that the propagator of the continuum limit has as a function of p^2. All quantities which in the continuum are functions of p^2 become, on finite lattices, functions of $\rho^2(k)$. In this way, the quantities $\rho^2(k)$ work as a kind of filter which allows us to compensate the distortions introduced by the finiteness of the box and the discrete character of the lattice. Besides this, there remains in explicit form a discrete remnant of the rotation symmetries, constituted by the rotations by $\pi/2$.

The spatial symmetries of translation are also modified by the introduction of the finite box and of the discretization. In the case of the introduction of the finite box the adoption of periodic boundary conditions still allows us to keep these symmetries in the form of periodic translation symmetries along the torus defined by these boundary conditions. The discretization on the lattice breaks the continuous character of these symmetries, changing them into discrete symmetries, in which we translate along the lattice by an integer number of sites in each direction. In this way, so long as there are no position-dependent external sources in the action of the model, the translation symmetries remain valid in a discrete form.

The spatial symmetries will play an important role in this work. In the absence of position-dependent external sources all physical quantities of the model, in particular the correlation length, will have discrete translation and rotation invariances. With this, it is evident that the geometry generated on the lattice by the quantization of the model will be flat. It is the breaking of these symmetries by the introduction of localized external sources which will be responsible for the generation of curvature.

Chapter 4

Local Observables for the Mass

We show here, by numerical means, that certain non-trivial relations among observables of the $\lambda\phi^4$ model are satisfied very precisely, possibly exactly so. These relations can be derived by means of perturbative methods and are identical in form to the corresponding relations for the free theory, differing from them only by the exchange of the mass by the renormalized mass.

4.1 Perturbation Theory on the Lattice

Let us consider the $\lambda\phi^4$ model defined by the action given in equation (2.2) and quantized on the lattice according to the scheme described in Chapter 2, using the lattice action given in equation (2.1). It is possible to develop for this model a perturbative method on finite lattices, in the way described in reference [5].

This approach is very useful and, although it has a perturbative character, the resulting approximations are better described as Gaussian approximations for the model. Properly speaking it is not an expansion but a good approximation for some of the observables of the theory. The approach is useful to deal with the one- and two-point functions, but not for the four-point function. In the symmetric phase the approximation for the renormalized mass is given, in terms of the parameters α and λ of the model, by

$$\alpha_R = \alpha + (\mathcal{N}+2)\lambda f'_{0,i}(N,d,\alpha_R),$$

for each i-th field component, with

$$f'_{0,i}(N,d,\alpha_R) = f_0(N,d,\alpha_R) + \frac{\delta_{i\mathcal{N}}-1}{N^d\alpha_R}, \tag{4.1}$$

where $f'_{0,i\neq\mathcal{N}}$ is the function f_0 defined in (3.1) without the zero-mode term and $f'_{0,\mathcal{N}} = f_0$. In the broken-symmetric phase we have

$$\alpha_R = -2\delta_{i\mathcal{N}}\left[\alpha + (\mathcal{N}+2)\lambda f_0(N,d,\alpha_R)\right].$$

Note that $\alpha_R = 0$ for the transversal components, which are Goldstone bosons.

These are not, in fact, explicit solutions for α_R but equations determining α_R in terms or α and λ, because their right-hand sides depend themselves on α_R. A comparison of these predictions for α_R with numerical estimates, as presented in [5], shows that they are very good approximations, even surprisingly so but, still, they are not exact and the differences can be clearly seen for large values of λ.

In this same perturbative scheme it is possible to derive results for other observables of the theory, which do not involve the renormalized coupling constant λ_R, for example for the expectation value of the field, $\vec{v}_R = (0, \ldots, 0, v_R)$, for which one gets, in the case $\vec{j} = \vec{0}$, $v_R = 0$ in the symmetric phase and, in the broken-symmetric phase,

$$v_R = \sqrt{\alpha_R/(2\lambda)}.$$

For the width of the fluctuations of the field at sites we have

$$\begin{aligned} \langle(\varphi_i - v_{R,i})^2\rangle &= \langle\varphi_i^2\rangle - v_{R,i}^2 \\ &= f'_{0,i}(N, d, \alpha_R). \end{aligned} \tag{4.2}$$

Finally, for the finite differences on the lattice we have

$$\begin{aligned} \langle(\Delta_l\varphi_i)^2\rangle &= \langle[\varphi_i(x + a_\mu) - \varphi_i(x)]^2\rangle \\ &= \frac{1}{N^d}\sum_k^{N^d} \frac{4\sin^2\left(\pi\frac{k_\mu}{N}\right)}{\rho^2(k) + \alpha_R} \\ &= f_1(N, d, \alpha_R), \\ \langle(\Delta_d\varphi_i)^2\rangle &= \langle[\varphi_i(x + a_{\mu_1} + a_{\mu_2}) - \varphi_i(x)]^2\rangle \\ &= \frac{1}{N^d}\sum_k^{N^d} \frac{4\sin^2\left(\pi\frac{k_{\mu_1}+k_{\mu_2}}{N}\right)}{\rho^2(k) + \alpha_R} \\ &= f_2(N, d, \alpha_R), \end{aligned} \tag{4.3}$$

where Δ_l is the difference between the fields at the two ends of a link, Δ_d is the difference between the fields at the two ends of a plaquette diagonal and a_μ is a displacement by the lattice spacing a in the direction μ. A plaquette is a set of four sites forming a square in one of the lattice planes, that is, it is the basic geometrical element of dimension two, which plays an important role in Gauge Theories.

4.2 Local Observables for α_R

Although the observables of the model are, in general, functions of N, d, α and λ independently, one can see that all these perturbative results can, with the exception of the one for v_R, be written in terms of $\alpha_R(\alpha, \lambda)$, instead of in terms of α e λ separately and independently. Note however that the relation (4.2) involves v_R in its left-hand

side and that, due to this, $\langle\varphi^2\rangle$ by itself cannot be expressed only in terms of α_R, unless $v_R \equiv 0$. On the other hand, the relations (4.3) do not depend on v_R and consequently may be written exclusively in terms of α_R. Besides, the functions $f'_{0,i}$, f_1 and f_2 have exactly the same form as the corresponding exact results for the free theory, differing from them only by the exchange of the parameter α of the free theory by α_R.

It is also possible to calculate the propagator of the theory in momentum space, resulting

$$\widetilde{g}_{(2),i}(k) = \langle\widetilde{\varphi}_i^*(k)\widetilde{\varphi}_i(k)\rangle = \frac{1}{N^d}\frac{1}{\rho^2(k)+\alpha_R}$$

in either phase, so long as α_R is the appropriate expression in each phase and for each field component. In this expression $\widetilde{\varphi}_i(k)$ is the finite Fourier transform of the field on the lattice [6], given by

$$\widetilde{\varphi}_i(k) = \frac{1}{N^d}\sum_s^{N^d}\varphi_i(s)e^{\imath\frac{2\pi}{N}k_\mu n^\mu}.$$

Besides, from a fit to the numerical propagator of an expression like

$$\frac{1}{N^d}\frac{\mathcal{R}}{\rho^2(k)+\alpha_R},$$

similar to the previous one, one can estimate very well α_R, as is shown in [5]. The fits done use a limited but sufficient number of values of the momenta. In general they are very good and it is observed that the residue of the propagator comes out consistently as $\mathcal{R} = 1$ within numerical errors, which we believe to be one more indication of the triviality of the models. The use of a limited number of values of the momenta is due to historical issues of a technical character in the development of our computer codes and we have plans to change this strategy and starts calculating the observables for a complete set of values of the momenta. There is a possibility that the use of this limited set of values of the momenta has introduced some small systematic errors which we detected in the numerical results.

Note that, unlike the momentum-space propagator, the observables defined in (4.2) and (4.3) are *local* objects on the lattice, involving at most two neighboring sites. Note also that the relation of these local observables to the renormalized mass is clear and intuitive, since they are directly related to the fluctuations of the fields at sites and the correlations between fields across links and diagonals,

$$\langle(\Delta_l\varphi_i)^2\rangle = 2\langle\varphi_i^2\rangle - 2\langle\varphi_i(l_+)\varphi_i(l_-)\rangle,$$

where $\varphi_i(l_+)$ and $\varphi_i(l_-)$ are the fields at the two ends of the link or diagonal, while the renormalized mass α_R is directly related to the correlation length of the theory.

These considerations lead to the possibility of testing the perturbative relations given in (4.2) and (4.3), verifying how well they are satisfied if used to relate the numerical values of α_R with the numerical values of $\langle\varphi_i^2\rangle - v_{R,i}^2$, $\langle(\Delta_l\varphi_i)^2\rangle$ and $\langle(\Delta_d\varphi_i)^2\rangle$. Note that everything here happens on finite lattices of arbitrary size.

4.3 Tests of the Local Observables

We performed such a comparison, which showed that the relations (4.3) are satisfied, within errors compatible with our numerical precision, despite their perturbative origin, for all values of the parameters of the model for which we were able to perform the comparisons. In the case of the relation (4.2) the same is valid for the transversal field components, for which $v_{R,i} = 0$, but a small difference appears for the longitudinal component, in the direction of which the symmetry is broken and for which, therefore, $v_{R,\mathcal{N}} \neq 0$.

To better understand these results it is important to point out that our treatment of the zero-mode in the computer simulations is very different for the transversal and longitudinal components: the zero-mode of the transversal components is eliminated from the theory by means of the symmetry transformations of the model, that of the longitudinal component is not. It is through these transformations that we keep the direction of symmetry breaking fixed along the component $\varphi_{\mathcal{N}}$.

As one can see, unlike the formulas $f'_{0,i\neq\mathcal{N}}$, f_1 and f_2, the formula $f'_{0,\mathcal{N}}$ contains an infra-red divergence involving the zero-mode, that is, a term proportional to $1/\alpha_R$, which diverges if $\alpha_R \to 0$. Note that there is no divergence in this term in the continuum limit, since in this case we have $\alpha_R \to 0$ as N^{-2} when $N \to \infty$, so that $1/(N^d \alpha_R)$ goes in fact to zero for $d > 2$. In the same manner as this term, the difference observed for the longitudinal component in the relation (4.2) decreases with the size of the lattice and should disappear in the continuum limit.

It becomes clear that the observed difference is due to the effect of the zero-mode. For the transversal component, the zero-mode of which was eliminated, this term is absent from the sum and the formula seems to be satisfied with precision. For the longitudinal component the term of the zero mode is present and the formula is not exactly satisfied. The presence of the zero-mode in $f'_{0,\mathcal{N}}$ is related to its dependence on v_R which, as we saw, cannot be written exclusively in terms of α_R. Note that the observables $\langle(\Delta_l\varphi_i)^2\rangle$ and $\langle(\Delta_d\varphi_i)^2\rangle$, the formulas for which seem to be realized exactly, do not involve the zero mode at all.

In order to perform the tests we measured α_R by means of the fit to the numerical propagator in momentum space and measured independently the observables $\vec{v}_R$, $\langle\varphi_i^2\rangle$, $\langle(\Delta_l\varphi_i)^2\rangle$ and $\langle(\Delta_d\varphi_i)^2\rangle$, for each set of values of the parameters. From these observables corresponding values for α_R were obtained by numerical inversion of the formulas $f'_{0,i}$, f_1 and f_2 given in (4.1) and (4.3).

A sampling of the results can be found in figures 4.1 and 4.2, while a mode complete set can be found in Appendix A.1. The parameters r and θ that appear in these graphs relate to α and λ by

$$\begin{aligned} \alpha &= -r\cos(\theta), \\ \lambda &= r\sin(\theta). \end{aligned}$$

As can be seen in these figures, with the exception of a few occasionally large statistical fluctuations or one or other possible imperfection in the fit used to obtain α_R from the

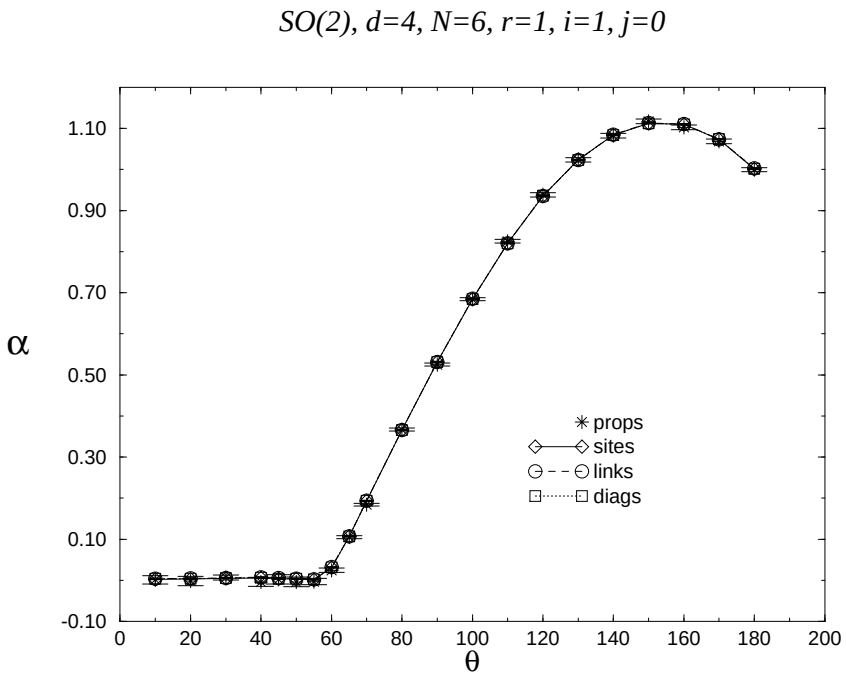

Figure 4.1: Test for the transversal component.

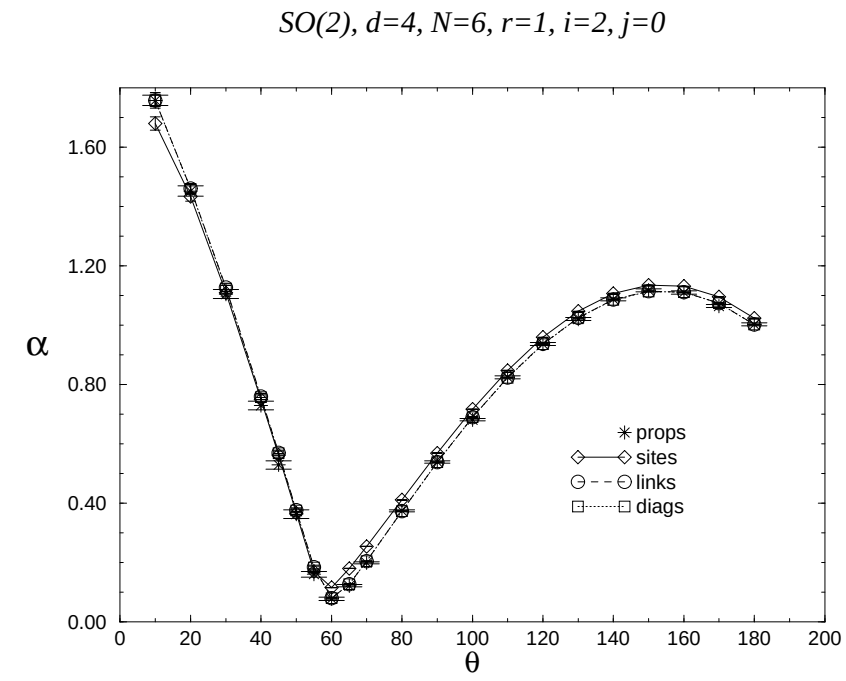

Figure 4.2: Test for the longitudinal component.

momentum-space propagator, the results coincide in an essentially exact way, even for large values of the coupling constant.

One can see that the local observables constitute a technically very good way to measure α_R in these models. The extreme regularity and precision of these results, as well as their remarkable consistency with one another, raised the conjecture that equations (4.2) for the case of the transversal components and (4.3) are in fact satisfied exactly on finite lattices. Furthermore, the following more general conjecture is strongly suggested: that there exists a pair of functions $h_1(\alpha, \lambda)$ and $h_2(\alpha, \lambda)$ such that, for every observable $\mathcal{O}$ of the theory, the expectation value

$$\langle \mathcal{O} \rangle = \frac{\int [d\varphi] \mathcal{O}[\varphi] e^{-S_E(\alpha,\lambda)}}{\int [d\varphi] e^{-S_E(\alpha,\lambda)}}$$

is equal to the corresponding expectation value in the free theory with mass parameter $\alpha_R = h_1(\alpha, \lambda)$ and field expectation value $v_R = h_2(\alpha, \lambda)$, that is,

$$\langle \mathcal{O} \rangle = \frac{\int [d\varphi] \mathcal{O}[\varphi] e^{-S_0(v_R,\alpha_R)}}{\int [d\varphi] e^{-S_0(v_R,\alpha_R)}}.$$

If this could be demonstrated it would immediately imply, of course, the triviality of the theory. Maybe this conjecture is valid on finite lattices only for some observables but, if the theory is in fact trivial, it must be true in the continuum limit for *all* observables. In any case it seems that the theory, which can have at most two free parameters, is such that h_1 e h_2 may be chosen as these parameters.

4.4 Extrapolation for the Use of the Observables

It is important to note that the observables of the type (4.3) involving Δ_l and Δ_d suffice to define the geometry on the lattice, because they allow us to measure the renormalized mass in a local way and, hence, the correlation lengths associated to links and diagonals. These elements are sufficient to define the lattice as a simplicial complex, that is, to define completely an intrinsic metrical geometry over it.

The observables which we used in this work relate only to the links between sites and to sites separated by a two-dimensional diagonal contained in one of the lattice planes. However, it is possible to define observables that measure α_R for two neighboring sites along any direction of a lattice of higher dimension:

$$\begin{aligned}
\langle [\varphi_i(x + a_{\mu_1} + \ldots + a_{\mu_3}) - \varphi_i(x)]^2 \rangle &= \frac{1}{N^d} \sum_k^{N^d} \frac{4 \sin^2\left(\pi \frac{k_{\mu_1} + \ldots + k_{\mu_3}}{N}\right)}{\rho^2(k) + \alpha_R} \\
&= f_3(N, d, \alpha_R), \\
\langle [\varphi_i(x + a_{\mu_1} + \ldots + a_{\mu_4}) - \varphi_i(x)]^2 \rangle &= \frac{1}{N^d} \sum_k^{N^d} \frac{4 \sin^2\left(\pi \frac{k_{\mu_1} + \ldots + k_{\mu_4}}{N}\right)}{\rho^2(k) + \alpha_R} \\
&= f_4(N, d, \alpha_R).
\end{aligned}$$

With this it is possible, in principle, to obtain the complete intrinsic geometry of a four-dimensional lattice. Here we limited ourselves to examine only the links and two-dimensional diagonals for technical reasons and due to the fact that this suffices for, at least, a first examination of the generated geometry, through its two-dimensional sections.

Note that, from the point of view of this work, the use of these local observables is only a technique which allows us to measure α_R in a local way in simulations with sizes limited by the current availability of computer resources. This is a technique that may apply only to the $\lambda\phi^4$ models, but it is possible to formulate, in principle, a scheme to do this in an arbitrary model. It is enough to imagine that we have a very large lattice, which can be divided into a large number of small boxes, each one still containing a sufficiently large number of sites.

Inside each of these small boxes we use Fourier transforms with momenta along each direction, with wavelengths sufficiently small to fit inside the boxes, to calculate the renormalized mass associated to each direction by means of a fit to the propagator. We assume, of course, that the boxes are much smaller than the typical distance in which the renormalized mass varies and that the number of available modes inside each box is very large, allowing a good fit to the propagator. For an approach like this to be successful, it is obvious that an extremely large lattice would be needed, which is currently out of our reach in practice.

In this work we will be, therefore, using the local observables to measure the metrical geometry of the lattice. However, we will be doing this under conditions differing from those in which it is possible to test them by comparison to the results obtained by means of Fourier transforms, for we will be introducing position-dependent external sources, which break the translation symmetries. It is necessary, therefore, to consider the errors that may be introduced by this extrapolation, even if the tests performed cover a considerable amplitude of situations with no important change in the results having being observed. We can argue in several different ways that this approach is at least qualitatively correct, providing at least a good approximation of the real situation.

A first justification is based in the very triviality of the theory: if the theory is in fact trivial, as all leads us to believe, then the two-point correlations are the same as those of the free theory and hence the local observables should produce good results, at least in the continuum limit, even in the presence of arbitrary external sources. Note that we are only interested in using the observables to measure α_R and not v_R or λ_R.

To formulate our second justification, we first observe that, for the calculation of the correlation length, the two-point correlation functions must be calculated for the shifted field $\vec{\varphi}'$ which has an expectation value equal to zero. As was discussed before, the precise functioning of the observables (4.3) seems to be related to the fact that, being constant, $\vec{v}_R$ does not appear in these observables, which involve derivatives, so that they can be written indifferently in terms of either $\vec{\varphi}$ or $\vec{\varphi}'$. With the introduction of position-dependent external sources $\vec{v}_R$ will be no longer constant and therefore will no longer cancel from these observables. We will have now for, as an example, the first

observable in (4.3)

$$\begin{aligned}
&\langle[\varphi_i'(l_+) - \varphi_i'(l_-)]^2\rangle \\
&\quad = \langle\{[\varphi_i(l_+) - v_{R,i}(l_+)] - [\varphi_i(l_-) - v_{R,i}(l_-)]\}^2\rangle \\
&\quad = \langle(\Delta_l\varphi_i - \Delta_l v_{R,i})^2\rangle.
\end{aligned}$$

We observe now that, while the quantum fields are discontinuous in the limit, the observables of the theory, as for example $\vec{v}_R$, are, in contrast to this, continuous. Therefore, while $\Delta_l\varphi_i \approx 1$, $\Delta_l v_{R,i} \to 0$ in the limit. With this it becomes clear that these observables are dominated by the discontinuous behavior of the fields and that the differences between the values of v_R at nearby sites can introduce, at most, small changes in the value of the observables, changes which should vanish in the continuum limit.

Finally, we note that the functions $f'_{0,i\neq\mathcal{N}}$, f_1 and f_2, considered as functions of α_R for given N and d, have as images finite intervals $(0, f_M)$, with f_M of the order of one, while α_R varies in the domain $(0, \infty)$. In this way, depending on the value obtained numerically for the observables, it may or may not be possible to invert these functions to obtain the corresponding values of α_R. In fact, for some test runs with very poor statistics we verified that the inversion sporadically fails due to the large numerical errors. However, it never fails for f_1 and f_2 in production runs with large statistics. This fact indicates that the observables are in fact closely related to the formulas f_1 and f_2 and that the values of α_R obtained from them should not contain excessively large errors.

Chapter 5

Geometry Generated on the Lattice

In order to examine the character of the geometry generated on the lattice we performed simulations of the model in four dimensions with a constant source located on a line of sites along the direction $\mu = 1$, which we chose arbitrarily as the temporal direction. In order to obtain the renormalized masses at each link and diagonal we measured over them the observables defined in (4.3), but using the shifted field variables $\vec{\varphi}'$ instead of $\vec{\varphi}$. We chose to examine the two-dimensional spatial sections containing the origin. In this way we can examine the resulting geometry through the construction of *embeddings* of these two-dimensional sections.

5.1 Numerical Results: Geometry of the Section

In figures 5.1 to 5.3 we can observe the result of this process for some interesting cases. A more complete set of graphs can be found in Appendix A.2. For the construction of the geometries shown in these graphs we used the mass of the longitudinal component and the largest value of the external source that we were able to run, $j_0 = 10$. In graph 5.1, which corresponds more clearly to the symmetric phase, we can see that the resulting geometry has a very localized curvature, with a short range around the location of the source. In graph 5.2, which corresponds to our being more deeply into the broken-symmetric phase, we see a clear tendency to conicity, that is, a geometry with little local curvature but with a conical singularity at the position of the source. In these cases a fold in the embedding frequently appears, along the border of the lattice. In the graph 5.3, which corresponds to a position close to the critical transition in the phase diagram, we have a clearly curved geometry, which seems to be developing a horizon in the immediacy of the source. It is very interesting that this behavior is related to the critical transition region, to where the continuum limits must tend.

In figures 5.4 to 5.6 we can see similar graphs, for the construction of which the mass of the transversal component was used. For this component we have, in the symmetric phase, an essentially flat geometry, with folds in the embedding probably associated to numerical errors at the origin, where the singular source is located. In the broken-

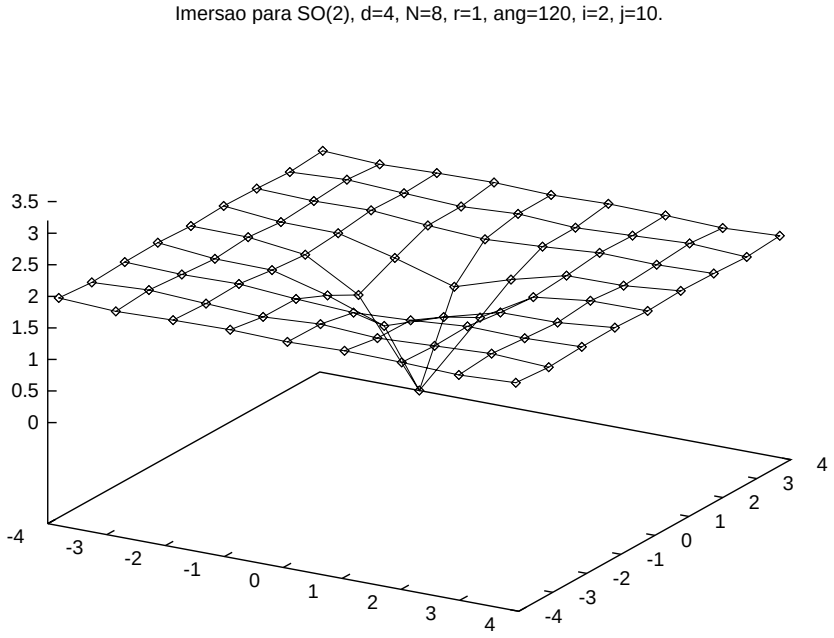

Figure 5.1: Embedding in the symmetric phase, in four dimensions, with $j_0 = 10$, longitudinal component.

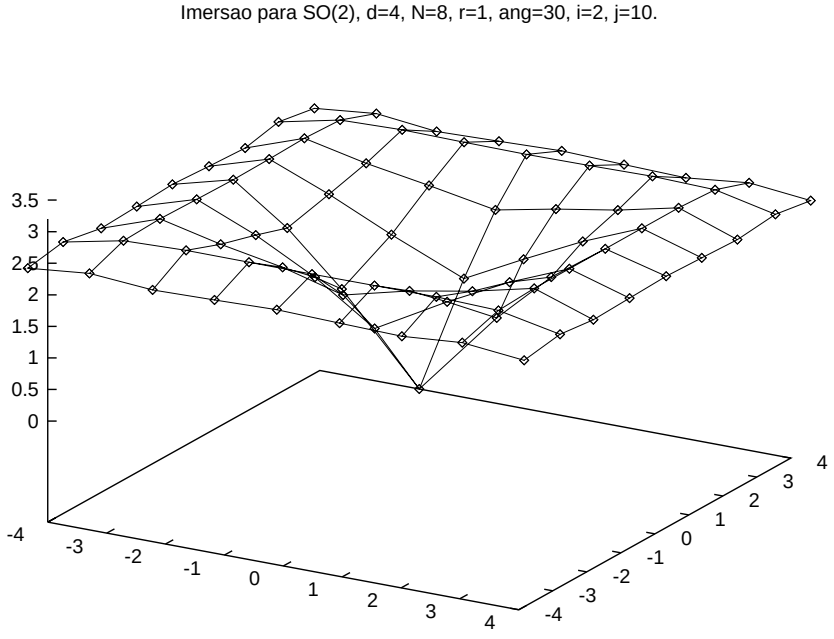

Figure 5.2: Embedding in the broken-symmetric phase, in four dimensions, with $j_0 = 10$, longitudinal component.

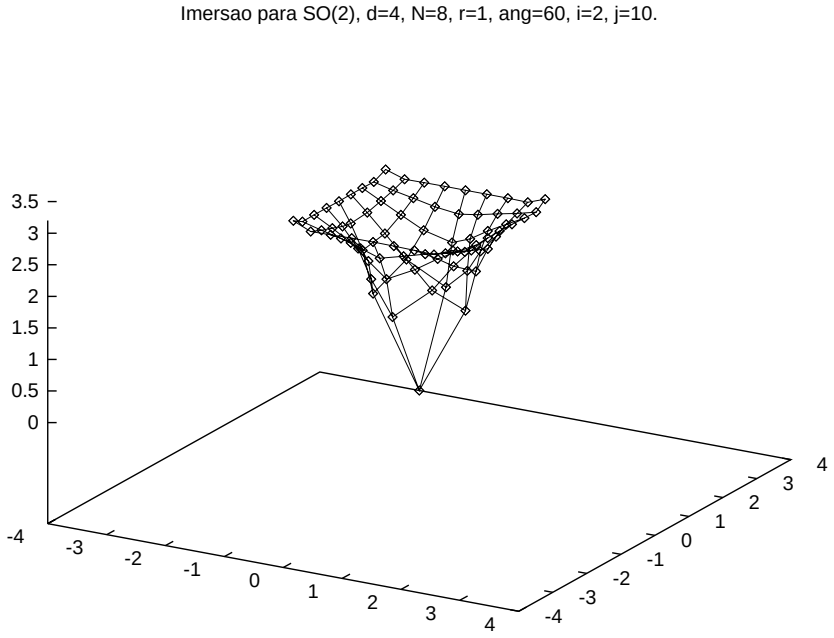

Figure 5.3: Embedding in the critical region, in four dimensions, with $j_0 = 10$, longitudinal component.

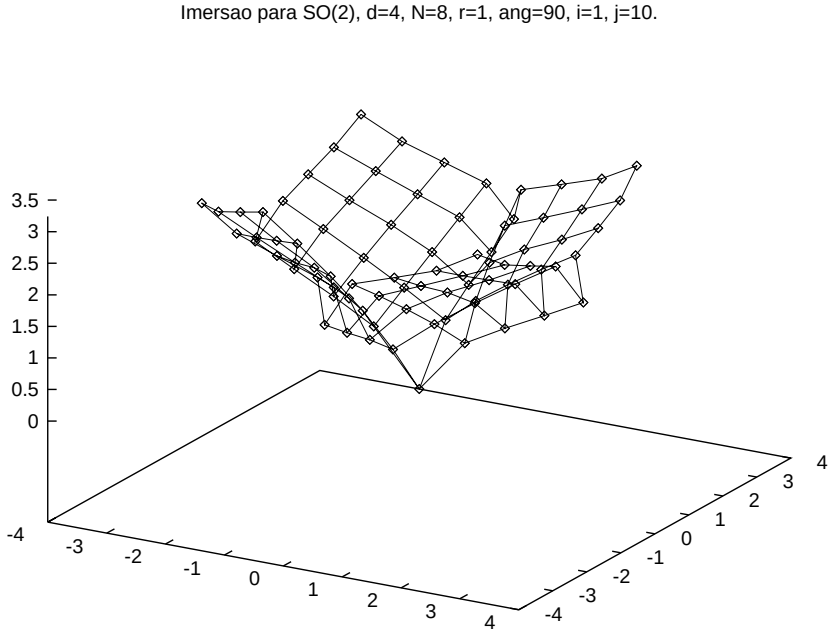

Figure 5.4: Embedding in the symmetric phase, in four dimensions, with $j_0 = 10$, transversal component.

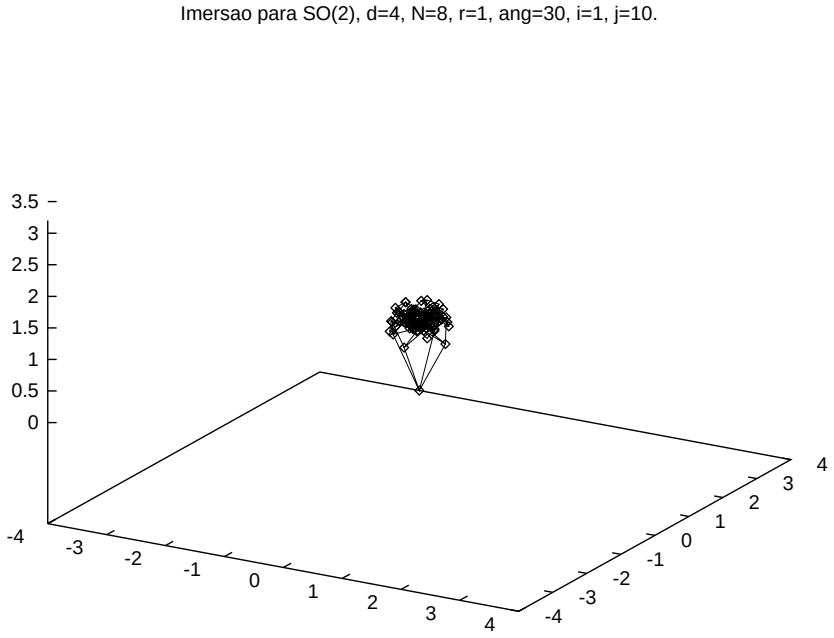

Figure 5.5: Embedding in the broken-symmetric phase, in four dimensions, with $j_0 = 10$, transversal component.

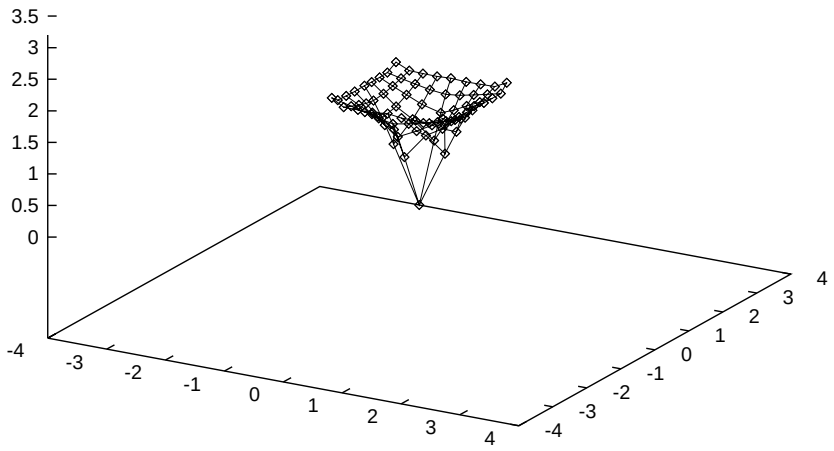

Figure 5.6: Embedding in the critical region, in four dimensions, with $j_0 = 10$, transversal component.

symmetric phase the geometry collapses, since the mass of this component goes to zero there and it cannot in fact define a geometry. It is interesting that in the critical region, unlike what happens in the other regions, the mass of the transversal component defines a geometry very similar with that defined by the mass of the longitudinal component. The main difference seems to be a global change of scale, probably due to the imperfect reconstitution of the symmetry in the transition region, which is characteristic of relatively small lattices with periodic boundary conditions.

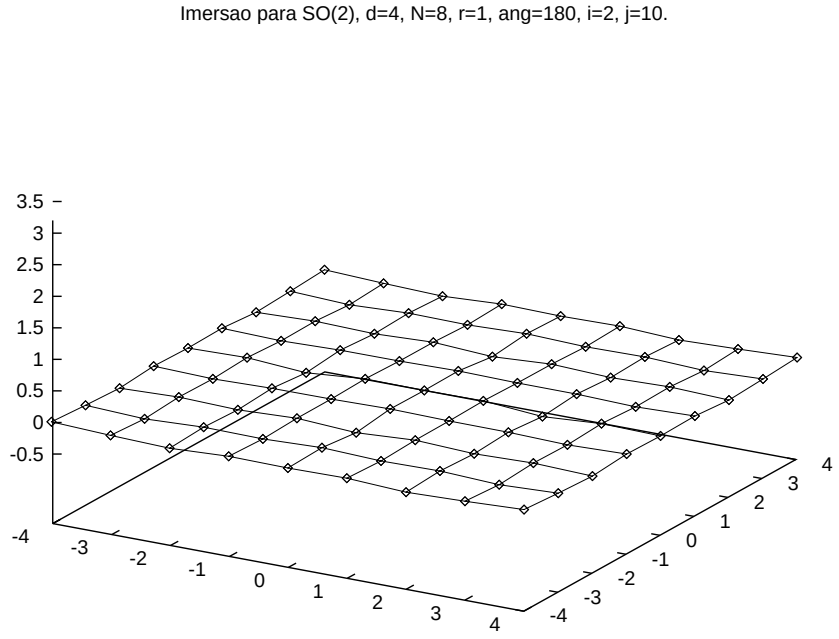

Figure 5.7: Embedding for the free theory, in four dimensions, with $j_0 = 10$, longitudinal component.

In these simulations $\theta = 180^o$ corresponds to the free theory, in which the geometry should be flat, with or without external source. This point was used as a reference for tests of the programs and an example of the results may be seen in figure 5.7. We also verified that the generated geometry is flat for the interacting theory, so long as j_0 is constant throughout the lattice.

We also performed some simulations with a somewhat smaller value of the external source, $j_0 = 5$, with the objective of determining the character of its influence on the formation and position of the horizon. We can see some results in figures 5.8 to 5.10. As we see, the formation of a horizon is less visible in this case, which probably indicates that it would be forming closer to the center, below the resolution of the lattice. Presumably, if we are to be able to see the formation of a horizon in this case a larger lattice will be needed.

Finally, we performed some simulations in three dimensions, with the same type and

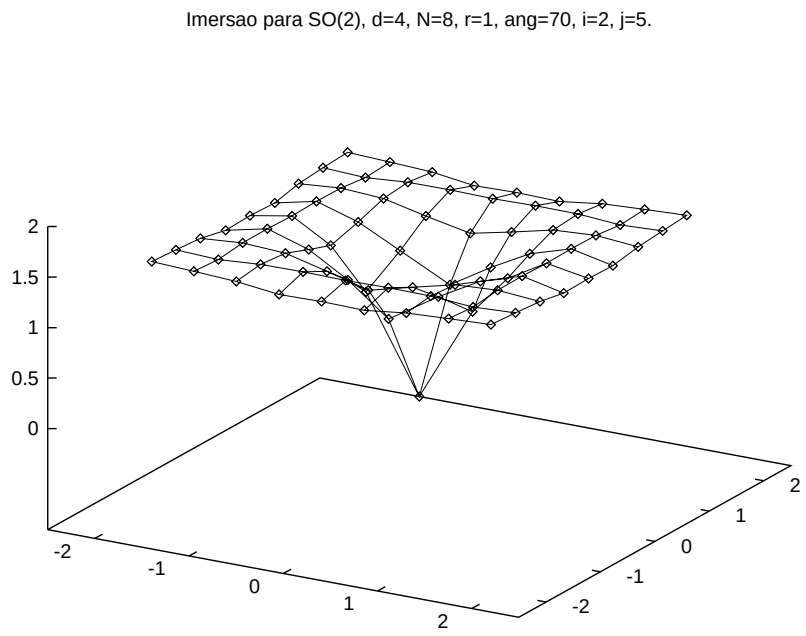

Figure 5.8: Embedding in symmetric the phase, in four dimensions, with $j_0 = 5$, longitudinal component.

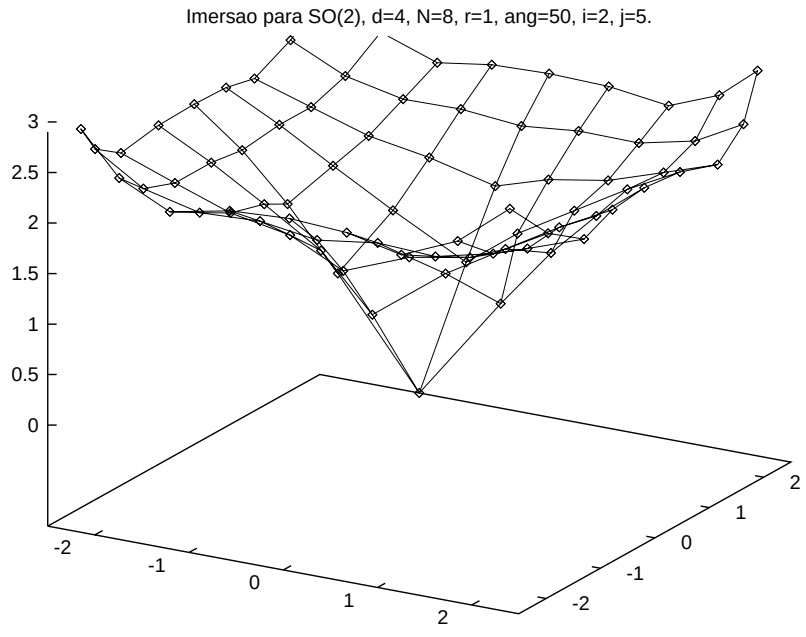

Figure 5.9: Embedding in the broken-symmetric phase, in four dimensions, with $j_0 = 5$, longitudinal component.

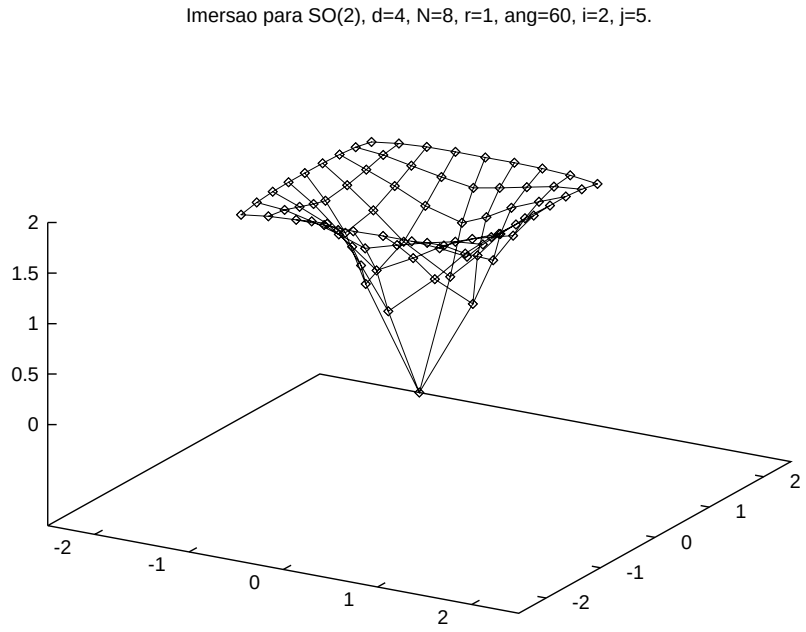

Figure 5.10: Embedding in the critical region, in four dimensions, with $j_0 = 5$, longitudinal component.

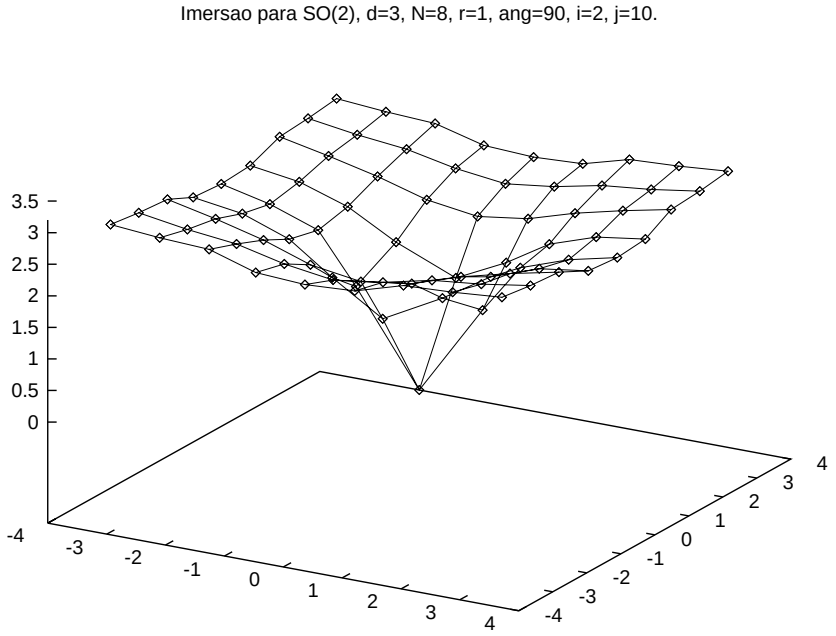

Figure 5.11: Embedding in the symmetric phase, in three dimensions, with $j_0 = 10$, longitudinal component.

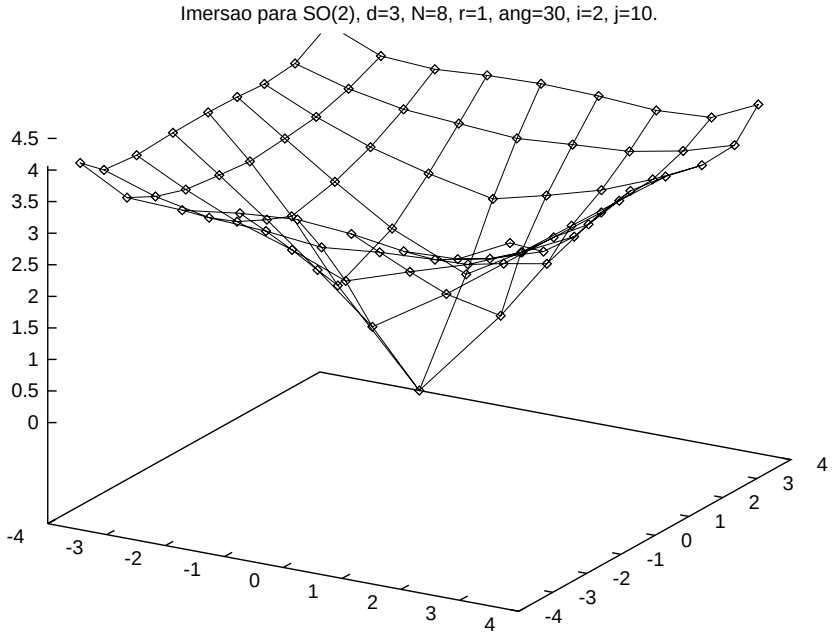

Figure 5.12: Embedding in the broken-symmetric phase, in three dimensions, with $j_0 = 10$, longitudinal component.

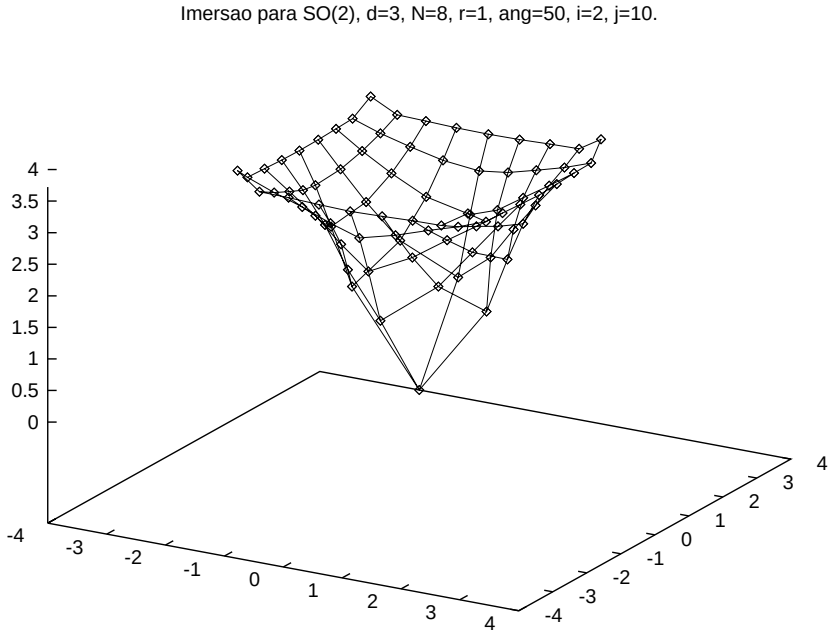

Figure 5.13: Embedding in the critical region, in three dimensions, with $j_0 = 10$, longitudinal component.

value of the source, with the objective of checking the kind of geometry which appears in this case. The main point of interest was verifying whether in this case the generated geometry is locally flat and, in particular, if there is a conical singularity at the origin. Graphs with the results can be seen in figures 5.11 to 5.13. As one can observe, on finite lattices the geometry in three dimensions is qualitatively similar to that which appears in four dimensions. Naturally, we should keep in mind that the dimensional variables of the theory scale in different ways in three and four dimensions and that, therefore, there may be a significant difference in the continuum limit.

5.2 Numerical Methods Used

The simulations turned out to be very long in the equipment which has been available for this work. For the largest lattice we could run, with $N = 8$, some points took almost 1000 hours in one processor of the fastest computer available for our use, so that we could generate good statistics. In order to improve the statistics, considering that the temporal translation symmetry is not broken by the source we introduced, we averaged over the N spatial sections perpendicular to the time axis. Still to improve the statistics we averaged, in the case of the four-dimensional space-time, over the three two-dimensional sections containing the origin which exist in the spatial section of three dimensions.

For the construction of the embeddings it is necessary to solve an embedding problem which consists, in this case, of finding a surface in a three-dimensional Euclidean space having the same intrinsic geometry of our section. This problem was solved numerically by a stochastic relaxation process of the type of a χ^2 fitting. Let ℓ_i be the lengths associated to each one of the $2dN^d$ links and diagonals, which result from the quantization process and let δ_i be the distances between the points at the two ends of each link or diagonal, measured in the embedding space. We define χ^2 as

$$\chi^2 = \sum_{i=1}^{2dN^d} w_i(\delta_i - \ell_i)^2,$$

where the sum runs over all the $2dN^d$ links and diagonals and w_i are weights inversely proportional to the statistical errors associated to each ℓ_i. The stochastic relaxation process is started with the N^d points of the lattice in arbitrarily chosen positions in the embedding space and begins to make random changes in these positions with the aim of minimizing χ^2. Each time that a change decreases χ^2 it is accepted, otherwise it is rejected and one tries again from the original position. In this way we approach the global minimum of χ^2, which is zero and corresponds to a perfect embedding, with each δ_i equal to the corresponding ℓ_i.

The relaxation process can be done in many different ways. If one makes only independent local variations at each point, it is susceptible of being very slow in approaching significantly the global minimum. There is also the risk of the system getting trapped

in local minima which are difficult to leave. Some of these local minima can be seen as folds in the resulting embedding. Whenever possible it is useful to make correlated changes of several points at the same time. However, if the number of correlated points in a certain change is too large the probability of rejecting trials increases quickly.

The process of embedding by stochastic relaxation tends to work better when the intrinsic geometry of the section is more curved. Note that the embedding problem does not necessarily have a unique solution. This is obvious, for example, in the case of the flat geometry and can be easily demonstrated by the crumpling up of a piece of paper. There is a drift within the set of possible solutions which happens along with the relaxation process. In order to minimize this drift we perform the relaxation using all the symmetry constraints which we can impose.

In our case we have a symmetry of 8 elements, composed by the four 90^o rotations and by a reflection of the section. Besides this, we fix the position of the central point and the direction of the symmetry axis of the section. However, this is not always enough to stabilize completely the embedding, which remains subject to foldings of various kinds, in special for the case of the flat geometry. Small errors in the lengths of the links and diagonals can have a dramatic effect on the embedding. This happens frequently for the links and diagonals which connect to the central point at which the singularity of the source is located, where the numerical errors tend to be larger. These errors are not purely statistical, including also numerical errors related to the representation of the potential of the theory in the presence of external sources.

The process of stochastic relaxation was executed in each case until the errors fell below a certain level, chosen to be compatible with our numerical errors and so as not to extend too much the execution time of the programs. Typical graphs of the final values of χ^2 can be seen in figures 5.14 to 5.16 and a more complete set can be found in Appendix A.3. In these graphs the scale of χ^2 is relative to the average length of the links and diagonals which connect to the point at which it is defined. In this way, the values presented correspond to the additional displacement which it would be necessary to do at each point in order that the errors become zero, which gives us a useful intuitive idea of the quality of the fit. Typically the errors are no more than a few percent in the worst cases, in general at the center of the lattice, where the singular source is located.

5.3 Analysis of the Geometry of the Section

The main result we have to present here about the relationship between the quantization of the fields and the curvature of the spatial geometry is of a qualitative character, that is, the simple fact that a curved geometry appears. The lattices which we were able to use until now are too small to allow us to do much better than evaluate visually the results. However, even a purely visual evaluation of the results can already give us an intuitively useful idea about the nature of the geometry. It is enough to compare the the embedding of figure 5.3, which corresponds to the critical region, to the embedding of a two-dimensional section of the Schwarzchild geometry shown in figure 5.17, to

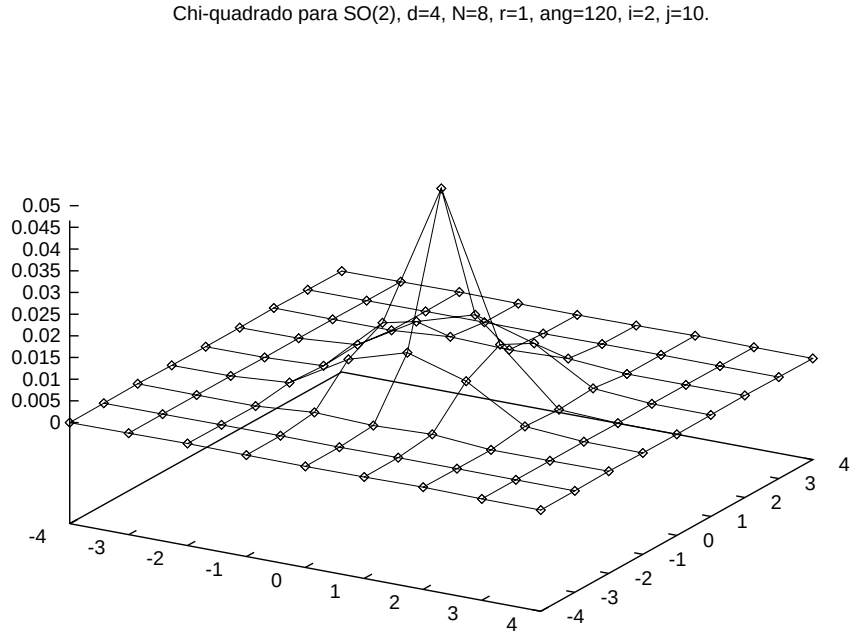

Figure 5.14: Residual errors in the symmetric phase, in four dimensions, with $j_0 = 10$, longitudinal component.

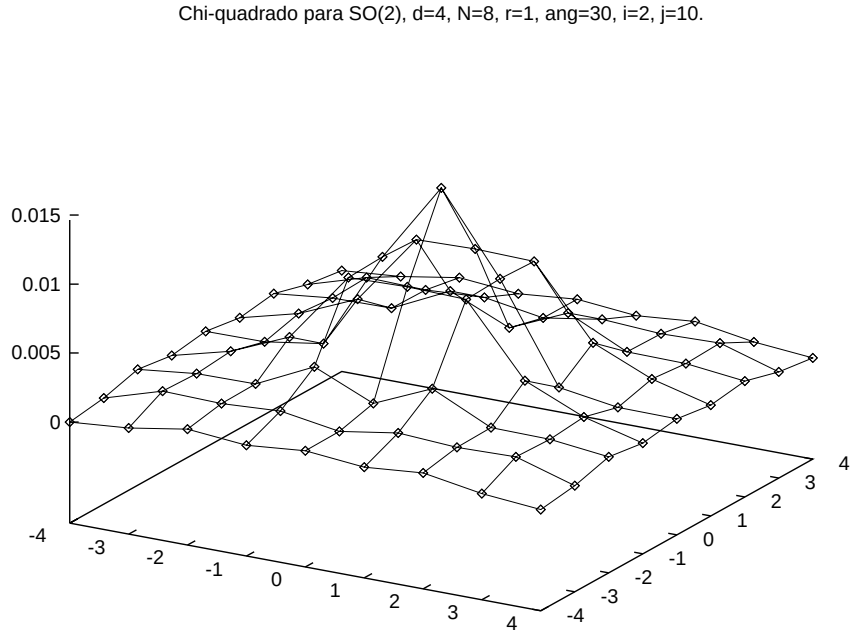

Figure 5.15: Residual errors in the broken-symmetric phase, in four dimensions, with $j_0 = 10$, longitudinal component.

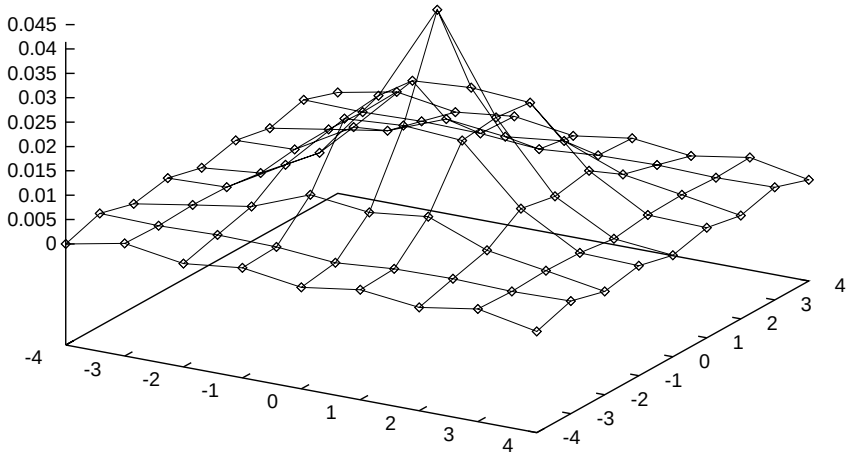

Figure 5.16: Residual errors in the critical region, in four dimensions, with $j_0 = 10$, longitudinal component.

verify the qualitative similarity between the two. In this last figure we included, for the comparison, an enlarged version of figure 5.3. The two graphs in figure 5.17 are drawn to the same scale and the Schwarzchild radius was chosen so as to make them as similar as possible.

There still are two aspects of the generated geometry which we can try to examine with more attention, even in these limited conditions from the point of view of the numerical explorations. The first one consists of a comparison of the scalar curvature of the generated section with that of the corresponding section of the Schwarzchild metric. It is easy to calculate the intrinsic curvature of a two-dimensional section containing the origin in the Schwarzchild geometry, outside the horizon. The complete metric of the geometry is

$$ds^2 = -\left(1 - \frac{r_0}{r}\right) dt^2 + \left(1 - \frac{r_0}{r}\right)^{-1} dr^2 + r^2 \left[d\theta^2 + \sin^2(\theta) d\phi^2\right],$$

where r_0 is the Schwarzchild radius. The section is given by the three-dimensional part of the metric, that is by $dt = 0$, if we impose also that $\theta = \pi/2$ with $d\theta = 0$. Since the metric is static outside the horizon the Euclidean and Lorentzian sections are identical and we obtain

$$ds^2 = \left(1 - \frac{r_0}{r}\right)^{-1} dr^2 + r^2 d\phi^2 = A^2(r) dr^2 + r^2 d\phi^2,$$

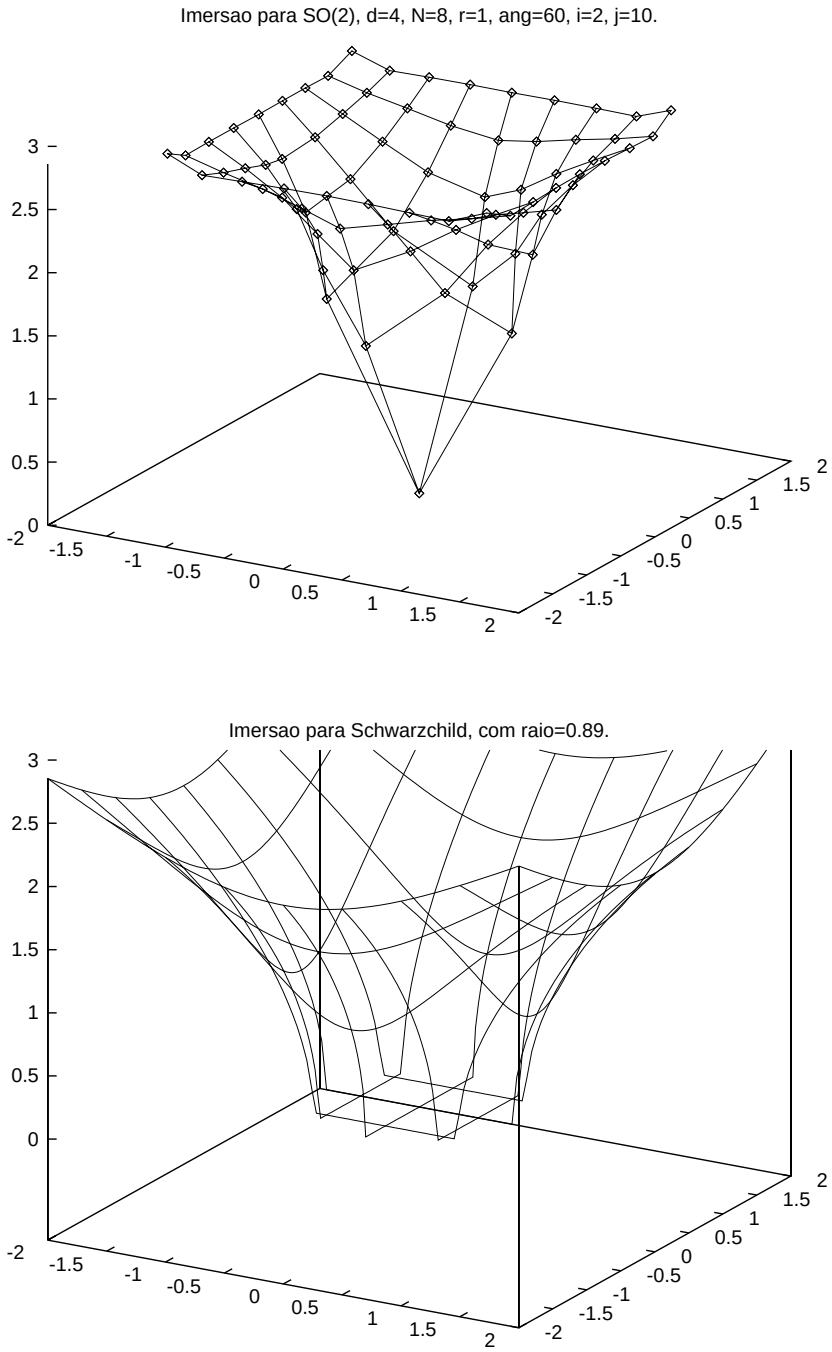

Figure 5.17: Comparison of the embedding in the critical region with the embedding of a section of the Schwarzchild geometry outside the horizon, shown with resolution compatible to that of the lattice.

where $A(r) = (1 - r_0/r)^{-1/2}$. Using the basis of 1-forms ω_μ given by

$$\begin{aligned} \omega_r &= A(r)dr, \\ \omega_\phi &= r d\phi, \end{aligned}$$

the metric of the section can be written as

$$ds^2 = (\omega_r)^2 + (\omega_\phi)^2,$$

which $g_{\mu\nu} = \delta_{\mu\nu}$, so that it is not necessary to differentiate between lower and upper indices. The connection 1-form $\omega_{\mu\nu}$ is in this case anti-symmetric and, solving the equations

$$\begin{aligned} dg_{\mu\nu} &= \omega_{\mu\nu} + \omega_{\nu\mu}, \\ d\omega_\mu &= -\omega_{\mu\nu} \wedge \omega_\nu \end{aligned}$$

we obtain

$$\begin{aligned} \omega_{rr} &= \omega_{\phi\phi} = 0, \\ \omega_{\phi r} &= -\omega_{r\phi} = \frac{1}{rA(r)}\omega_\phi. \end{aligned}$$

The curvature 2-form $\Omega_{\mu\nu}$ is obtained from

$$\Omega_{\mu\nu} = d\omega_{\mu\nu} + \omega_{\mu\alpha} \wedge \omega_{\alpha\nu},$$

from which it follows that the non-zero components are all equal up to a sign, being given by

$$\Omega_{r\phi} = \frac{\dot{A}(r)}{rA^3(r)}\omega_r \wedge \omega_\phi,$$

where $\dot{A}(r) = dA(r)/dr$. From this we obtain the curvature tensor $R_{\mu\nu\alpha\beta}$, which relates to $\Omega_{\mu\nu}$ by

$$\Omega_{\mu\nu} = R_{\mu\nu|\alpha>\beta|}\omega_\alpha \wedge \omega_\beta,$$

from which it follows that the non-zero components have all the same magnitude, with

$$R_{r\phi r\phi} = \frac{\dot{A}(r)}{rA^3(r)},$$

the others being obtainable by anti-symmetry. It follows that the non-zero components of the tensor $R_{\mu\nu}$ are

$$R_{rr} = R_{\phi\phi} = \frac{\dot{A}(r)}{rA^3(r)},$$

and that the scalar curvature R is given by

$$R = \frac{2\dot{A}(r)}{rA^3(r)} = -\frac{r_0}{r^3}.$$

This result is valid at any point outside the horizon, that is for $r > r_0$. What matters most to us about it is that it is negative and that its magnitude falls when we move away from the center.

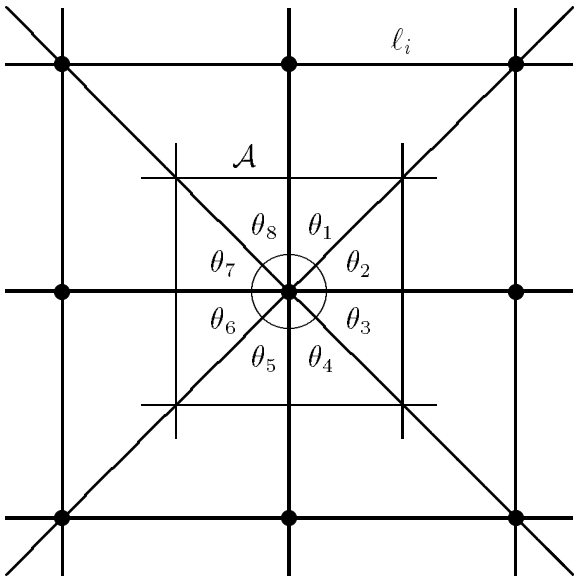

Figure 5.18: A cell of the simplicial complex.

It is also easy to calculate the scalar curvature of our numerical section by means of the Regge calculus. For this, we use the interpretation of our lattice as a simplicial complex. Taking all the links and diagonals which depart from a point, as well as all the neighbors connected by these links and diagonals, we can build around each point of the section a part of the complex, as figure 5.18 shows. It is composed of 8 triangles. If we connect the middle points of the links and diagonals, we build a small region or *cell* around each point. It is easy to verify that the section can be divided in such a way that each point has around it a cell like this, while the union of all cells reconstitutes the section. Under these condition we may define the scalar curvature at the central point of the cell as

$$R = \frac{2\pi - \theta_T}{\mathcal{A}},$$

where $\mathcal{A}$ is the area of the cell which is around the point and $\theta_T = \sum_{i=1}^{8} \theta_i$ is the sum of the 8 internal angles of the triangles the vertices of which are at the central point of the cell at issue. Both the areas and the angles can be obtained trigonometrically from our knowledge of the lengths ℓ_i of the links and diagonals. With this we can calculate R at each point along our numerical section. Since in $d = 2$ the scalar curvature suffices to define completely the intrinsic geometry, this allows for a useful comparison. It must be recorder here that, as we defined it, the simplicial complex associated to the two-dimensional section is, in fact, three-dimensional. This is due to the fact that we use both the diagonals of each square of the lattice, which effectively gives origin to tetrahedra. However these tetrahedra are quasi-degenerate on finite lattices and become flat in the continuum limit.

This calculation was performed and the result qualitatively compared to the result for the Schwarzchild section. Naturally, the absolute numbers are not of much interest, since we are comparing a relatively small lattice to the continuum limit. But the resulting sign is correct, being negative except at the central point where the singularity is, at the points directly connected to it by a link or diagonal and at the border of the lattice, where there are deformations due to the periodic boundary conditions. Naturally, one realizes that, with the exclusion of so many points in relatively small lattices, not many significant points remain for a quantitative comparison. Even so, on the lattice with $N = 8$, where there still are two significant points along the radial direction, one can see that the magnitude of R decreases as we move away from the center, as is the case for the Schwarzchild geometry.

The second aspect which we can try to examine is related to the possibility that the generated geometry be conformally flat. Since the geometry is generated by the variation of a single parameter, the renormalized mass, one may think at first that this leads inevitable to a conformally flat geometry. This is due to the fact that a geometry is conformally flat if its invariant interval ds^2 is proportional to the invariant interval of the flat geometry. The proportionality factor may depend on position, so that the geometry is not really flat, but it may be flattened by a simple change of scale made in a local way, at each point. The crucial point is that, in order that the geometry be conformally flat, the proportionality factor cannot depend on *direction*, but only on position.

Therefore, we may judge whether or not the generated geometry will be conformally flat examining the magnitude of the scale generated by the renormalized mass in each direction through a given point. Note that the renormalized mass, as we measure it in this work, is not associated to sites but to links and diagonals, which is a reflection of the fact that it is related to correlation lengths. Hence, it is possible that there is in fact a dependence of it on direction. Since the renormalized masses are associated to the links and diagonals and not directly to the sites, it is necessary to define on each site mass parameters, associated to each direction, which interpolate the values of the masses at the links and diagonals which connect to the point from each of the two sides in each direction.

In our two-dimensional sections we have 4 independent directions available at each site. For each of these directions we make an average of the masses associates to the two corresponding links or diagonals, one in each side of the site, and associate the result to the site. We check then whether or not the values obtained at each site depend on the direction. The result is that in the more curved geometries they clearly depend on direction, with differences significantly larger than the statistical errors. It follows, therefore, that the geometry generated in the four-dimensional space is not conformally flat, except when it is completely flat. This indicates that the correlations are affected in a differentiated form by the central source, depending on being measured in the radial or angular directions. It is necessary not to confuse this statement about the geometry of the space as a whole with any statement about the intrinsic geometry of the section, which, being two-dimensional, is always conformally flat.

Chapter 6

Conclusions and Outlook

We believe that the simulations performed leave little doubt about the fact that the introduction of strong localized external sources in the $\lambda\phi^4$ model generates on the lattice *some* form of metrical geometry with intrinsic curvature. Two important questions remain open: first, we have the question of whether or not the curvature of the geometry generated on finite lattices by the process of quantization of the fields survives the continuum limit; second, we have the question of whether or not the resulting geometry is the one predicted by Einstein's equation,

$$R_{\mu\nu} - \frac{1}{2} g_{\mu\nu} R = 8\pi G\, T_{\mu\nu}.$$

We have not had, until now, access to enough computer power to answer these questions through numerical explorations. All that we can say at the moment about the second question is that the geometry generated on a finite lattice by a point source, judged through the two-dimensional spatial sections going through the origin, is qualitatively similar to the corresponding section of the Schwarzchild solution. However, with the rapid progress of computing technology, we may expect that the numerical explorations will advance very much in a relatively short time.

As to the question of the continuum limit, certainly the size of the lattices we could use so far is not large enough to enable us to draw definitive conclusions. It should be said that it is possible that the curvature does not survive the continuum limit in physically acceptable conditions. The reason is that the variation of the mass with position is apparently due, in this laboratory model, to the shifting of the minimum of the potential, that is, to the emergence of a non-zero expectation value $\vec{v}_R$. This only reflects the fact that the model seems to be unable to generate two independent dimensional scales. In four dimensions, a limit with a source representing a fixed and finite point charge is such that j_0 is constant, while $J_0 \to \infty$ as $1/a^3$. In such a limit we will have $\vec{V}_R$ finite at all points except the origin. As we saw before, if we wish to have a finite $\vec{V}_R$ in the continuum limit, it is necessary that $\vec{v}_R$ vanish in this limit. Hence, we should have in the limit that $\vec{v}_R \to 0$ for all points except the origin, where the external source is located and where $\vec{V}_R$ diverges. We are not able at the moment

to decide whether or not it is enough to have $\vec{V}_R \neq 0$ in order to generate a curved geometry. Because of this, it is possible that in the limit α_R becomes constant over all the extent of the lattice and that the generated geometry becomes locally flat.

Note that, if this mechanism is actually realized in the continuum limit, one can look at it as a second kind of triviality of the model, associated to the triviality in its usual sense. This possible result may be interpreted as the fact that the generated geometry is short ranged, just as the correlation functions of the massive longitudinal component of our model. With this, the curvature of the geometry may collapse to the origin in the limit. It is true that there are long-range correlations in the broken phases of the models with $\mathcal{N} > 1$, due to the particles of zero mass, the Goldstone bosons associated to the transversal components. However, the geometry is defined by the finite and non-zero renormalized mass of the longitudinal component and, if the various particles do not interact due to the triviality of the theory, there is no way in which these long-range modes may affect the geometry. There remains a possibility that there is a remnant of a topological character of the generated geometry, in the form of a conical singularity at the origin, resulting from the collapse of the curvature of the geometry to that point.

This leads to the discussion of an objection formulated by Prof. H. B. Nielsen about the issue of the generated geometry being Einstein's geometry. Since it is necessary to have $m_R \neq 0$ in order to define a scale and hence the geometry, the field correlations will be short-ranged. It is therefore to be expected that the variations Δm_R of the mass decay exponentially and the geometry resulting from them should be localized and not the long-range geometry Einstein's equation. As we said before, it is possible that, in this laboratory model, the triviality of the theory prevents the Goldstone bosons from transmitting the effects of generation of curvature to long distances but, in a more realistic case, for example in a Gauge Theory, we will have a similar situation, with zero-mass vector particles and finite-mass spinor particles, except that in that case the particles do interact in fact with one another.

Another objection about the generated geometry satisfying Einstein's equation comes from the study of the geometry in three dimensions. Apparently the behavior is qualitatively the same which is seen in four dimensions, unlike what is implied by Einstein's equation. According to it, in three dimensions we should have only conical singularities at the location of the source. Naturally, it is possible that this is realized in the continuum limit, but it should be expected that the differences between the situations in three and four dimensions would be clearly visible even on finite lattices. Once more, in order to make progress in this kind of analysis it is necessary that we be able to use larger lattices both in three and four dimensions.

Naturally, a most important task lying ahead consists of discovering and developing ideas and techniques which may enable us to realize a program like the one we presented here in the standard model, including the vector and spinor fields. It would be very interesting to start this program with a study of the case of Electrodynamics.

We close with an observation about the possible origin of the principle of equivalence in a program like the one we presented here. In a more complex theory, like the

standard model, we will have several independent dimensional physical scales, related to the renormalized masses of the various particles present in the model. It is natural that we use one of them, possibly that of the lightest massive particle, as a scale unit, measuring all the others in terms of this one. Besides, we may now introduce external sources of several types, one for each type of particle present in the model. Presumably the independent introduction of any of these sources should affect the values of all the masses, since the fields interact with one another.

However, in order that the principle of equivalence be valid, it is necessary that the *ratios between masses do not depend on position or direction*, so that the generated geometry be the same from the point of view of any of the masses, except for the global change of scale due to the exchange of units. For this, it is necessary that, whatever the type of external source present, all the masses vary in the *same way* with position and direction. Hence, the principle of equivalence, in the context of the ideas presented here, takes the form of a certain kind of *universality* of the mechanism of generation of curvature, which should hold, at least, for the types of particles and fields that we do in fact find in nature. The determination of the existence or not of this universality is, certainly, one of the most important tasks we have ahead.

Appendix A

Graphs

We present in this Appendix a reasonably complete sampling of the simulations and the numerical tests performed. More than to simply record the available data, the intention is to give an idea of the extension of the numerical work which it was possible to do.

Tests and simulations were performed in three and four dimensions, for the $\lambda\phi^4$ model with $SO(2)$ symmetry. With regard to the external sources, tests were realized examining the cases $\vec{j}_0 = \vec{0}$ and $\vec{j}_0 = (0, \ldots, 0, j_0)$, where j_0 is a constant along that lattice, with values between 1 e 10. Lattices were used with even N between 2 and 8, values of the parameter r between 0.1 and 10 and of the parameter θ between 10^o and 180^o. The angle to which some figures refer is always the angle θ.

The statistics used in each run was of 200 blocks of 50000 lattice sweeps each. The partial averages over each block were recorded and the dispersion among the blocks was used for the evaluation of the statistical errors. We also measured the auto-correlation between consecutive individual sweeps, the corresponding correlation lengths being taken into account in the final calculation of the errors.

Whenever permitted by the existing symmetries, averages over the lattice were made in order to improve the statistics. The effect on the final errors of the correlations which exist between different points of the lattice was automatically taken into account, since the errors were calculated through blocks of sweeps obtained with these averages already included.

The coordinates of the lattice being $i_1, \ldots, i_d = 1, \ldots, N$ we chose arbitrarily $i_1 = 1, \ldots, N$ as the coordinate of the time axis for the simulations and we put the external source along this axis, in the position $i_{\mu \neq 1} = N/2$. We make averages of the observables over all the spatial sections perpendicular to the time axis. In $d = 3$ a two-dimensional space described by $i_2, i_3 = 1, \ldots, N$ results. In $d = 4$ a three-dimensional space described by $i_2, i_3, i_4 = 1, \ldots, N$ results. In this case we make averages over the three two-dimensional sections given by $i_2 = N/2$, $i_3 = N/2$ e $i_4 = N/2$.

The scales of the embedding graphs were maintained constant for all values of θ, for each lattice size and collection of values of the other parameters of the model.

A.1 Observable Tests

Tests in $d = 4$:
(transversal component)

SO(2), d=4, N=4, r=0.1, i=1, j=0

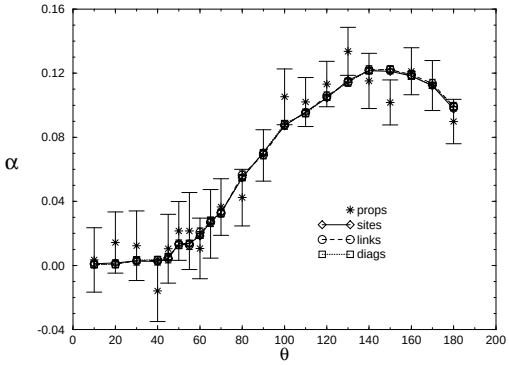

Fig. T-4-1.1

SO(2), d=4, N=4, r=1, i=1, j=0

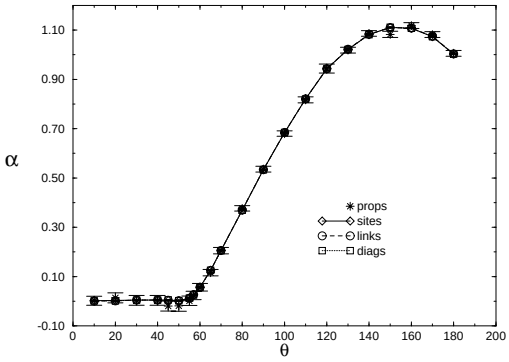

Fig. T-4-1.2

SO(2), d=4, N=4, r=10, i=1, j=0

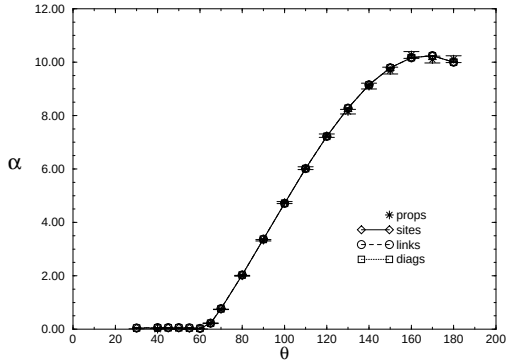

Fig. T-4-1.3

SO(2), d=4, N=6, r=0.1, i=1, j=0

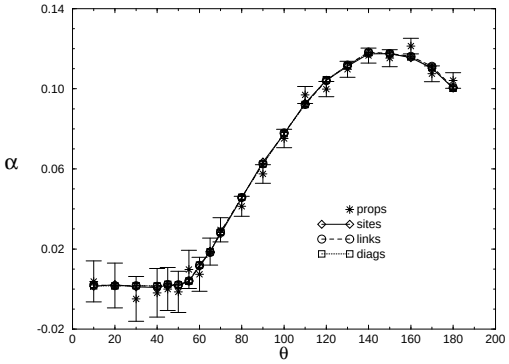

Fig. T-4-1.4

SO(2), d=4, N=6, r=1, i=1, j=0

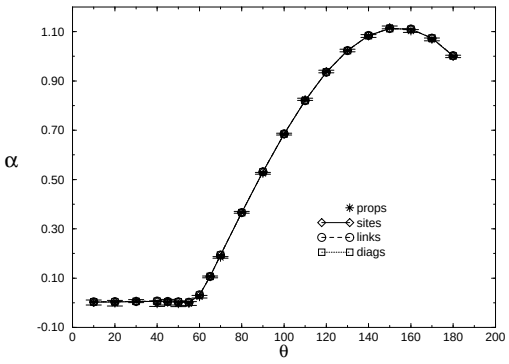

Fig. T-4-1.5

SO(2), d=4, N=6, r=10, i=1, j=0

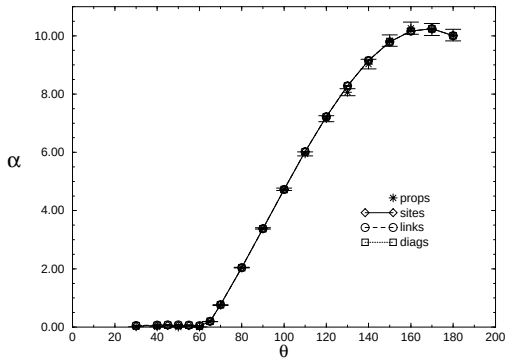

Fig. T-4-1.6

SO(2), d=4, N=8, r=0.1, i=1, j=0

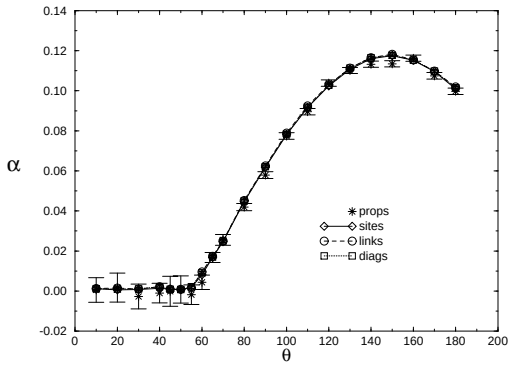

Fig. T-4-1.7

SO(2), d=4, N=4, r=1, i=2, j=0

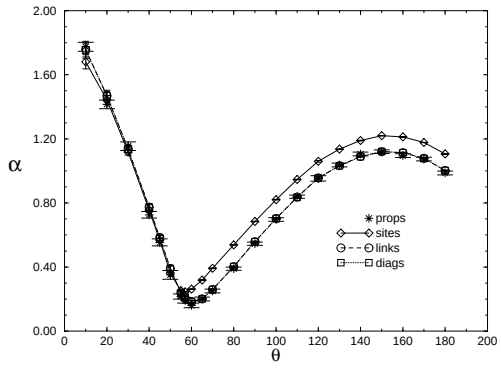

Fig. T-4-2.2

SO(2), d=4, N=8, r=1, i=1, j=0

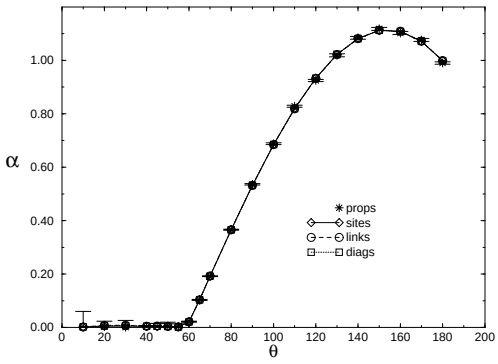

Fig. T-4-1.8

SO(2), d=4, N=4, r=10, i=2, j=0

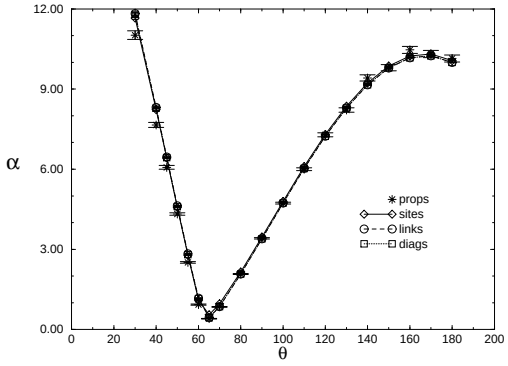

Fig. T-4-2.3

Tests in $d = 4$:
(longitudinal component)

SO(2), d=4, N=4, r=0.1, i=2, j=0

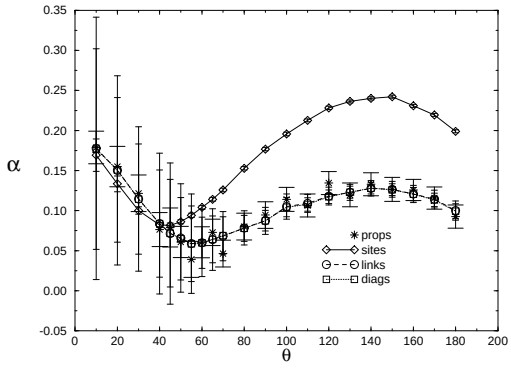

Fig. T-4-2.1

SO(2), d=4, N=6, r=0.1, i=2, j=0

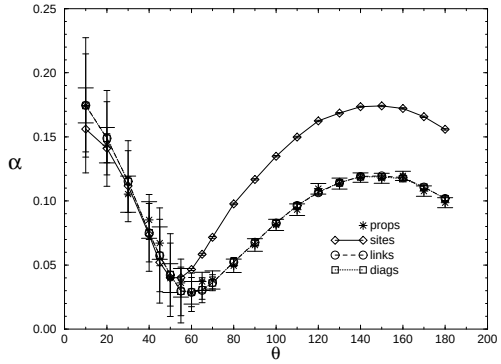

Fig. T-4-2.4

SO(2), d=4, N=6, r=1, i=2, j=0

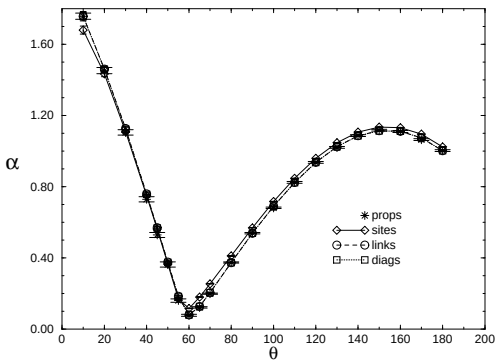

Fig. T-4-2.5

SO(2), d=4, N=8, r=1, i=2, j=0

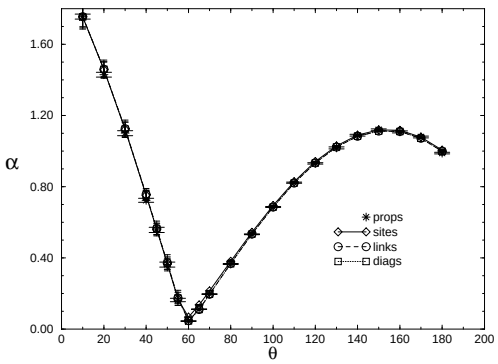

Fig. T-4-2.8

SO(2), d=4, N=6, r=10, i=2, j=0

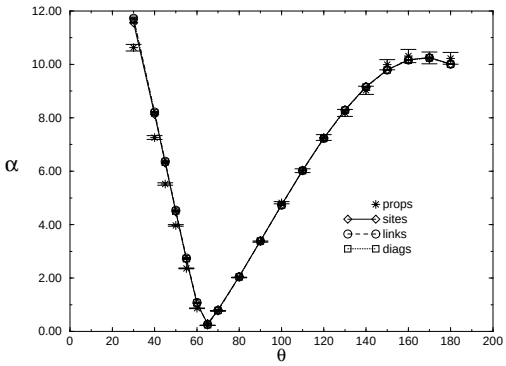

Fig. T-4-2.6

SO(2), d=4, N=8, r=0.1, i=2, j=0

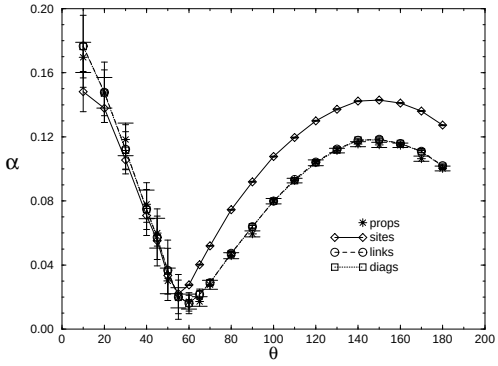

Fig. T-4-2.7

Tests in $d = 3$:

SO(2), d=3, N=4, r=1, i=1, j=0

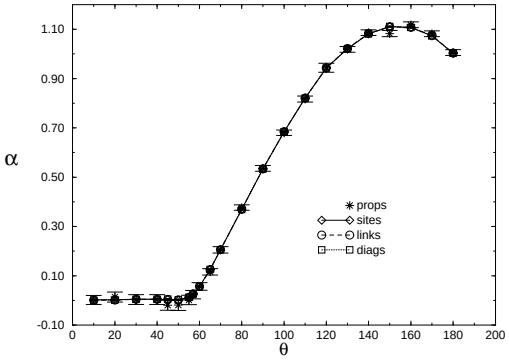

Fig. T-3.1

SO(2), d=3, N=4, r=1, i=2, j=0

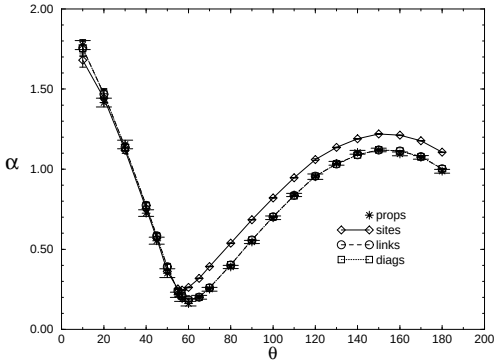

Fig. T-3.2

A.2 Section Embeddings

Embeddings in $d = 4$:
(longitudinal component)

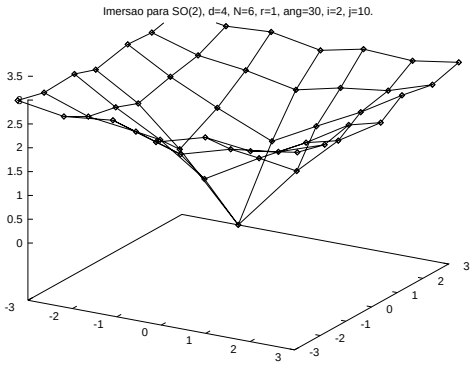

Fig. I-4-2.1

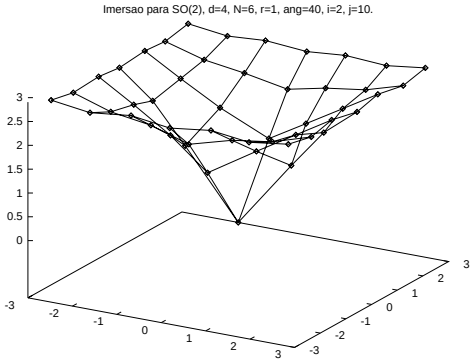

Fig. I-4-2.2

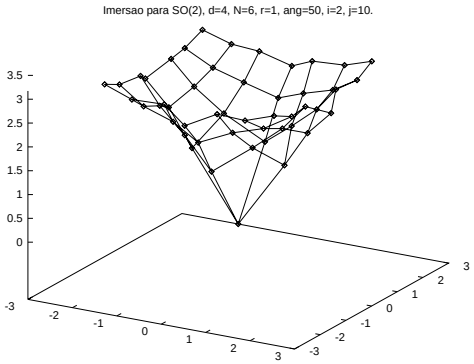

Fig. I-4-2.3

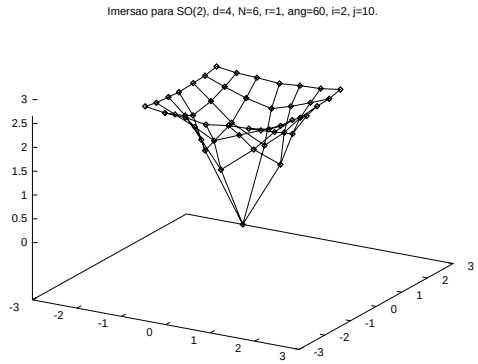

Fig. I-4-2.4

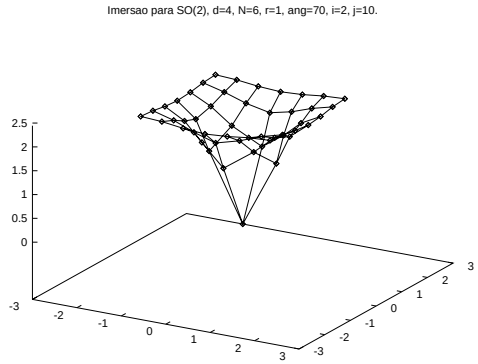

Fig. I-4-2.5

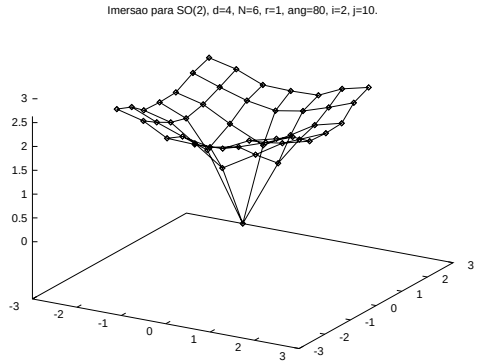

Fig. I-4-2.6

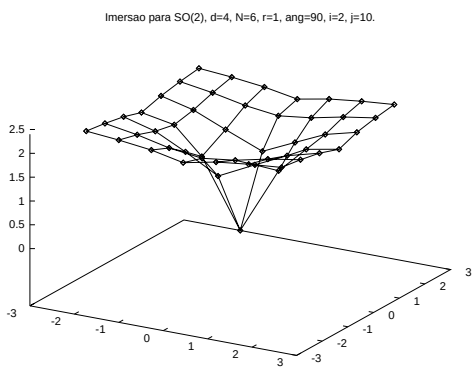

Fig. I-4-2.7

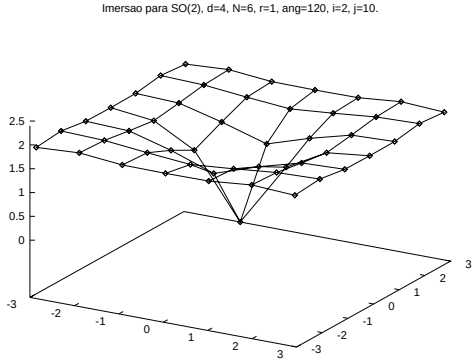

Fig. I-4-2.8

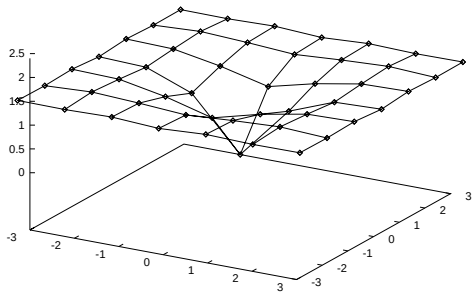

Fig. I-4-2.9

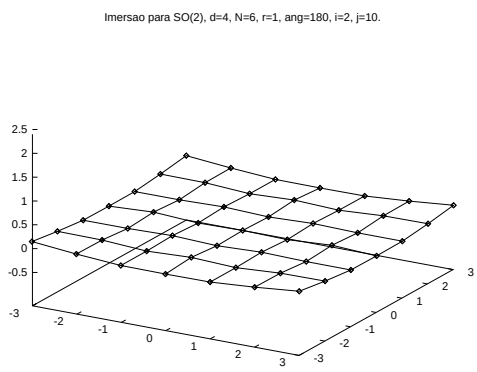

Fig. I-4-2.10

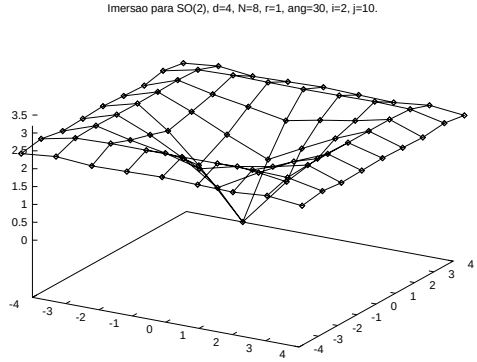

Fig. I-4-2.11

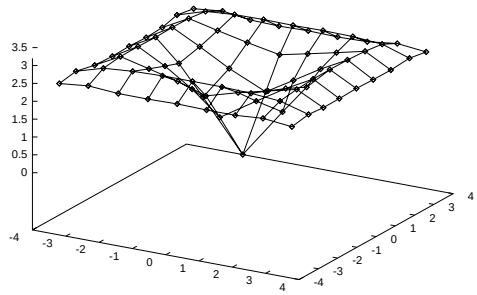

Fig. I-4-2.12

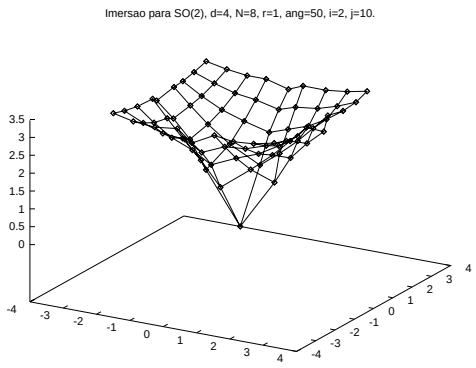

Fig. I-4-2.13

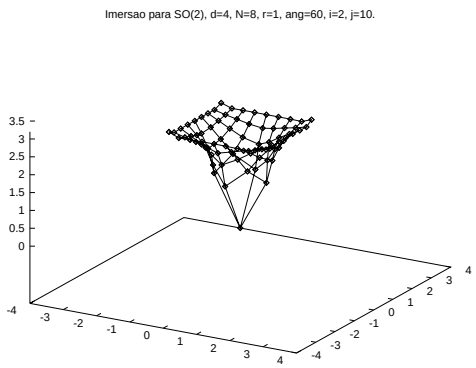

Fig. I-4-2.14

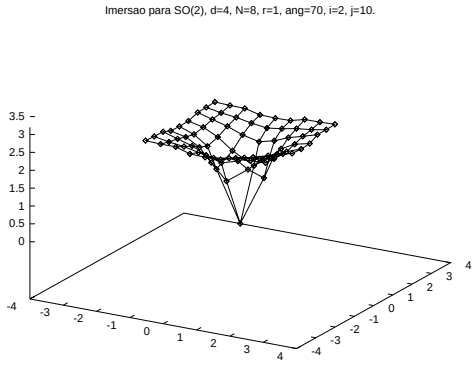

Fig. I-4-2.15

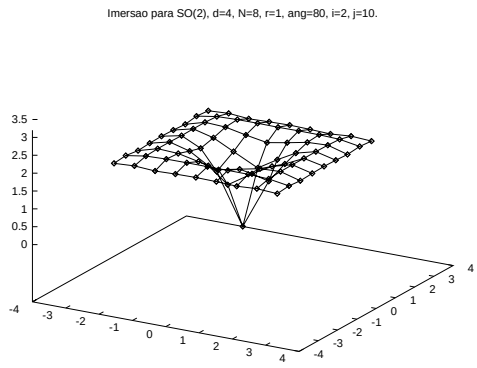

Fig. I-4-2.16

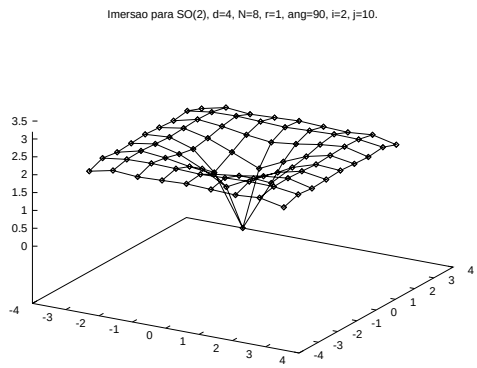

Fig. I-4-2.17

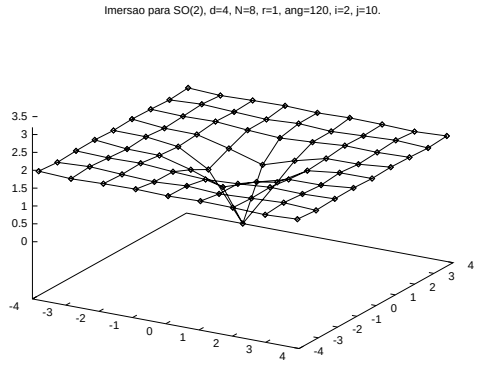

Fig. I-4-2.18

Imersao para SO(2), d=4, N=8, r=1, ang=150, i=2, j=10.

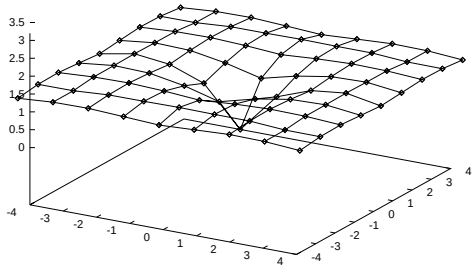

Fig. I-4-2.19

Imersao para SO(2), d=4, N=8, r=1, ang=180, i=2, j=10.

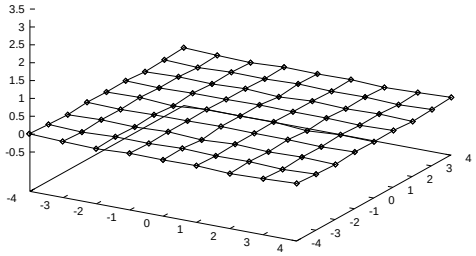

Fig. I-4-2.20

Embeddings in $d = 4$:
(transversal component)

Imersao para SO(2), d=4, N=6, r=1, ang=30, i=1, j=10.

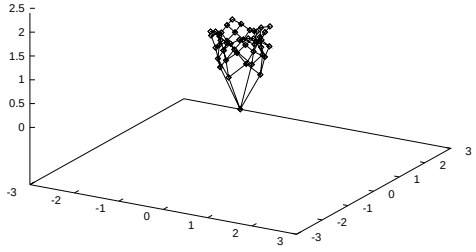

Fig. I-4-1.1

Imersao para SO(2), d=4, N=6, r=1, ang=40, i=1, j=10.

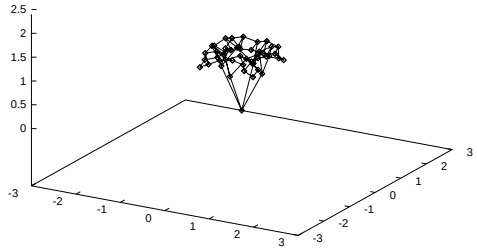

Fig. I-4-1.2

Imersao para SO(2), d=4, N=6, r=1, ang=50, i=1, j=10.

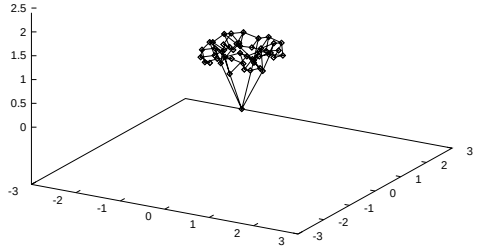

Fig. I-4-1.3

Imersao para SO(2), d=4, N=6, r=1, ang=60, i=1, j=10.

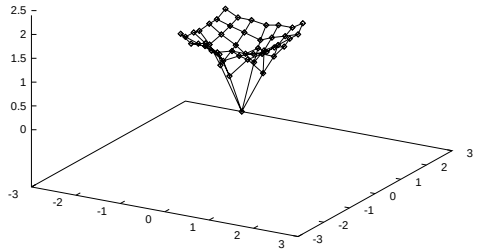

Fig. I-4-1.4

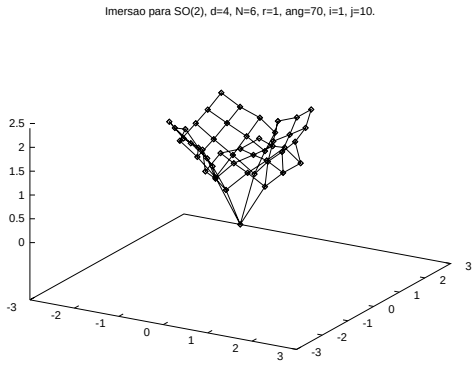

Fig. I-4-1.5

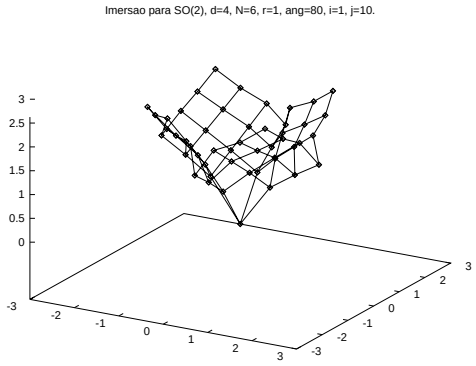

Fig. I-4-1.6

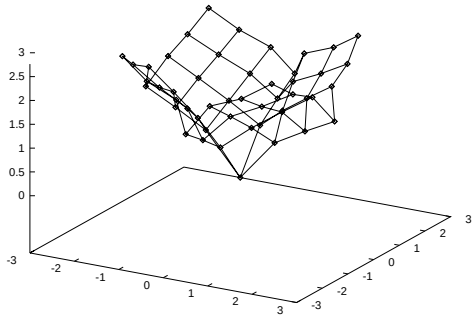

Fig. I-4-1.7

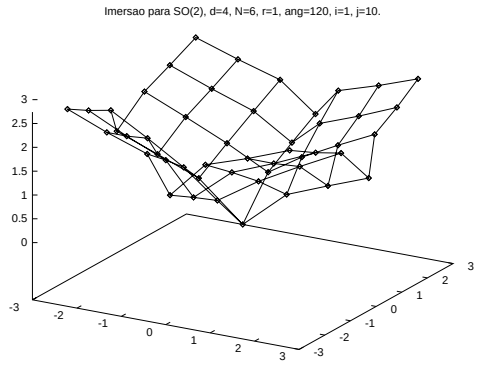

Fig. I-4-1.8

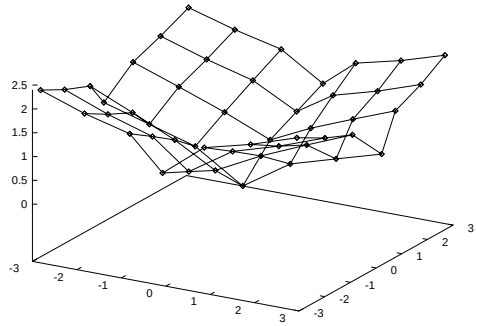

Fig. I-4-1.9

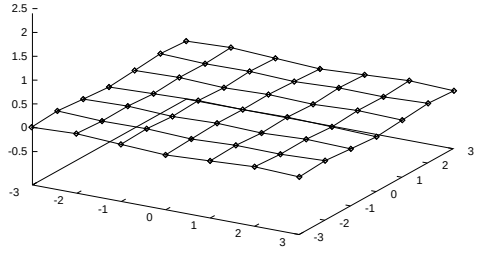

Fig. I-4-1.10

Imersao para SO(2), d=4, N=8, r=1, ang=30, i=1, j=10.

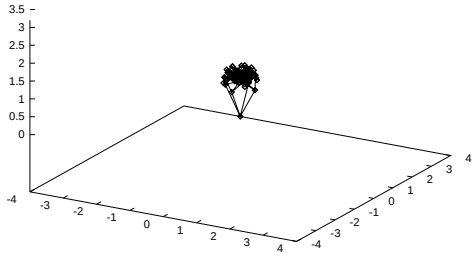

Fig. I-4-1.11

Imersao para SO(2), d=4, N=8, r=1, ang=40, i=1, j=10.

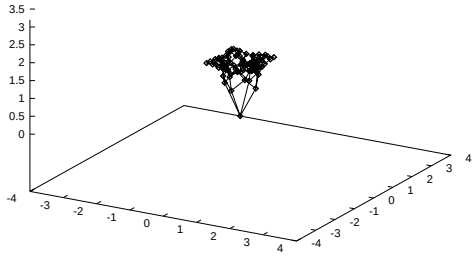

Fig. I-4-1.12

Imersao para SO(2), d=4, N=8, r=1, ang=50, i=1, j=10.

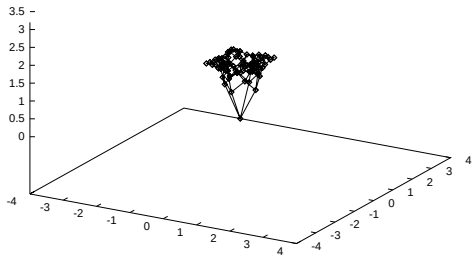

Fig. I-4-1.13

Imersao para SO(2), d=4, N=8, r=1, ang=60, i=1, j=10.

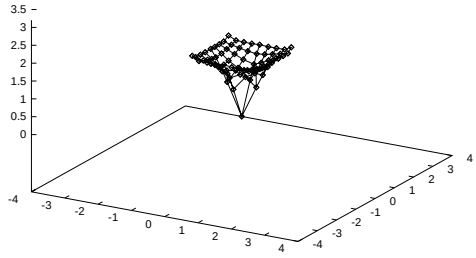

Fig. I-4-1.14

Imersao para SO(2), d=4, N=8, r=1, ang=70, i=1, j=10.

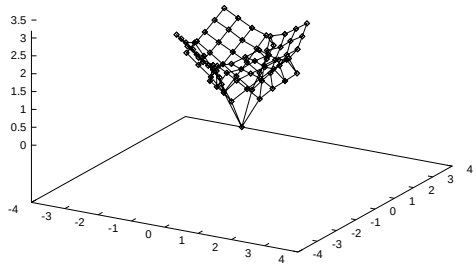

Fig. I-4-1.15

Imersao para SO(2), d=4, N=8, r=1, ang=80, i=1, j=10.

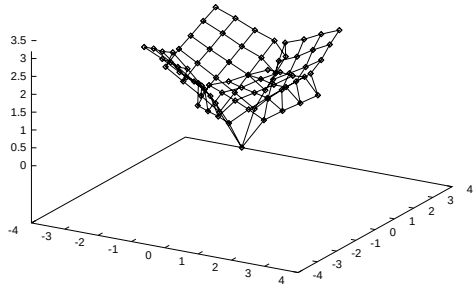

Fig. I-4-1.16

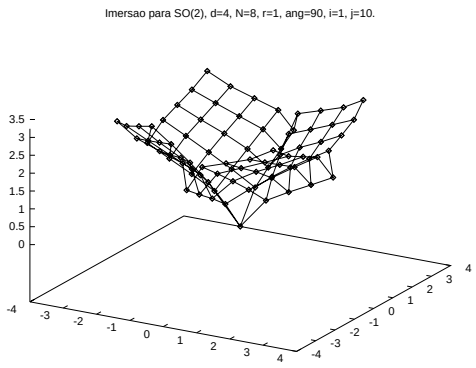

Fig. I-4-1.17

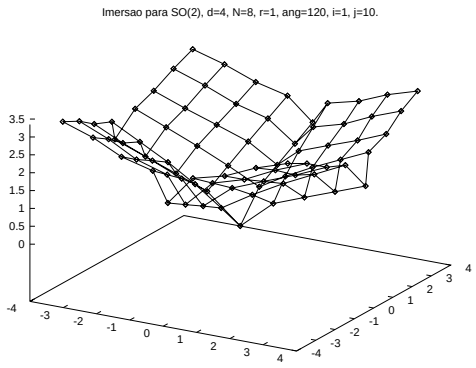

Fig. I-4-1.18

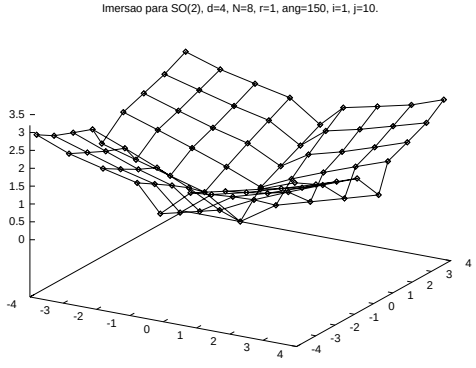

Fig. I-4-1.19

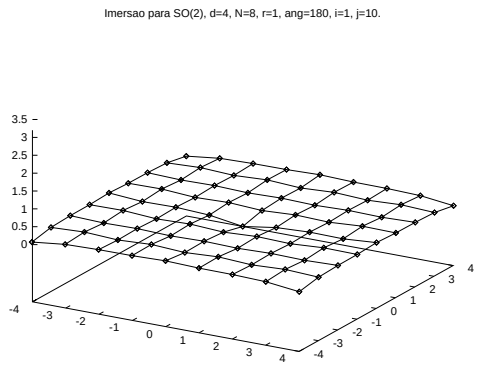

Fig. I-4-1.20

Embeddings in $d = 3$: (longitudinal component)

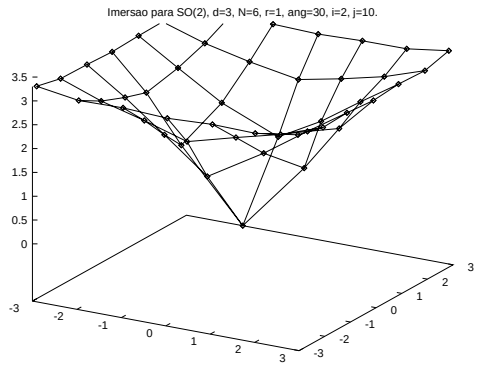

Fig. I-3-2.1

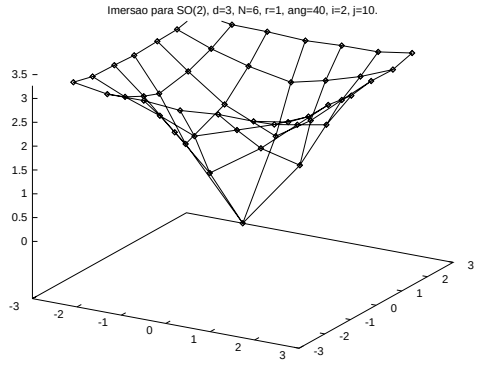

Fig. I-3-2.2

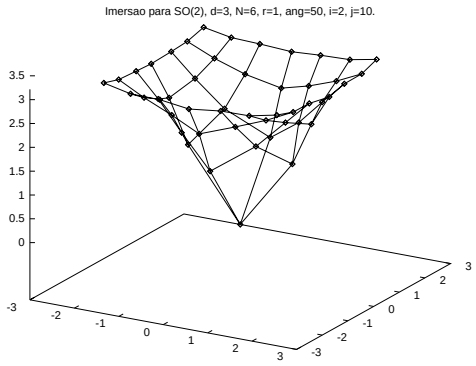

Fig. I-3-2.3

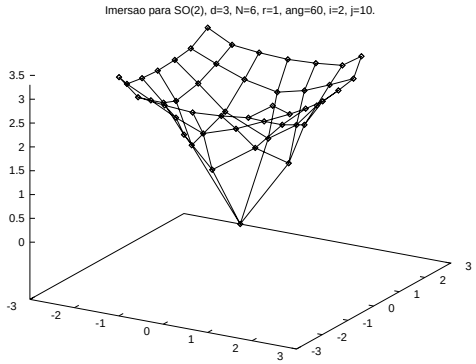

Fig. I-3-2.4

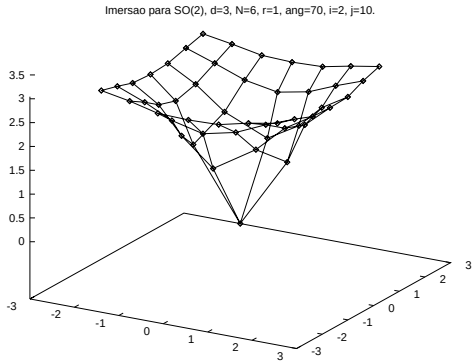

Fig. I-3-2.5

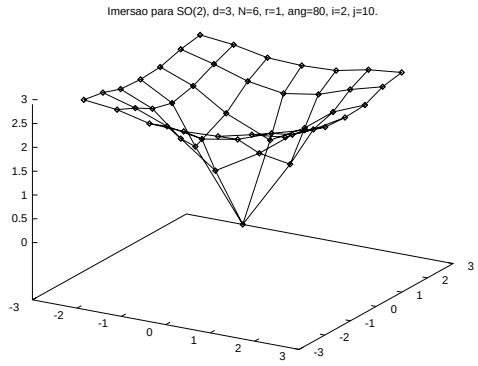

Fig. I-3-2.6

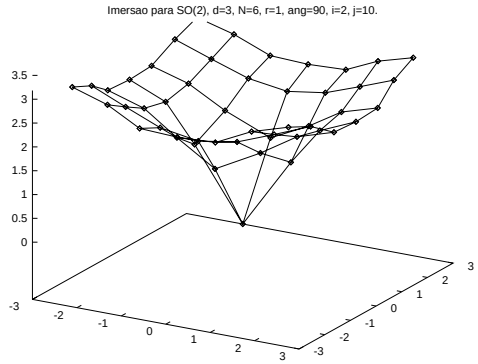

Fig. I-3-2.7

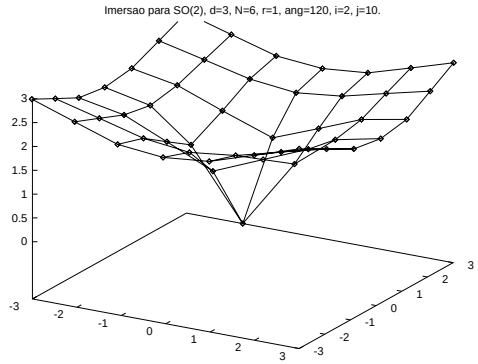

Fig. I-3-2.8

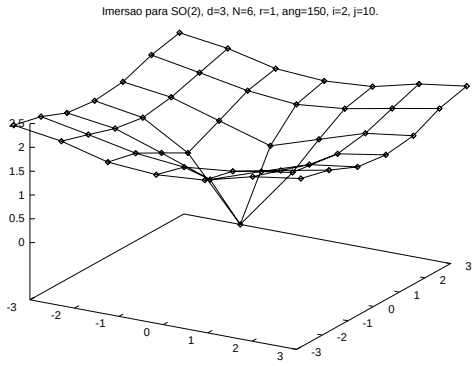

Fig. I-3-2.9

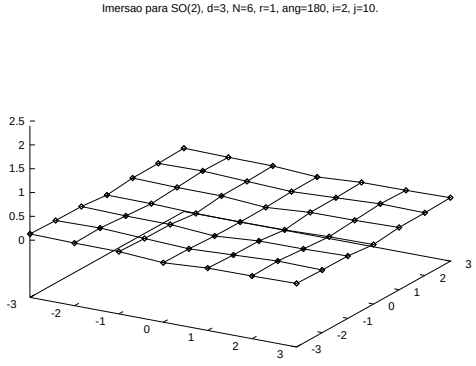

Fig. I-3-2.10

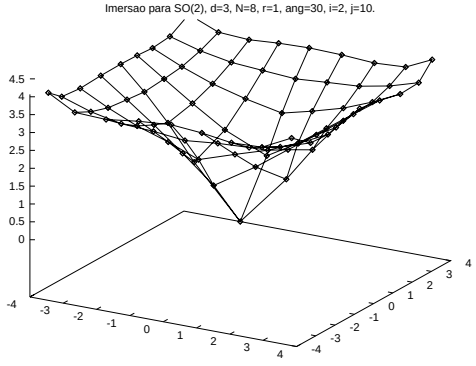

Fig. I-3-2.11

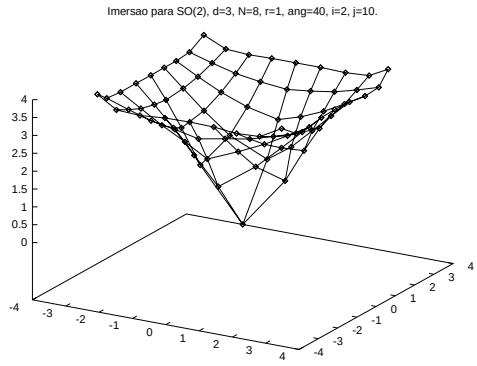

Fig. I-3-2.12

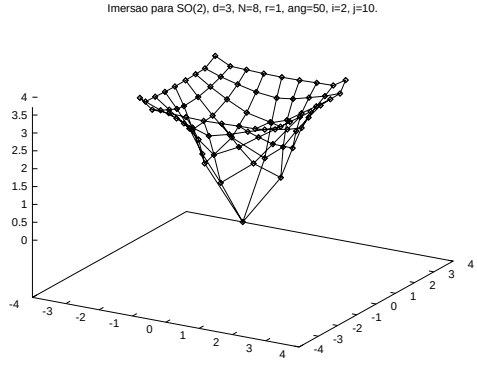

Fig. I-3-2.13

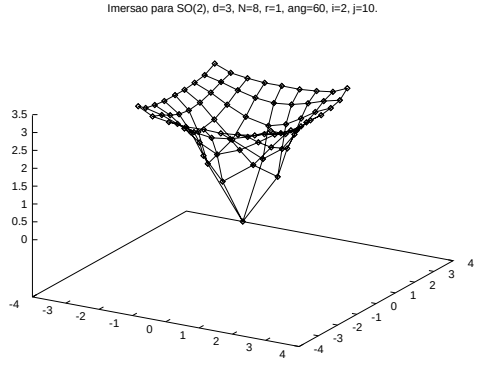

Fig. I-3-2.14

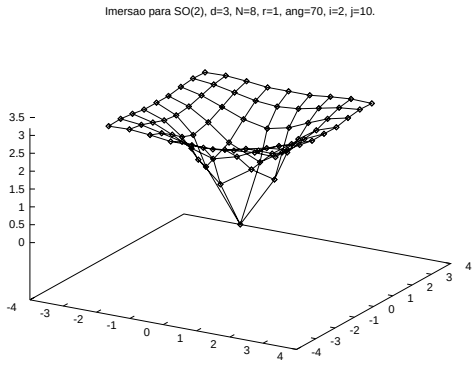

Fig. I-3-2.15

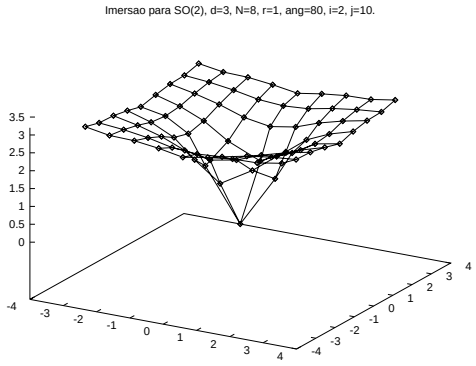

Fig. I-3-2.16

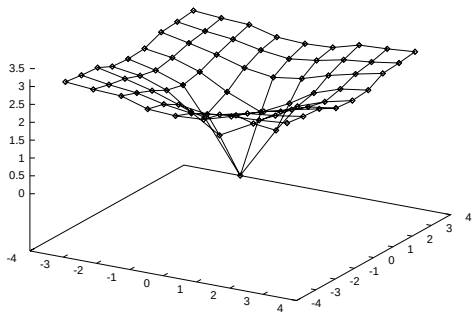

Fig. I-3-2.17

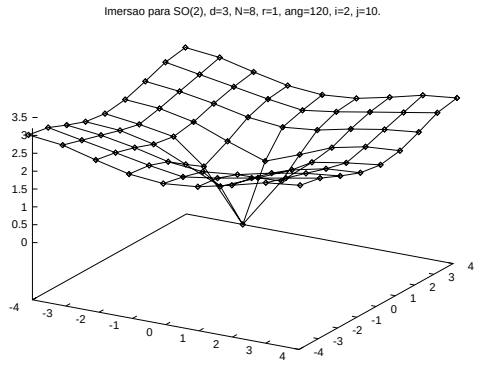

Fig. I-3-2.18

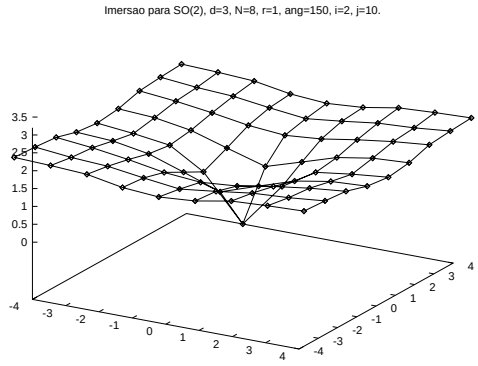

Fig. I-3-2.19

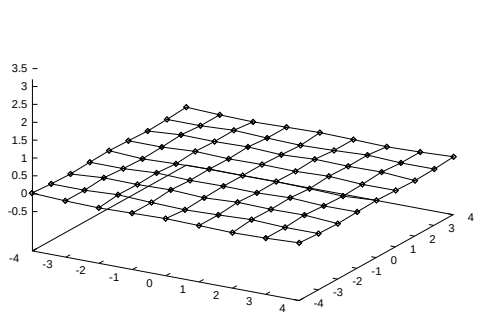

Fig. I-3-2.20

Embeddings in $d = 3$:
(transversal component)

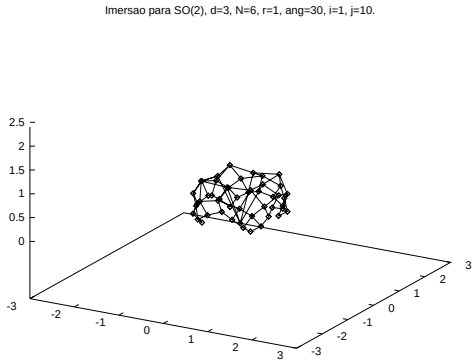

Fig. I-3-1.1

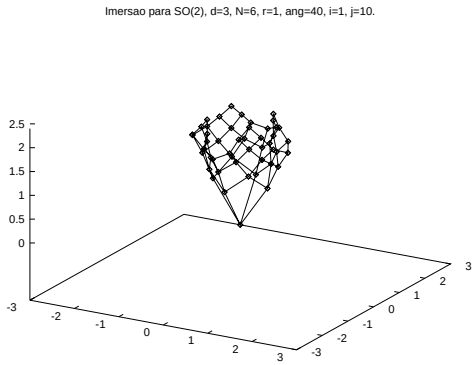

Fig. I-3-1.2

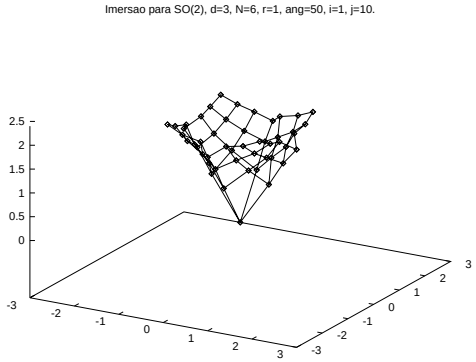

Fig. I-3-1.3

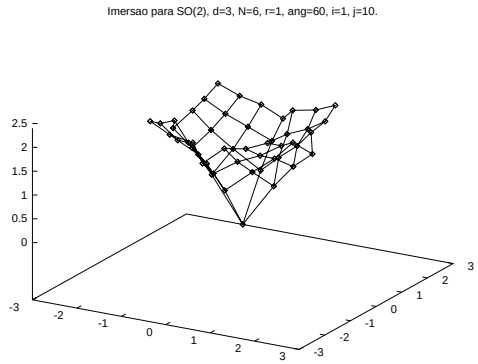

Fig. I-3-1.4

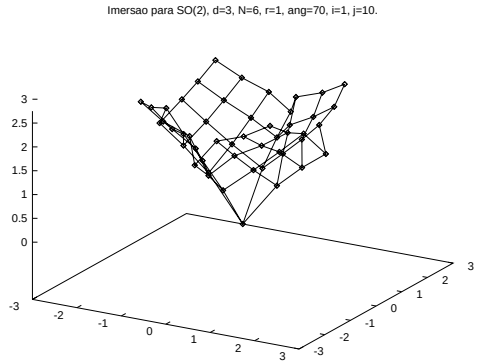

Fig. I-3-1.5

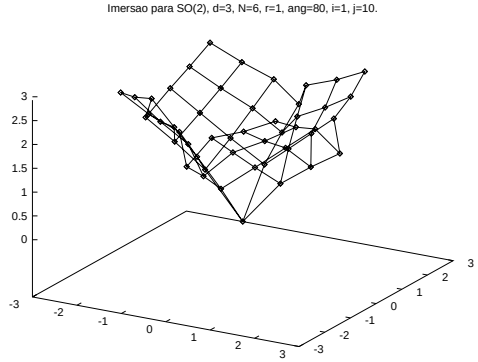

Fig. I-3-1.6

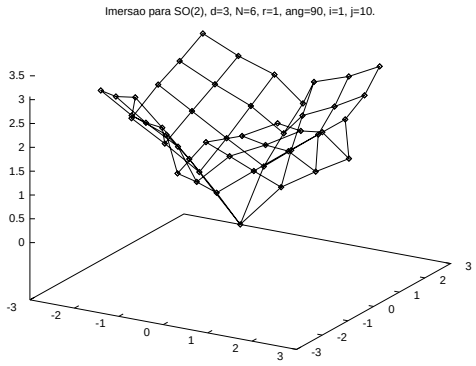

Fig. I-3-1.7

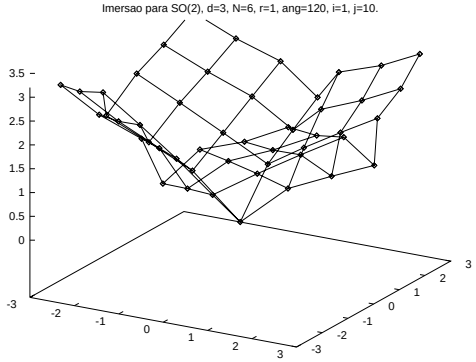

Fig. I-3-1.8

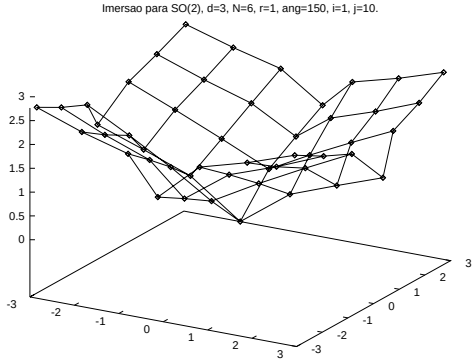

Fig. I-3-1.9

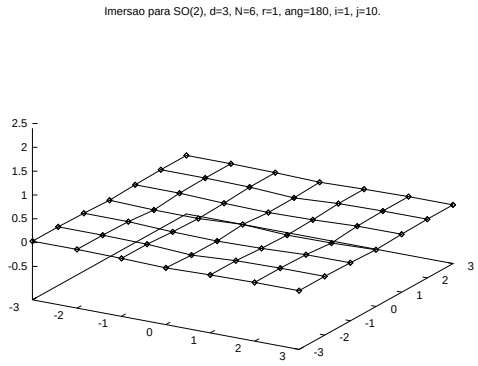

Fig. I-3-1.10

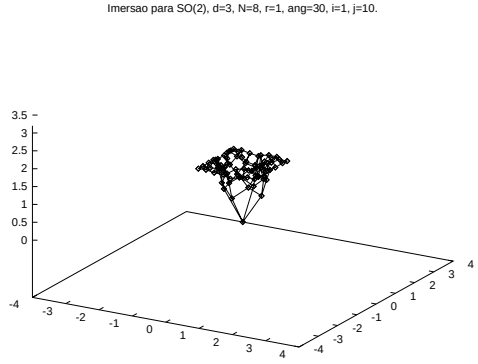

Fig. I-3-1.11

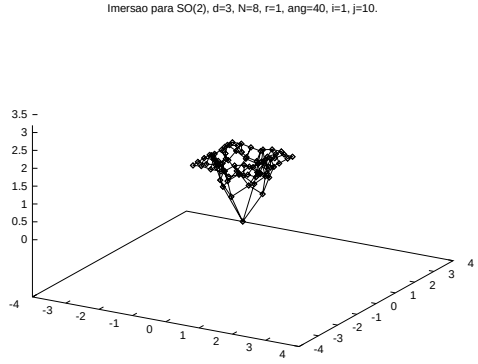

Fig. I-3-1.12

Imersao para SO(2), d=3, N=8, r=1, ang=50, i=1, j=10.

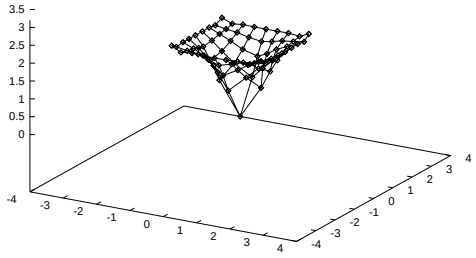

Fig. I-3-1.13

Imersao para SO(2), d=3, N=8, r=1, ang=60, i=1, j=10.

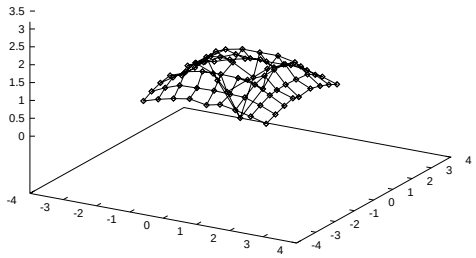

Fig. I-3-1.14

Imersao para SO(2), d=3, N=8, r=1, ang=70, i=1, j=10.

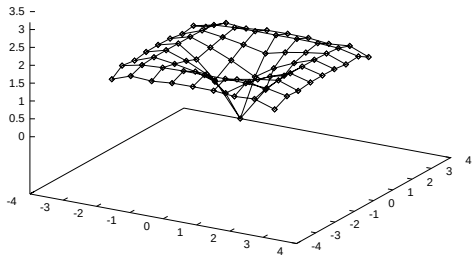

Fig. I-3-1.15

Imersao para SO(2), d=3, N=8, r=1, ang=80, i=1, j=10.

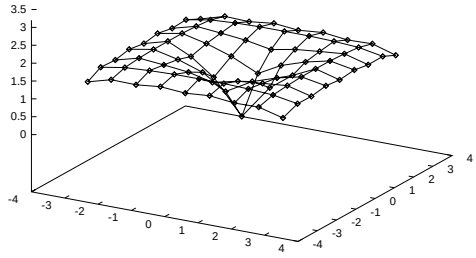

Fig. I-3-1.16

Imersao para SO(2), d=3, N=8, r=1, ang=90, i=1, j=10.

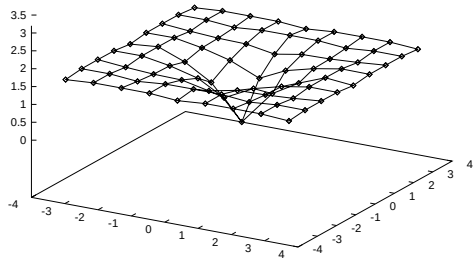

Fig. I-3-1.17

Imersao para SO(2), d=3, N=8, r=1, ang=120, i=1, j=10.

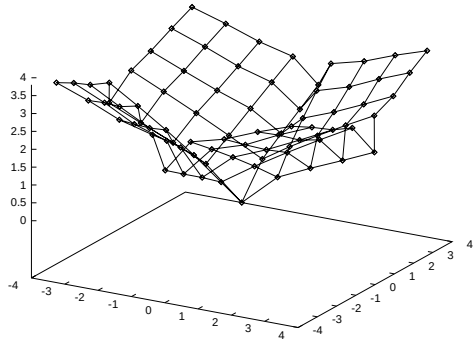

Fig. I-3-1.18

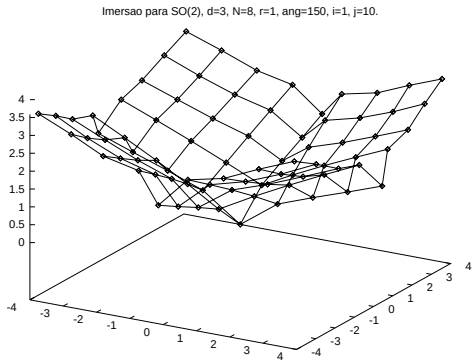

Fig. I-3-1.19

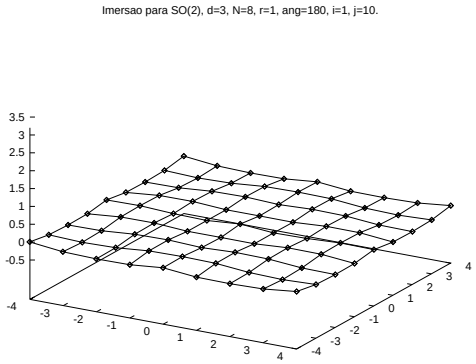

Fig. I-3-1.20

Embeddings with $j = 5$: (longitudinal component)

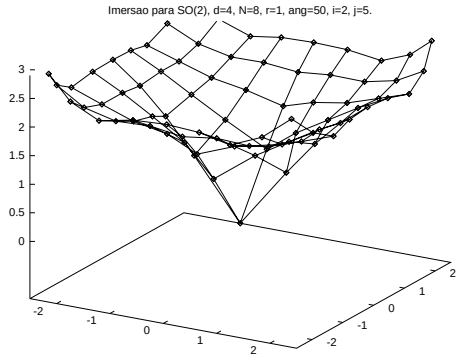

Fig. I-4-2-J.1

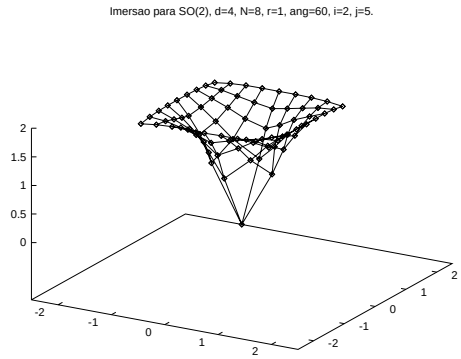

Fig. I-4-2-J.2

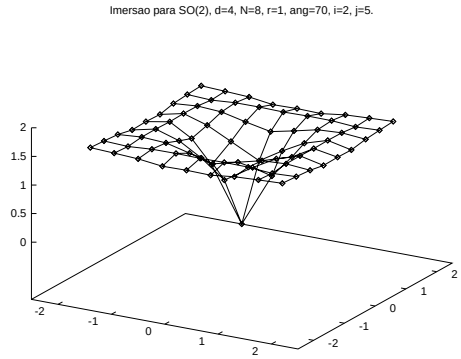

Fig. I-4-2-J.3

Embeddings with $j = 5$: (transversal component)

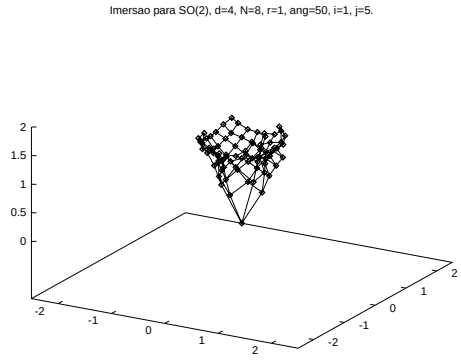

Fig. I-4-1-J.1

Imersao para SO(2), d=4, N=8, r=1, ang=60, i=1, j=5.

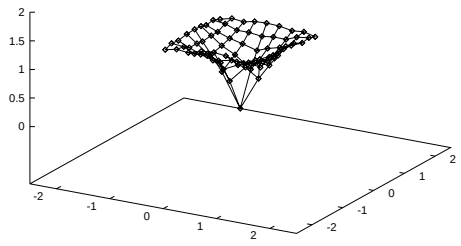

Fig. I-4-1-J.2

Imersao para SO(2), d=4, N=8, r=1, ang=70, i=1, j=5.

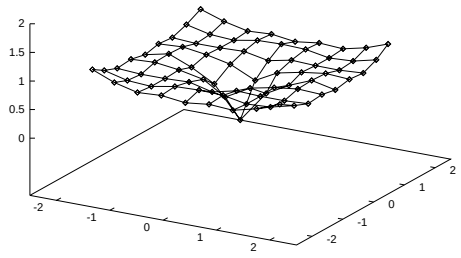

Fig. I-4-1-J.3

A.3 Residual Errors

Errors in $d = 4$:
(longitudinal component)

Chi-quadrado para SO(2), d=4, N=6, r=1, ang=30, i=2, j=10.

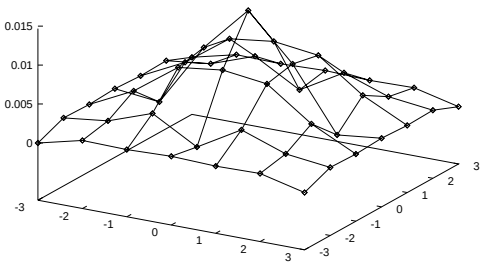

Fig. E-4-2.1

Chi-quadrado para SO(2), d=4, N=6, r=1, ang=40, i=2, j=10.

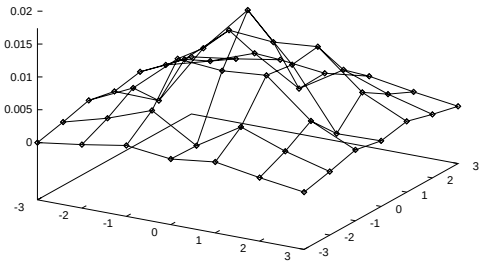

Fig. E-4-2.2

Chi-quadrado para SO(2), d=4, N=6, r=1, ang=50, i=2, j=10.

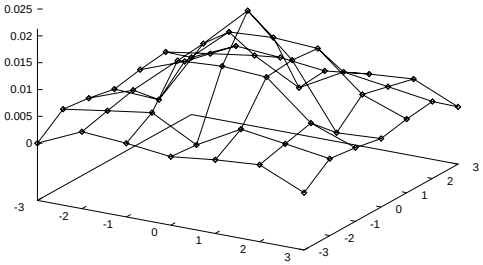

Fig. E-4-2.3

Chi-quadrado para SO(2), d=4, N=6, r=1, ang=60, i=2, j=10.

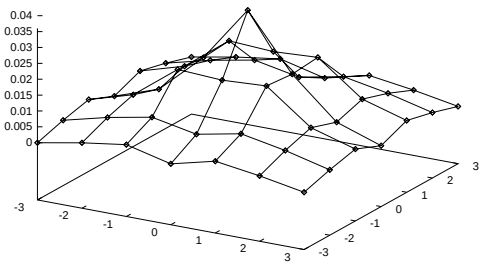

Fig. E-4-2.4

Chi-quadrado para SO(2), d=4, N=6, r=1, ang=70, i=2, j=10.

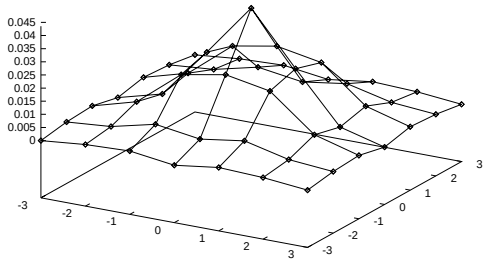

Fig. E-4-2.5

Chi-quadrado para SO(2), d=4, N=6, r=1, ang=80, i=2, j=10.

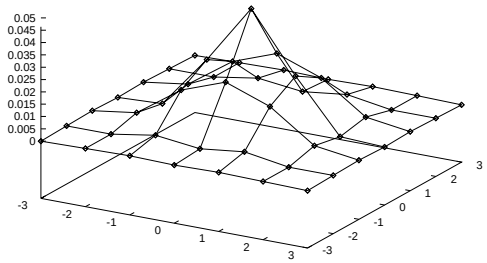

Fig. E-4-2.6

Chi-quadrado para SO(2), d=4, N=6, r=1, ang=90, i=2, j=10.

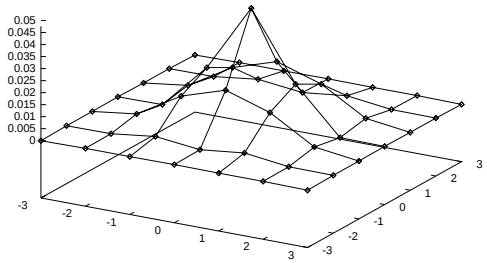

Fig. E-4-2.7

Chi-quadrado para SO(2), d=4, N=6, r=1, ang=120, i=2, j=10.

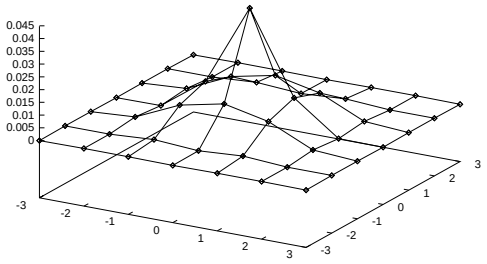

Fig. E-4-2.8

Chi-quadrado para SO(2), d=4, N=6, r=1, ang=150, i=2, j=10.

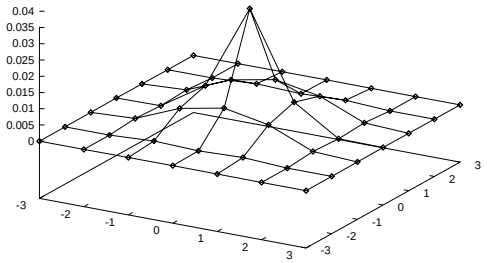

Fig. E-4-2.9

Chi-quadrado para SO(2), d=4, N=6, r=1, ang=180, i=2, j=10.

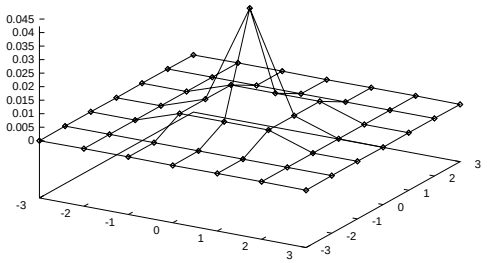

Fig. E-4-2.10

Chi-quadrado para SO(2), d=4, N=8, r=1, ang=30, i=2, j=10.

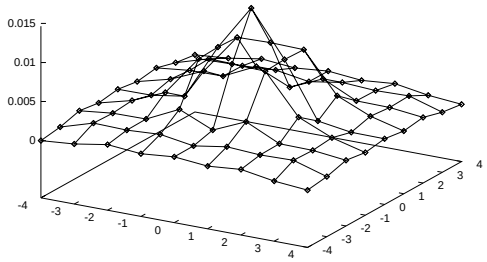

Fig. E-4-2.11

Chi-quadrado para SO(2), d=4, N=8, r=1, ang=40, i=2, j=10.

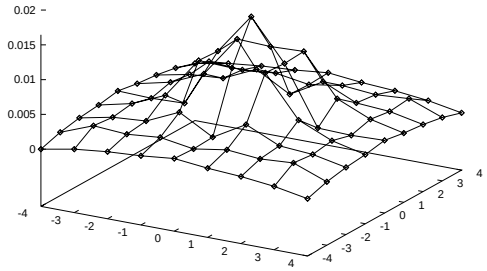

Fig. E-4-2.12

Chi-quadrado para SO(2), d=4, N=8, r=1, ang=50, i=2, j=10.

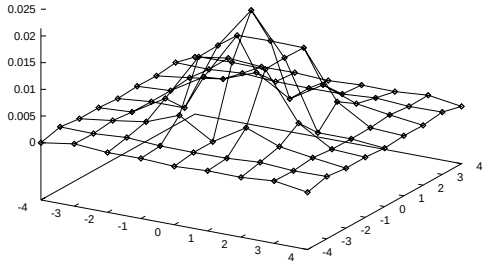

Fig. E-4-2.13

Chi-quadrado para SO(2), d=4, N=8, r=1, ang=60, i=2, j=10.

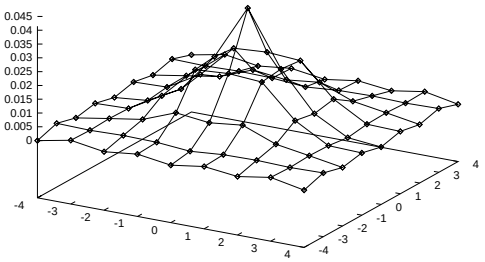

Fig. E-4-2.14

Chi-quadrado para SO(2), d=4, N=8, r=1, ang=70, i=2, j=10.

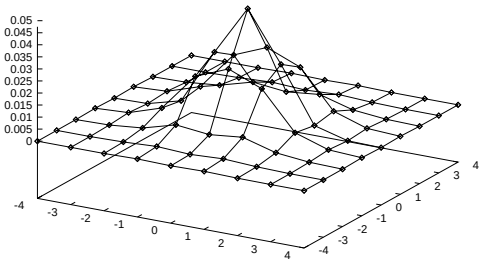

Fig. E-4-2.15

Chi-quadrado para SO(2), d=4, N=8, r=1, ang=80, i=2, j=10.

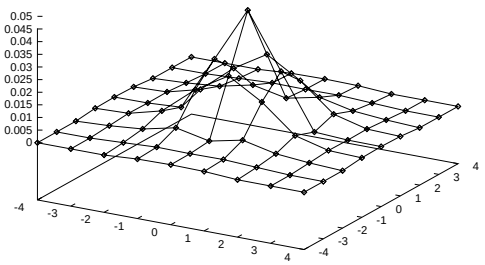

Fig. E-4-2.16

Chi-quadrado para SO(2), d=4, N=8, r=1, ang=90, i=2, j=10.

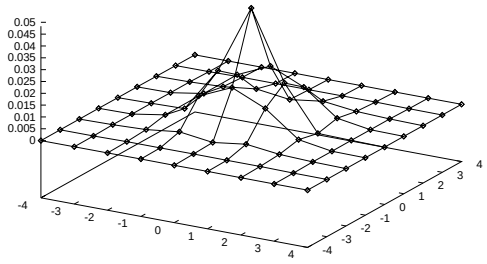

Fig. E-4-2.17

Chi-quadrado para SO(2), d=4, N=8, r=1, ang=120, i=2, j=10.

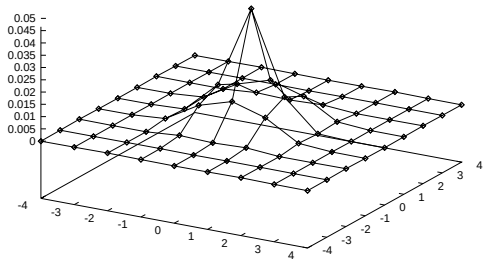

Fig. E-4-2.18

Chi-quadrado para SO(2), d=4, N=8, r=1, ang=150, i=2, j=10.

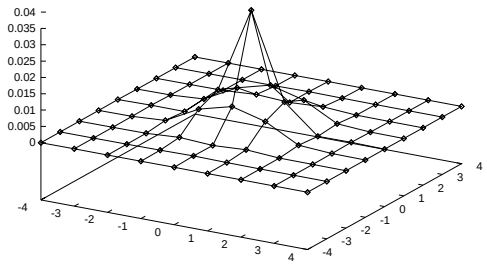

Fig. E-4-2.19

Chi-quadrado para SO(2), d=4, N=8, r=1, ang=180, i=2, j=10.

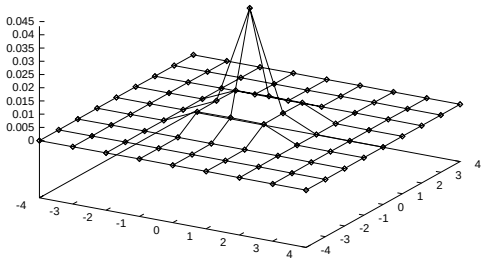

Fig. E-4-2.20

Errors in $d = 4$:
(transversal component)

Chi-quadrado para SO(2), d=4, N=6, r=1, ang=30, i=1, j=10.

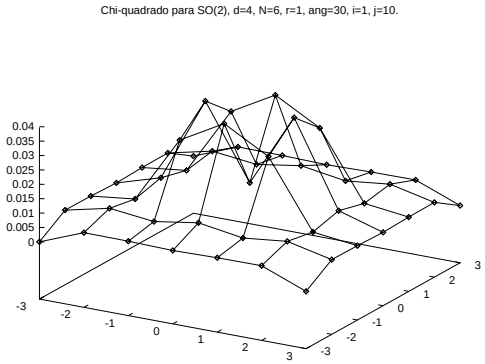

Fig. E-4-1.1

Chi-quadrado para SO(2), d=4, N=6, r=1, ang=40, i=1, j=10.

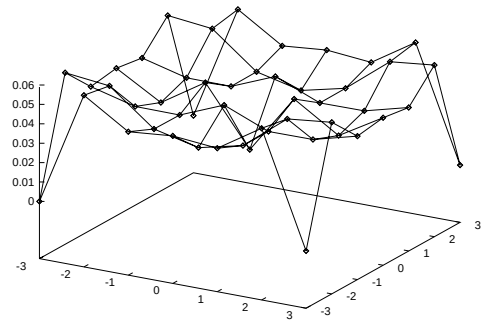

Fig. E-4-1.2

Chi-quadrado para SO(2), d=4, N=6, r=1, ang=50, i=1, j=10.

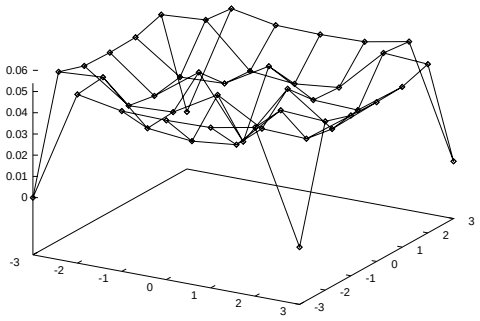

Fig. E-4-1.3

Chi-quadrado para SO(2), d=4, N=6, r=1, ang=60, i=1, j=10.

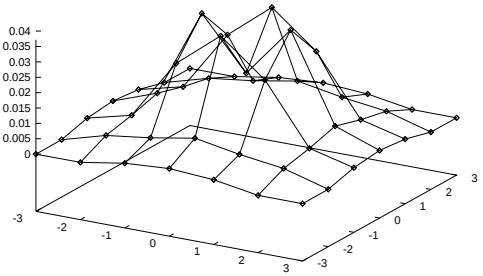

Fig. E-4-1.4

Chi-quadrado para SO(2), d=4, N=6, r=1, ang=70, i=1, j=10.

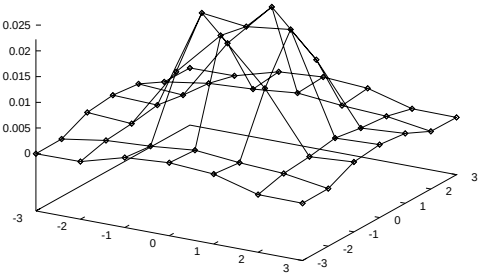

Fig. E-4-1.5

Chi-quadrado para SO(2), d=4, N=6, r=1, ang=80, i=1, j=10.

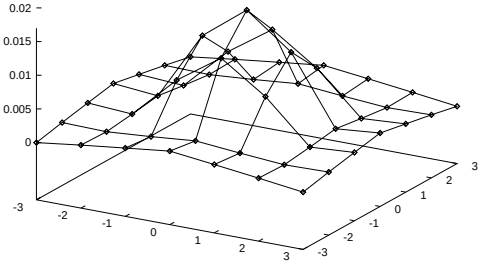

Fig. E-4-1.6

Chi-quadrado para SO(2), d=4, N=6, r=1, ang=90, i=1, j=10.

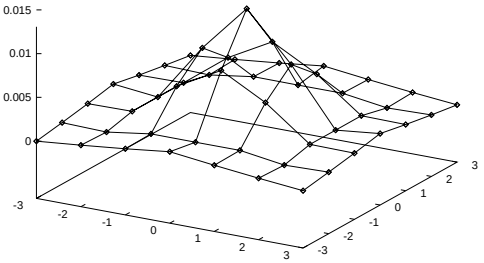

Fig. E-4-1.7

Chi-quadrado para SO(2), d=4, N=6, r=1, ang=120, i=1, j=10.

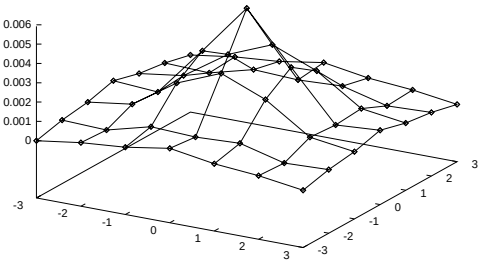

Fig. E-4-1.8

Chi-quadrado para SO(2), d=4, N=6, r=1, ang=150, i=1, j=10.

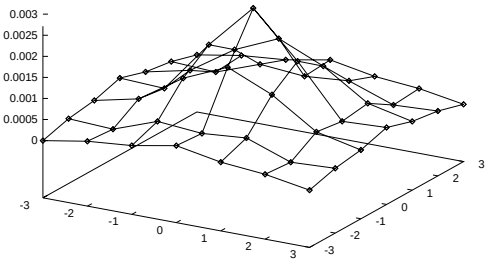

Fig. E-4-1.9

Chi-quadrado para SO(2), d=4, N=6, r=1, ang=180, i=1, j=10.

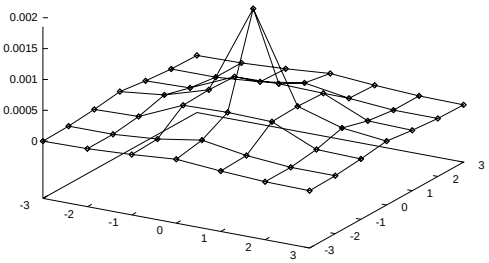

Fig. E-4-1.10

Chi-quadrado para SO(2), d=4, N=8, r=1, ang=30, i=1, j=10.

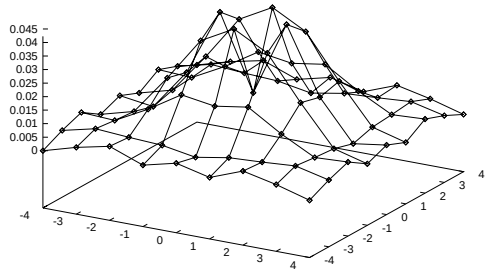

Fig. E-4-1.11

Chi-quadrado para SO(2), d=4, N=8, r=1, ang=40, i=1, j=10.

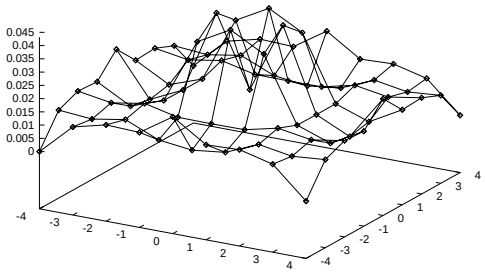

Fig. E-4-1.12

Chi-quadrado para SO(2), d=4, N=8, r=1, ang=50, i=1, j=10.

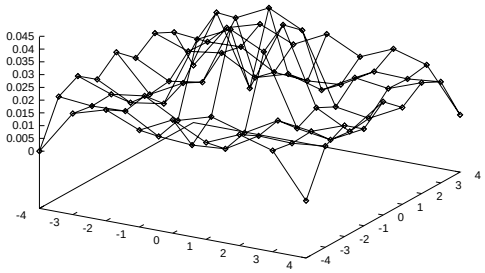

Fig. E-4-1.13

Chi-quadrado para SO(2), d=4, N=8, r=1, ang=60, i=1, j=10.

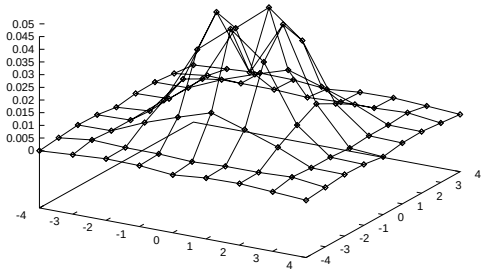

Fig. E-4-1.14

Chi-quadrado para SO(2), d=4, N=8, r=1, ang=70, i=1, j=10.

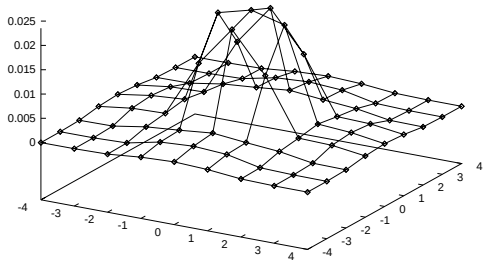

Fig. E-4-1.15

Chi-quadrado para SO(2), d=4, N=8, r=1, ang=80, i=1, j=10.

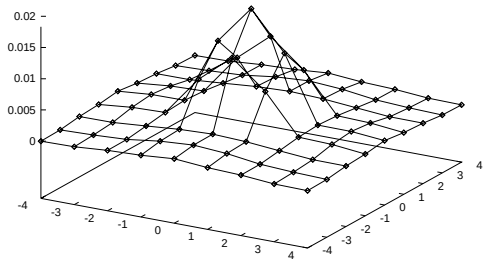

Fig. E-4-1.16

Chi-quadrado para SO(2), d=4, N=8, r=1, ang=90, i=1, j=10.

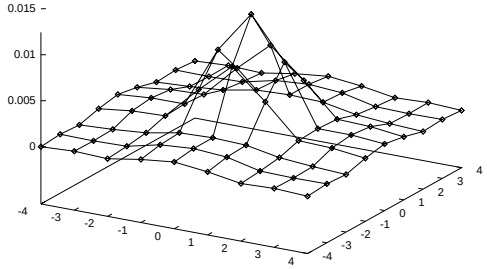

Fig. E-4-1.17

Chi-quadrado para SO(2), d=4, N=8, r=1, ang=120, i=1, j=10.

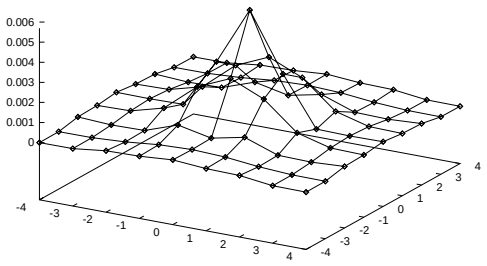

Fig. E-4-1.18

Chi-quadrado para SO(2), d=4, N=8, r=1, ang=150, i=1, j=10.

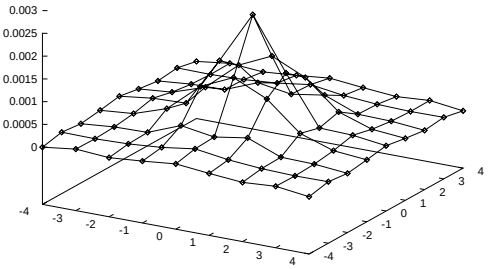

Fig. E-4-1.19

Chi-quadrado para SO(2), d=4, N=8, r=1, ang=180, i=1, j=10.

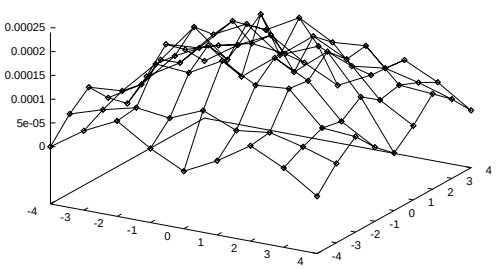

Fig. E-4-1.20

Errors in $d = 3$:
(longitudinal component)

Chi-quadrado para SO(2), d=3, N=6, r=1, ang=30, i=2, j=10.

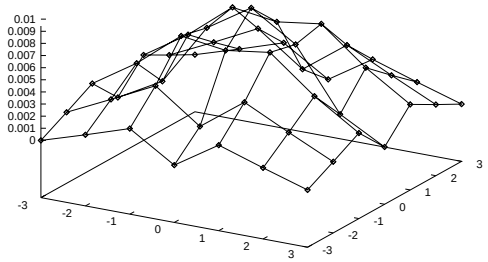

Fig. E-3-2.1

Chi-quadrado para SO(2), d=3, N=6, r=1, ang=40, i=2, j=10.

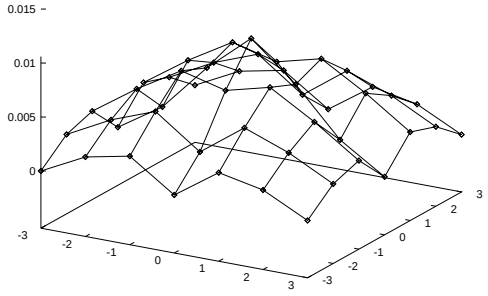

Fig. E-3-2.2

Chi-quadrado para SO(2), d=3, N=6, r=1, ang=50, i=2, j=10.

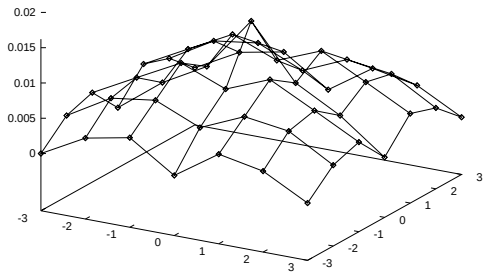

Fig. E-3-2.3

Chi-quadrado para SO(2), d=3, N=6, r=1, ang=60, i=2, j=10.

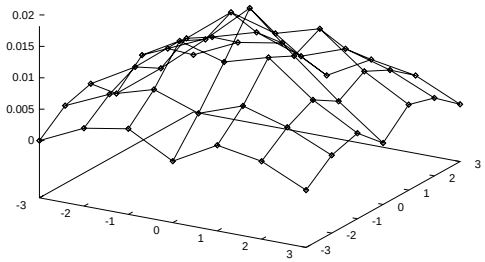

Fig. E-3-2.4

Chi-quadrado para SO(2), d=3, N=6, r=1, ang=70, i=2, j=10.

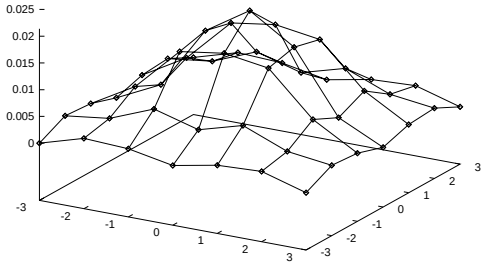

Fig. E-3-2.5

Chi-quadrado para SO(2), d=3, N=6, r=1, ang=80, i=2, j=10.

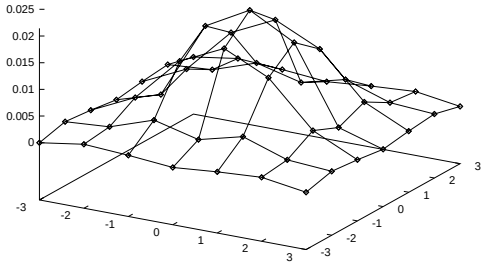

Fig. E-3-2.6

Chi-quadrado para SO(2), d=3, N=6, r=1, ang=90, i=2, j=10.

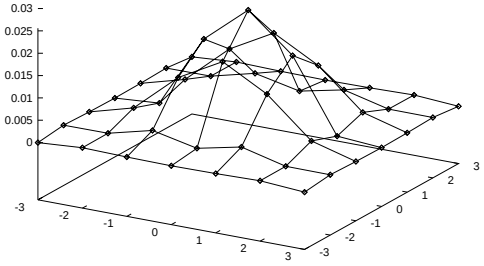

Fig. E-3-2.7

Chi-quadrado para SO(2), d=3, N=6, r=1, ang=120, i=2, j=10.

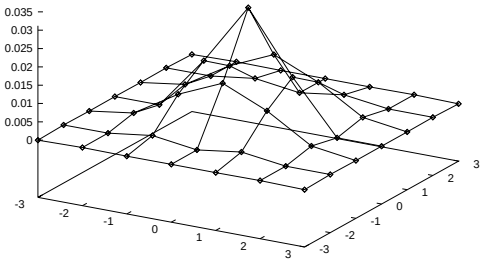

Fig. E-3-2.8

Chi-quadrado para SO(2), d=3, N=6, r=1, ang=150, i=2, j=10.

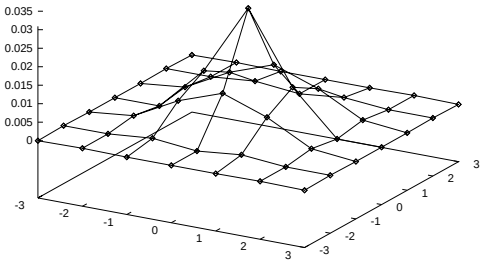

Fig. E-3-2.9

Chi-quadrado para SO(2), d=3, N=6, r=1, ang=180, i=2, j=10.

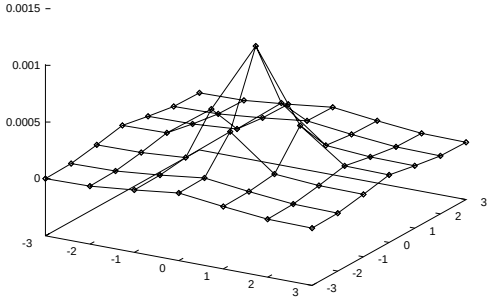

Fig. E-3-2.10

Chi-quadrado para SO(2), d=3, N=8, r=1, ang=30, i=2, j=10.

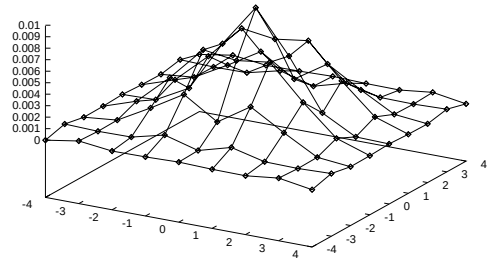

Fig. E-3-2.11

Chi-quadrado para SO(2), d=3, N=8, r=1, ang=40, i=2, j=10.

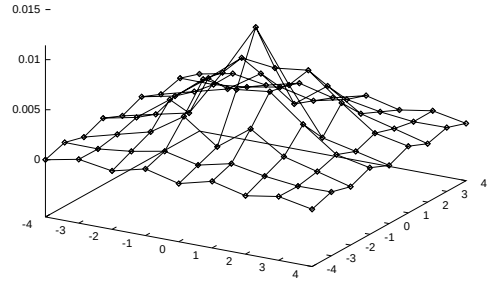

Fig. E-3-2.12

Chi-quadrado para SO(2), d=3, N=8, r=1, ang=50, i=2, j=10.

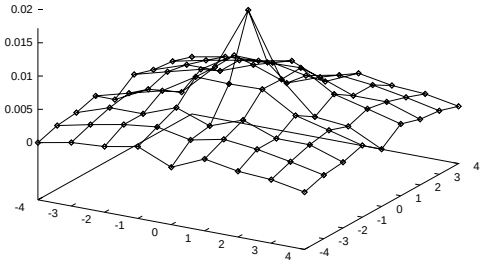

Fig. E-3-2.13

Chi-quadrado para SO(2), d=3, N=8, r=1, ang=60, i=2, j=10.

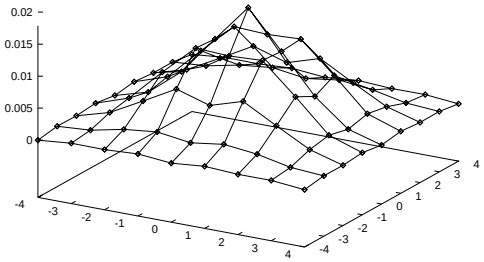

Fig. E-3-2.14

Chi-quadrado para SO(2), d=3, N=8, r=1, ang=70, i=2, j=10.

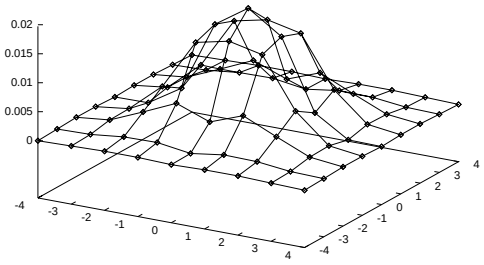

Fig. E-3-2.15

Chi-quadrado para SO(2), d=3, N=8, r=1, ang=80, i=2, j=10.

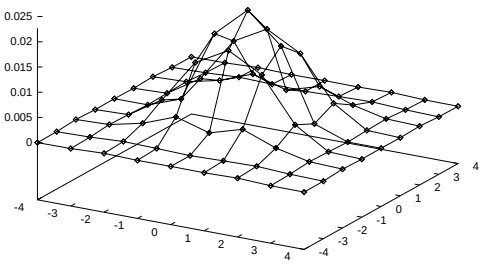

Fig. E-3-2.16

Chi-quadrado para SO(2), d=3, N=8, r=1, ang=90, i=2, j=10.

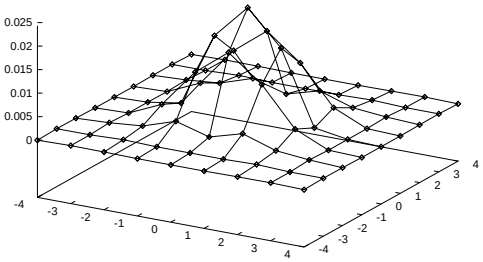

Fig. E-3-2.17

Chi-quadrado para SO(2), d=3, N=8, r=1, ang=120, i=2, j=10.

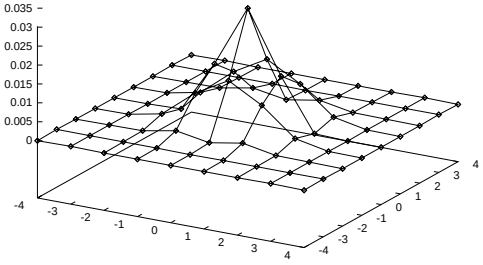

Fig. E-3-2.18

Chi-quadrado para SO(2), d=3, N=8, r=1, ang=150, i=2, j=10.

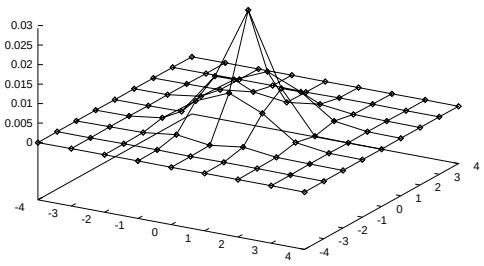

Fig. E-3-2.19

Chi-quadrado para SO(2), d=3, N=8, r=1, ang=180, i=2, j=10.

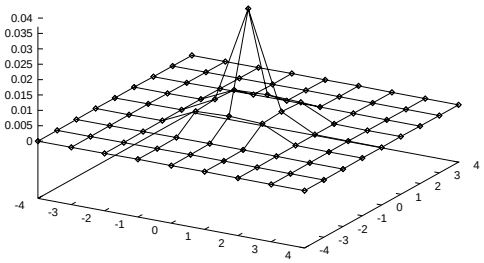

Fig. E-3-2.20

Errors in $d = 3$:
(transversal component)

Chi-quadrado para SO(2), d=3, N=6, r=1, ang=30, i=1, j=10.

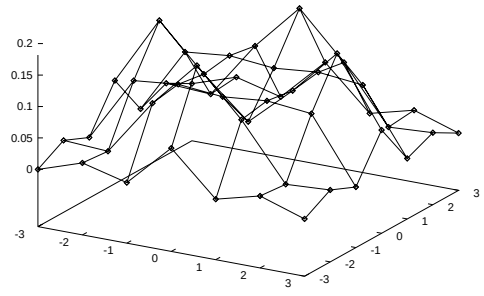

Fig. E-3-1.1

Chi-quadrado para SO(2), d=3, N=6, r=1, ang=40, i=1, j=10.

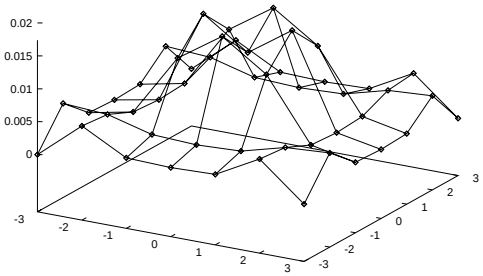

Fig. E-3-1.2

Chi-quadrado para SO(2), d=3, N=6, r=1, ang=50, i=1, j=10.

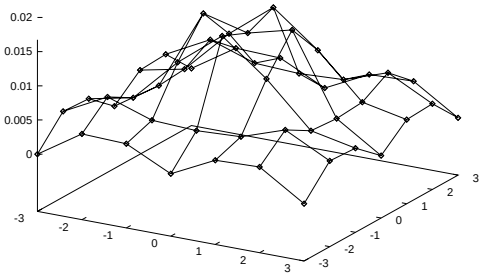

Fig. E-3-1.3

Chi-quadrado para SO(2), d=3, N=6, r=1, ang=60, i=1, j=10.

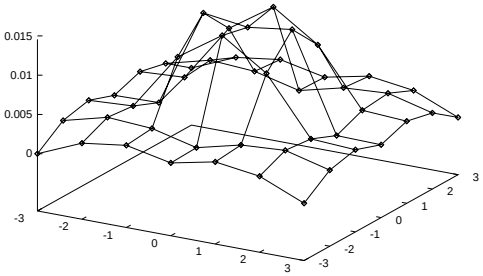

Fig. E-3-1.4

Chi-quadrado para SO(2), d=3, N=6, r=1, ang=70, i=1, j=10.

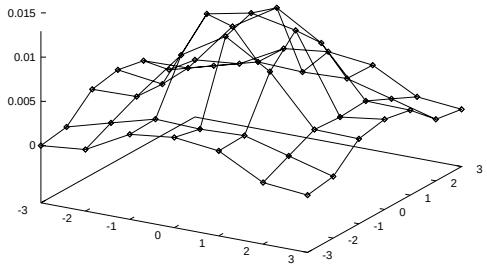

Fig. E-3-1.5

Chi-quadrado para SO(2), d=3, N=6, r=1, ang=80, i=1, j=10.

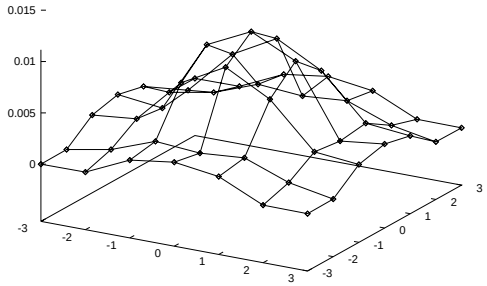

Fig. E-3-1.6

Chi-quadrado para SO(2), d=3, N=6, r=1, ang=90, i=1, j=10.

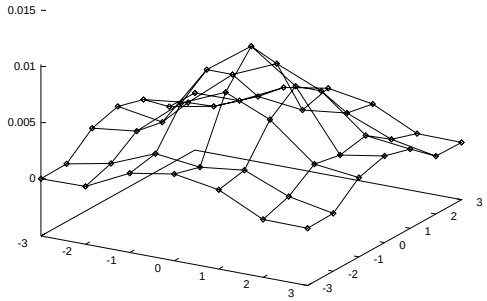

Fig. E-3-1.7

Chi-quadrado para SO(2), d=3, N=6, r=1, ang=120, i=1, j=10.

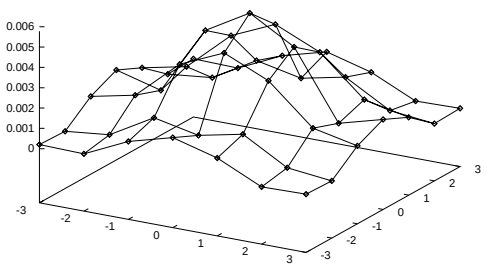

Fig. E-3-1.8

Chi-quadrado para SO(2), d=3, N=6, r=1, ang=150, i=1, j=10.

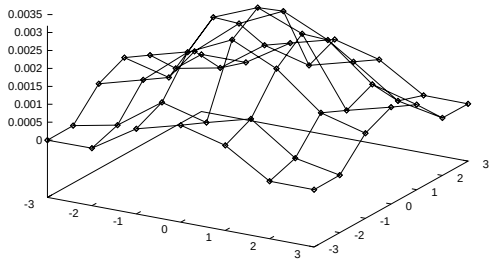

Fig. E-3-1.9

Chi-quadrado para SO(2), d=3, N=6, r=1, ang=180, i=1, j=10.

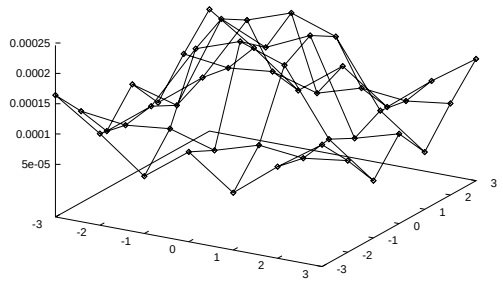

Fig. E-3-1.10

Chi-quadrado para SO(2), d=3, N=8, r=1, ang=30, i=1, j=10.

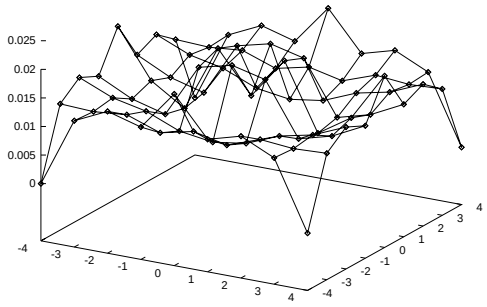

Fig. E-3-1.11

Chi-quadrado para SO(2), d=3, N=8, r=1, ang=40, i=1, j=10.

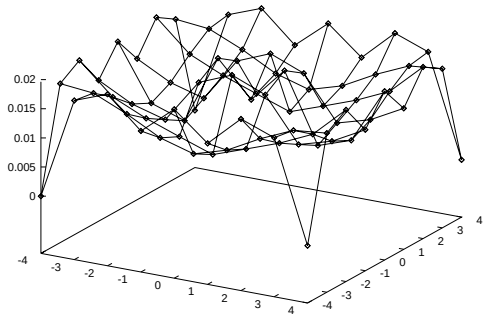

Fig. E-3-1.12

Chi-quadrado para SO(2), d=3, N=8, r=1, ang=50, i=1, j=10.

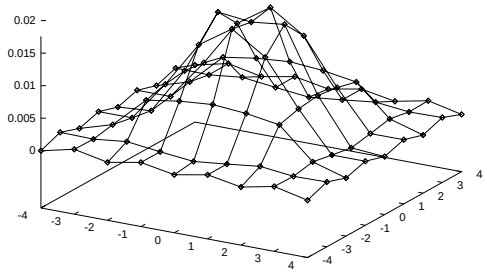

Fig. E-3-1.13

Chi-quadrado para SO(2), d=3, N=8, r=1, ang=60, i=1, j=10.

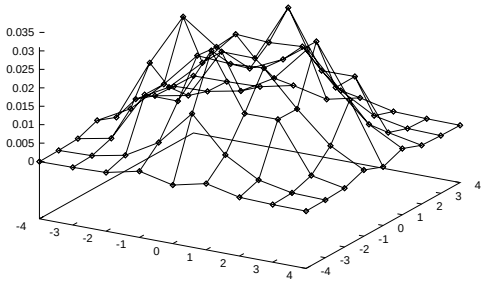

Fig. E-3-1.14

Chi-quadrado para SO(2), d=3, N=8, r=1, ang=70, i=1, j=10.

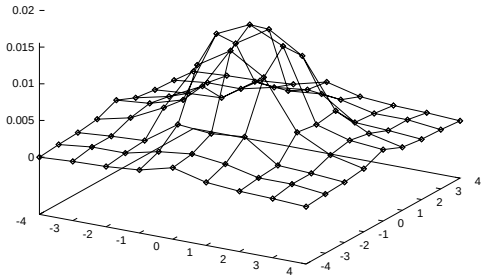

Fig. E-3-1.15

Chi-quadrado para SO(2), d=3, N=8, r=1, ang=80, i=1, j=10.

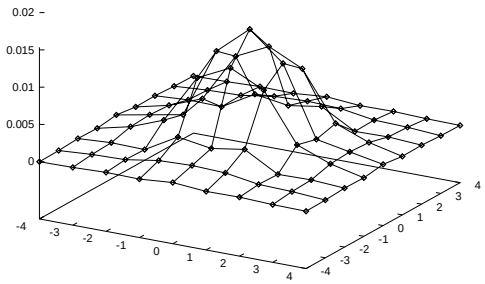

Fig. E-3-1.16

Chi-quadrado para SO(2), d=3, N=8, r=1, ang=90, i=1, j=10.

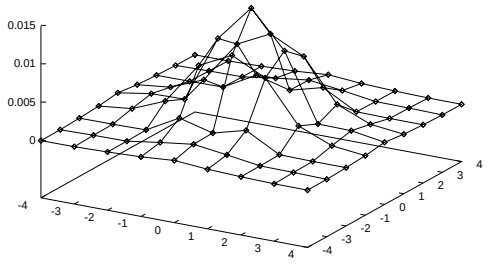

Fig. E-3-1.17

Chi-quadrado para SO(2), d=3, N=8, r=1, ang=120, i=1, j=10.

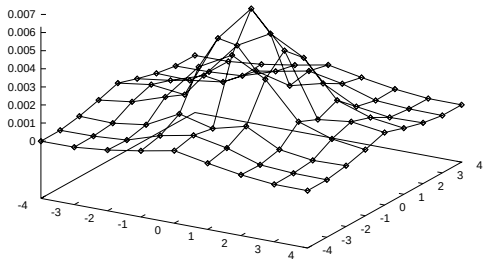

Fig. E-3-1.18

Chi-quadrado para SO(2), d=3, N=8, r=1, ang=150, i=1, j=10.

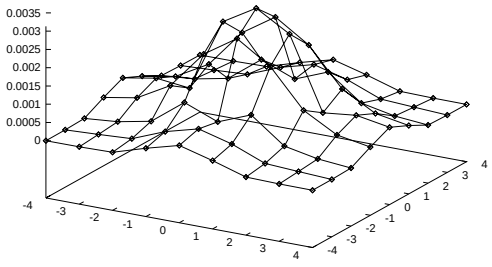

Fig. E-3-1.19

Chi-quadrado para SO(2), d=3, N=8, r=1, ang=180, i=1, j=10.

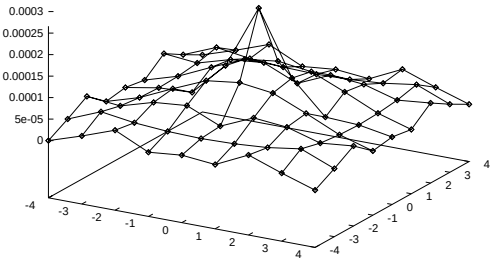

Fig. E-3-1.20

Errors for $j = 5$:
(longitudinal component)

Chi-quadrado para SO(2), d=4, N=8, r=1, ang=50, i=2, j=5.

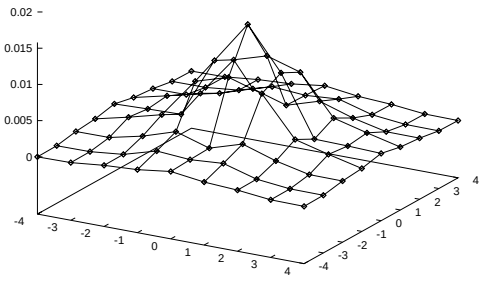

Fig. E-4-2-J.1

Chi-quadrado para SO(2), d=4, N=8, r=1, ang=60, i=2, j=5.

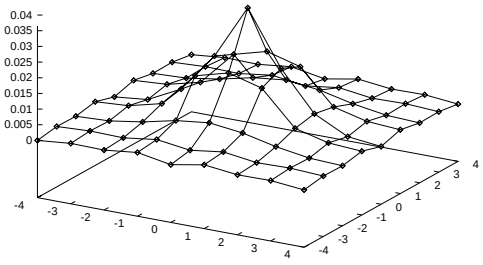

Fig. E-4-2-J.2

Chi-quadrado para SO(2), d=4, N=8, r=1, ang=70, i=2, j=5.

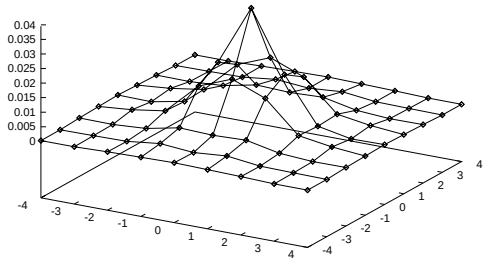

Fig. E-4-2-J.3

Chi-quadrado para SO(2), d=4, N=8, r=1, ang=70, i=1, j=5.

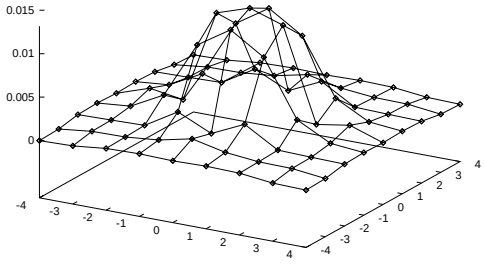

Fig. E-4-1-J.3

Errors for $j = 5$:
(transversal component)

Chi-quadrado para SO(2), d=4, N=8, r=1, ang=50, i=1, j=5.

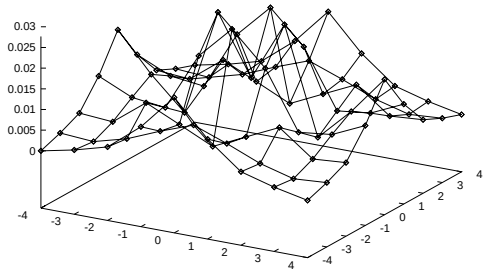

Fig. E-4-1-J.1

Chi-quadrado para SO(2), d=4, N=8, r=1, ang=60, i=1, j=5.

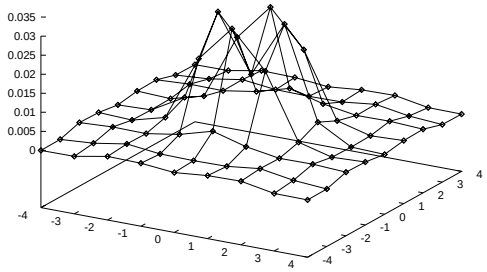

Fig. E-4-1-J.2

Bibliography

[1] J.-S. Wang and R. H. Swendsen, Physica **A 167**, (1990), 565; U. Wolff, Phys. Rev. Lett. **62**, (1989), 361; R. C. Brower e P. Tamaio, Phys. Rev. Lett. **62** (1989), 1087.

[2] N. Metropolis, A. W. Rosenbluth, M. N. Rosenbluth, A. H. Teller and E. Teller, J. Chem. Phys. 21 (1953), 1087; J. M. Hammersley and D. C. Handscomb, "Monte Carlo Methods", Methuen (1964).

[3] "Um Estudo sobre Quebra de Simetria e Comportamento Crítico em Teorias Quânticas de Campos na Rede", A. C. R. Martins, Doctoral Thesis submitted to the "Instituto de Física" of the "Universidade de São Paulo", 1996.

[4] "Differentiability and continuity of quantum fields on a lattice", Jorge L. deLyra, Timothy E. Gallivan and See Kit Foong, Phys. Rev. **D43** (1991) 476–484.

[5] "Symmetry breaking on a finite euclidean lattice", J. L. deLyra and A. C. R. Martins, Nucl. Phys. **B432** (1994) 621–640.

[6] "Finite lattice systems with true critical behavior", Jorge L. deLyra, Timothy E. Gallivan and See Kit Foong, Phys. Rev. **D46** (1992) 1643–1657.